Copy 6
RM L55I23

NACA

RESEARCH MEMORANDUM

WIND-TUNNEL INVESTIGATION OF THE STATIC LONGITUDINAL AND LATERAL STABILITY OF THE BELL X-1A AT SUPERSONIC SPEEDS

By Arthur Henderson, Jr.

Langley Aeronautical Laboratory
Langley Field, Va.

NATIONAL ADVISORY COMMITTEE
FOR AERONAUTICS

WASHINGTON

October 27, 1955

NACA RM L55I23

NATIONAL ADVISORY COMMITTEE FOR AERONAUTICS

RESEARCH MEMORANDUM

WIND-TUNNEL INVESTIGATION OF THE STATIC LONGITUDINAL AND LATERAL STABILITY OF THE BELL X-1A AT SUPERSONIC SPEEDS

By Arthur Henderson, Jr.

SUMMARY

An investigation to determine the static longitudinal and lateral stability characteristics of a 1/62-scale model of the Bell X-1A has been conducted in the Langley 9-inch supersonic tunnel. Tests were made at Mach numbers of 1.62, 1.94, 2.22, 2.40, and 2.62 on the wing-body, wing—body—vertical-tail, and complete configurations. Data are presented for both the body and stability axes. Detailed analysis of the test results is omitted.

INTRODUCTION

During recent flight tests the Bell X-1A was found to have some highly undesirable handling qualities. In the vicinity of Mach number 2 the airplane commenced rolling uncontrollably while at the same time diverging in pitch and yaw. In order to obtain more information on the airplane's aerodynamic characteristics, a 1/62-scale model of the Bell X-1A has been tested in the Langley 9-inch supersonic tunnel at Mach numbers of 1.62, 1.94, 2.22, 2.40, and 2.62. Tests were conducted on the complete configuration with three different stabilizer settings (0°, 5°, -10°), the model with horizontal tail off, and the model with horizontal and vertical tail off. Tests were made through an angle-of-attack range at zero yaw angle and through an angle-of-yaw range at zero angle of attack. Detailed analysis of the test results is omitted in order to expedite release of this information.

SYMBOLS

A	axial force
b	wing span
B	body
$\bar{c}$	wing mean aerodynamic chord
c.g.	center of gravity (located at 22.3-percent $\bar{c}$)
C_A	axial-force coefficient, A/qS
C_D	drag coefficient, D/qS
C_{D_o}	minimum drag coefficient
C_{F_N}	normal-force coefficient, F_N/qS
C_L	lift coefficient, L/qS
C_l	rolling-moment coefficient, L'/qSb
C_m	pitching-moment coefficient, M/qS$\bar{c}$
C_n	yawing-moment coefficient, N/qSb
C_Y	side-force coefficient, Y/qS
D	drag
F_N	normal force
L	lift
L'	rolling moment about axis through center of base and parallel to body axis
M	pitching moment about center of gravity
N	yawing moment about center of gravity

[redacted]

q	dynamic pressure
R	Reynolds number based on wing mean aerodynamic chord
S	wing area or stabilizer
T	vertical tail
W	wing
x	longitudinal distance ahead or behind center of gravity
$x/\bar{c}$	longitudinal center-of-pressure location measured in mean aerodynamic chords from center-of-gravity position
α	angle of attack
β	angle of sideslip
$C_{I_\alpha} = \left(\frac{\partial C_L}{\partial \alpha}\right)_{\alpha=0}$	
$C_{m_\alpha} = \left(\frac{\partial C_m}{\partial \alpha}\right)_{\alpha=0}$	
$\frac{\partial C_m}{\partial C_L}$	longitudinal aerodynamic-center location in units of $\bar{c}$ measured from center of gravity at $\alpha = 0^\circ$, $\frac{(C_{m_\alpha})_{\alpha=0}}{(C_{I_\alpha})_{\alpha=0}}$
$C_{Y_\beta} = \left(\frac{\partial C_Y}{\partial \beta}\right)_{\beta=0}$	
$C_{l_\beta} = \left(\frac{\partial C_l}{\partial \beta}\right)_{\beta=0}$	
$C_{n_\beta} = \left(\frac{\partial C_n}{\partial \beta}\right)_{\beta=0}$	
$\frac{\partial C_n}{\partial C_Y}$	aerodynamic-center location of side force in units of b measured from center of gravity at $\beta = 0^\circ$, $\frac{(C_{n_\beta})_{\beta=0}}{(C_{Y_\beta})_{\beta=0}}$

[redacted]

APPARATUS AND TESTS

Wind Tunnel

The Langley 9-inch supersonic tunnel is a closed-throat, single return, continuous operating tunnel in which the test section is approximately 9 inches square. Different test Mach numbers are achieved through the use of interchangeable nozzle blocks. Eleven fine-mesh turbulence-damping screens are installed in the settling chamber ahead of the supersonic nozzle. The pressure, temperature, and humidity can be controlled during the tunnel operation.

Models

The configurations used for the present tests consisted of the complete model with stabilizer settings of 0°, 5°, and -10° ($WBTS_0$, $WBTS_5$, $WBTS_{-10}$), wing—body—vertical-tail (WBT), and wing-body (WB). A three-view drawing of the complete model is shown in figure 1.

Six-Component Balance and Model-Support System

The six-component balance and model-support system used in these tests is described in reference 1.

Tests

In an attempt to simulate flight boundary-layer conditions, all configurations were run with transition strips near: the model nose, wing leading edges, vertical-tail leading edges, and stabilizer leading edges. Transition strip material was pulverized salt which had been passed through an 80-mesh screen. The Mach number, Reynolds number, and α and β ranges for each configuration are given in table I. The two Reynolds numbers at each of Mach numbers 2.22, 2.40, and 2.62 were not run as part of a Reynolds number investigation. The higher Reynolds number was the result of increasing the stagnation pressure in order to increase the sensitivity of the balance through the zero α and zero β range at the higher Mach numbers. The lower Reynolds number was that for atmospheric pressure in the stagnation chamber, which allowed the α and β ranges to be extended while keeping the maximum loads on the model consistent with allowable sting stresses.

[redacted]

PRECISION OF DATA

The estimated probable errors in the force and moment coefficients are as follows:

M	R	C_{F_N}	C_A	C_{Y_l}	C_l	C_n	C_m	C_L	C_D
1.62	0.32×10^6	±0.0011	±0.0005	±0.0007	±0.0015	±0.0009	±0.0038	±0.0011	±0.0005
1.94	.29	±.0006	±.0003	±.0006	±.0022	±.0014	±.0041	±.0006	±.0003
2.22	.45	±.0005	±.0002	±.0003	±.0008	±.0008	±.0052	±.0005	±.0002
	.26	±.0006	±.0004	±.0003	±.0012	±.0008	±.0080	±.0006	±.0005
2.40	.40	±.0002	±.0004	±.0004	±.0006	±.0005	±.0026	±.0002	±.0004
	.23	±.0006	±.0003	±.0005	±.0006	±.0017	±.0082	±.0006	±.0003
2.62	.45	±.0003	±.0004	±.0004	±.0004	±.0005	±.0027	±.0003	±.0004
	.21	±.0006	±.0003	±.0005	±.0010	±.0008	±.0058	±.0006	±.0004

RESULTS

The static longitudinal and lateral force and moment characteristics of the configurations tested are presented in figures 2 to 26 as follows:

Configuration	Figures for Mach number of -				
	1.62	1.94	2.22	2.40	2.62
WB	2	3	4	5	6
WBT	7	8	9	10	11
$WBTS_0$	12	13	14	15	16
$WBTS_5$	17	18	19	20	21
$WBTS_{-10}$	22	23	24	25	26

[redacted]

Each figure has three parts: part (a) presents the longitudinal force and moment characteristics in the body-axis system; part (b) presents the longitudinal force characteristics in the stability-axis system; part (c) presents the lateral force and moment characteristics in the body-axis system. The flagged symbols on the $M = 2.22$, $M = 2.40$, and $M = 2.62$ curves represent atmospheric stagnation-pressure data, whereas the unflagged symbols are for greater than atmospheric stagnation-pressure data.

Figure 27 presents the static longitudinal and lateral stability derivatives and the minimum drag coefficients of the configurations as a function of Mach number. It may be seen from this figure that the variation with Mach number of the minimum drag and the static longitudinal stability derivatives is qualitatively what would be expected. The general trends with Mach number of the static lateral stability derivatives are also about what would be expected; with the exception, that at approximately $M = 2.2$ some of the C_{Y_β} curves undergo reversal of direction. The level of the C_{n_β} curves is such that the Bell X-1A becomes directionally unstable between $M = 2.3$ and $M = 2.4$, depending on the configuration. It is interesting to note that the difference between BWT and BWTS can be more than 0.0005 in C_{n_β}, depending upon the stabilizer setting and Mach number.

Langley Aeronautical Laboratory,
National Advisory Committee for Aeronautics,
Langley Field, Va., September 7, 1955.

REFERENCE

1. Rainey, Robert W.: Investigation of the Effects of Bomb-Bay Configuration Upon the Aerodynamic Characteristics of a Body With Circular Cross Section at Supersonic Speeds. NACA RM L55E27, 1955.

[redacted]

TABLE I

M	R	α, deg	β, deg
1.62	0.32×10^6	-6 to 8	-8 to 2
1.94	.29	-6 to 8	-8 to 2
2.22	.45 .26	-6 to 8 +4 to 10	-8 to 2 -10 to -4
2.40	.40 .23	-6 to 8 +6 to 12	-8 to 2 -12 to -6
2.62	.45 .21	-6 to 8 6 to ≈13	-8 to 2 ≈ -13 to -6

[redacted]

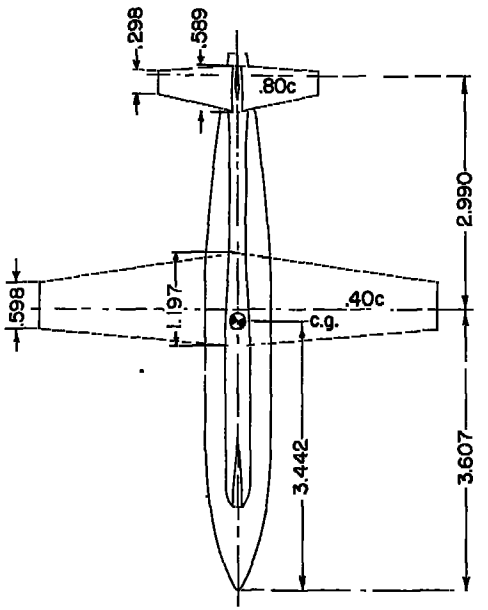

Wing	
Area	4.864 sq in.
Span	5.420 in.
Aspect ratio	6
Section	65$_1$-008 (a=1)
Root incidence	2.5°
Tip incidence	1.5°
Mean aerodyamic chord	0.931 in.
Stabilizer	
Area	0.974 sq in.
Section	65-006
Vertical tail	
Area	0.958 sq in.
Section	65-008

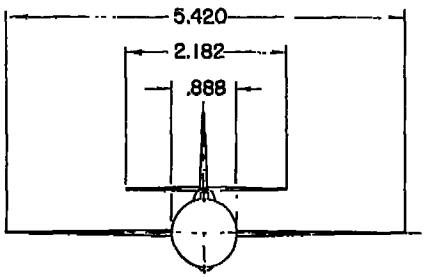

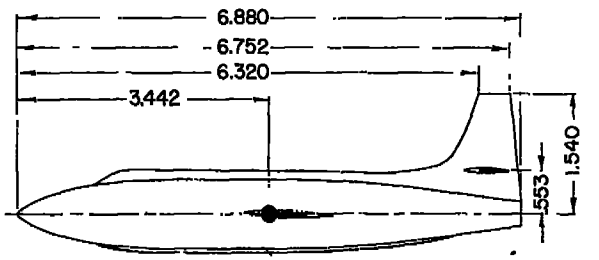

Figure 1.- Three-view drawing of 1/62-scale model of Bell X-1A. All dimensions are in inches.

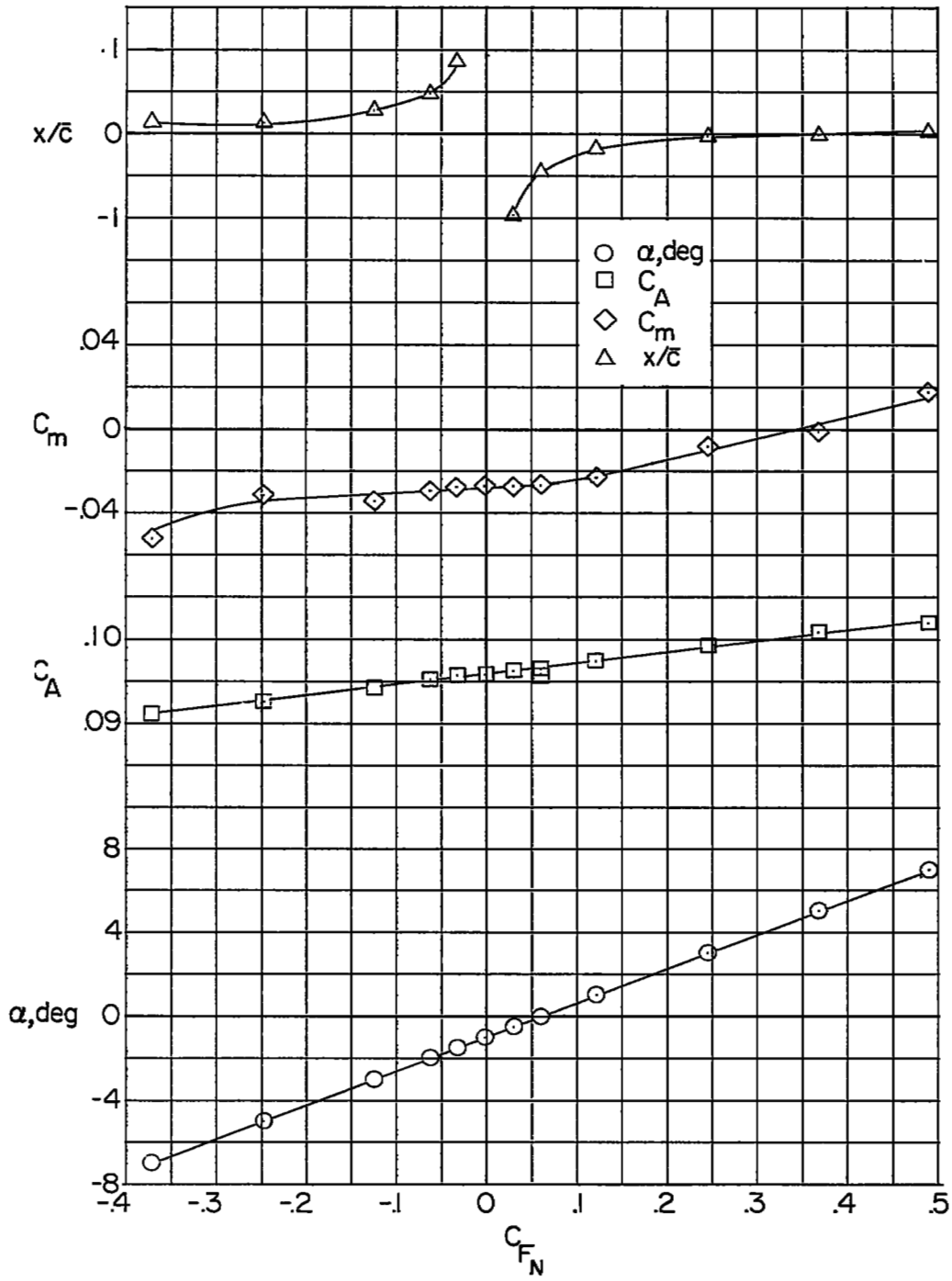

(a) Longitudinal characteristics in body-axis system at $\beta = 0^{\circ}$.

Figure 2.- Wing-body configuration at $M = 1.62$.

[redacted]

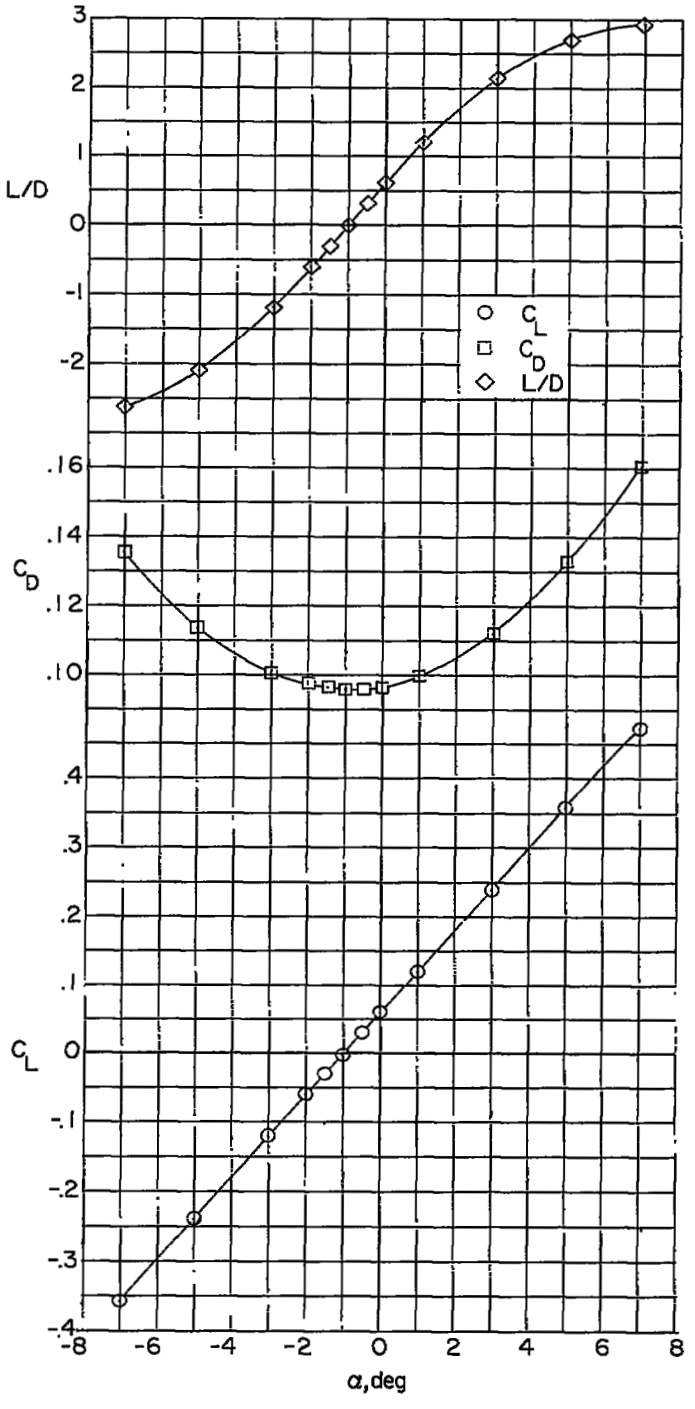

(b) Longitudinal force characteristics in stability-axis system at $\beta = 0^{\circ}$.

Figure 2.- Wing-body configuration at $M = 1.62$. Continued.

[redacted]

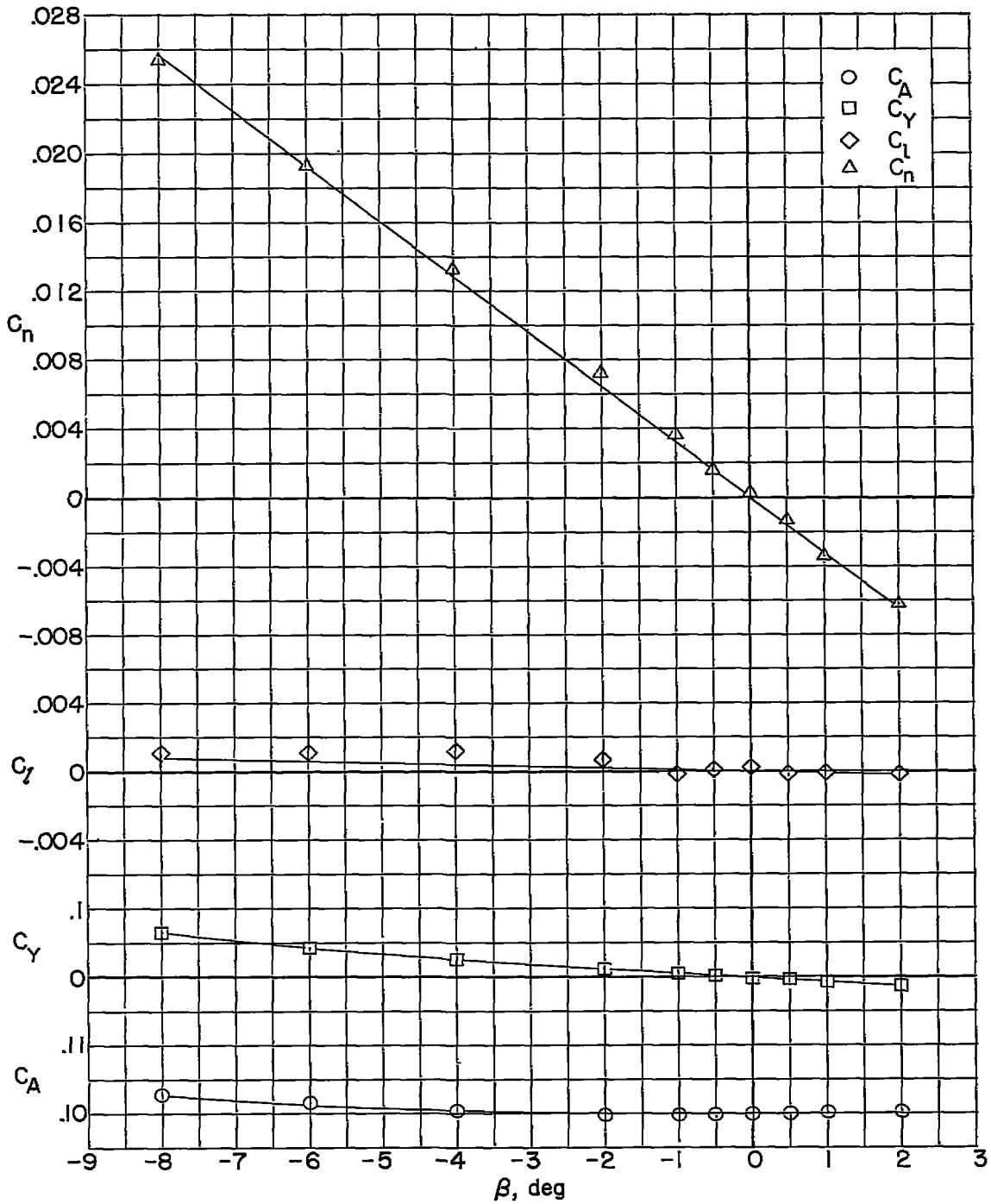

(c) Lateral characteristics in body-axis system at $\alpha = 0^\circ$.

Figure 2.- Wing-body configuration at M = 1.62. Concluded.

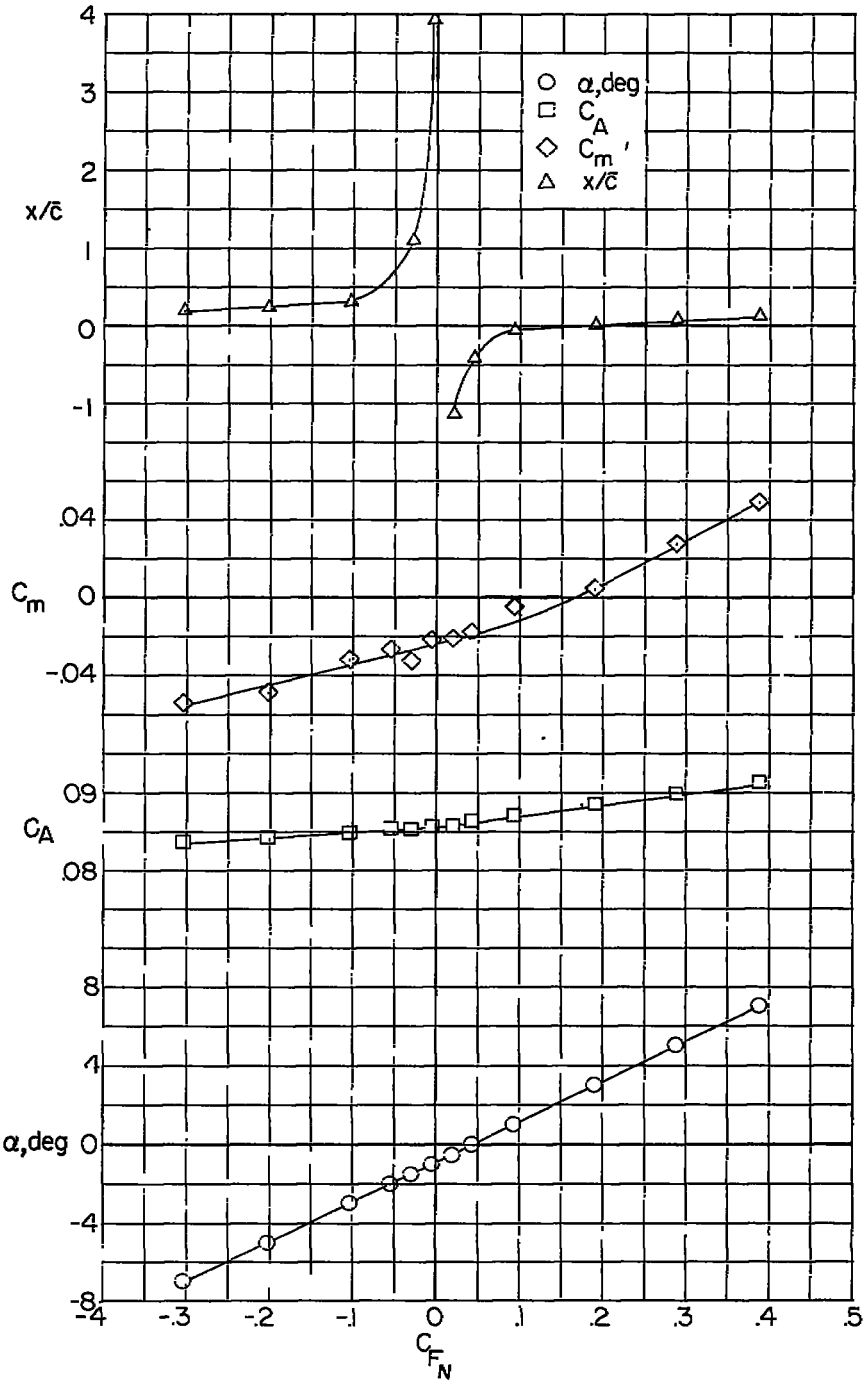

(a) Longitudinal characteristics in body-axis system at $\beta = 0^\circ$.

Figure 3.- Wing-body configuration at $M = 1.94$.

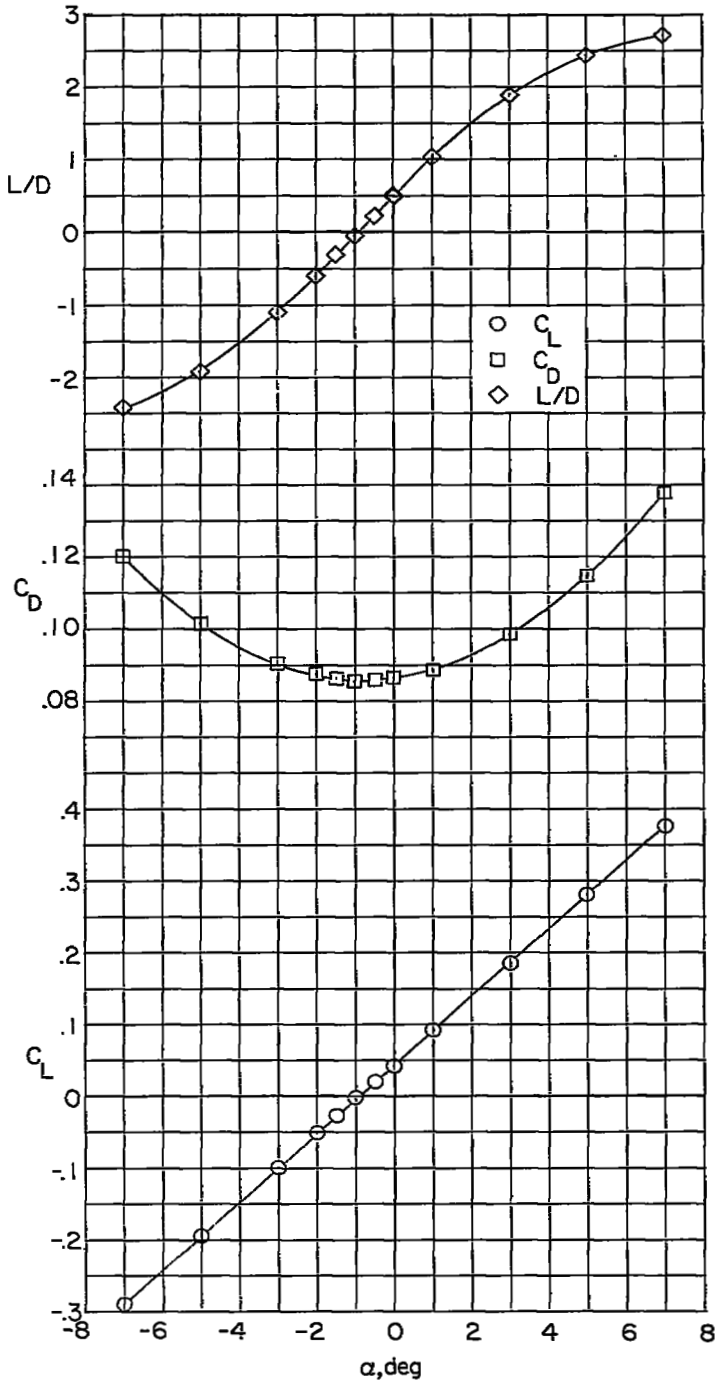

(b) Longitudinal force characteristics in stability-axis system at $\beta = 0^{\circ}$.

Figure 3.- Wing-body configuration at $M = 1.94$. Continued.

[redacted]

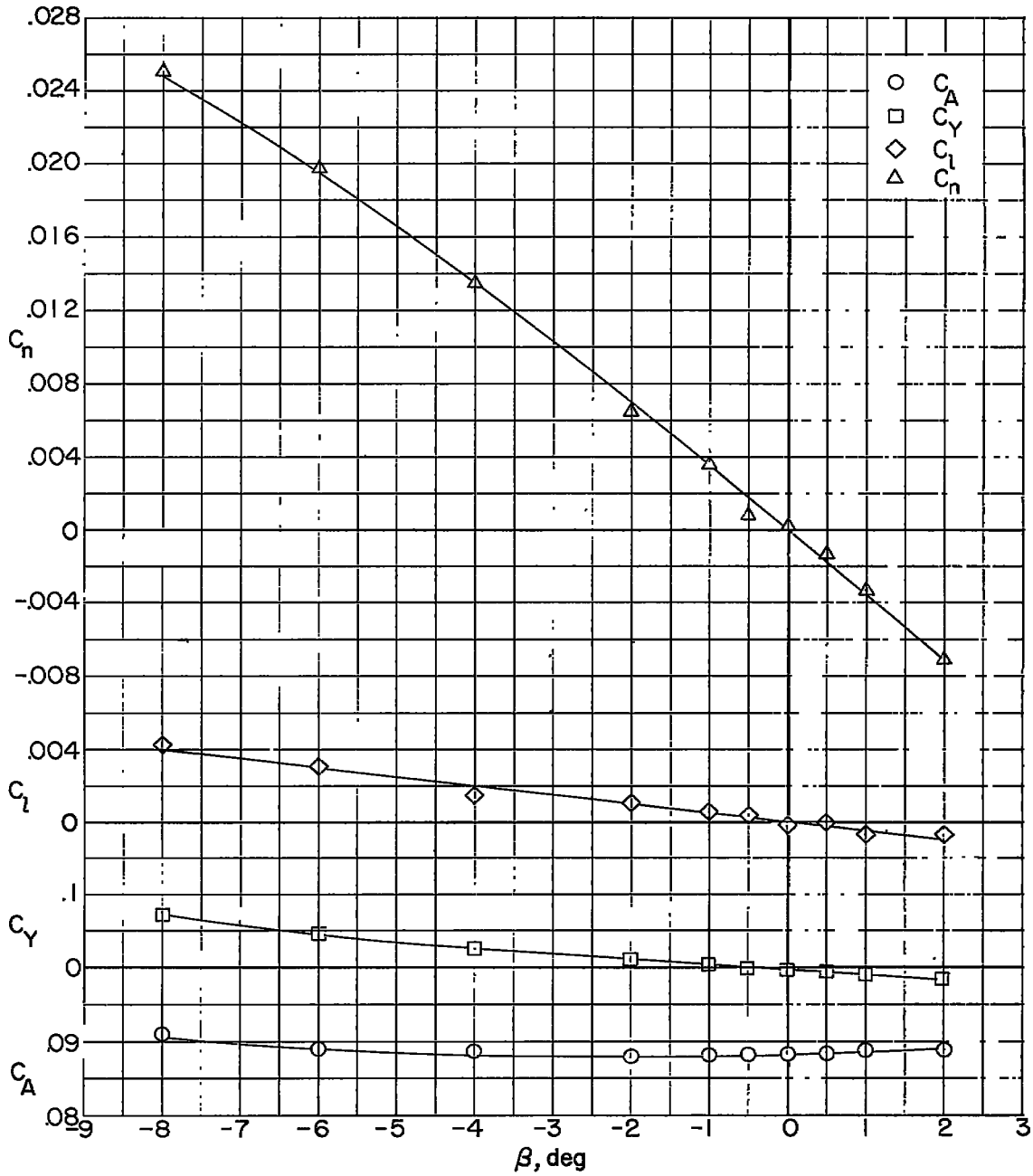

(c) Lateral characteristics in body-axis system at $\alpha = 0^\circ$.

Figure 3.- Wing-body configuration at M = 1.94. Concluded.

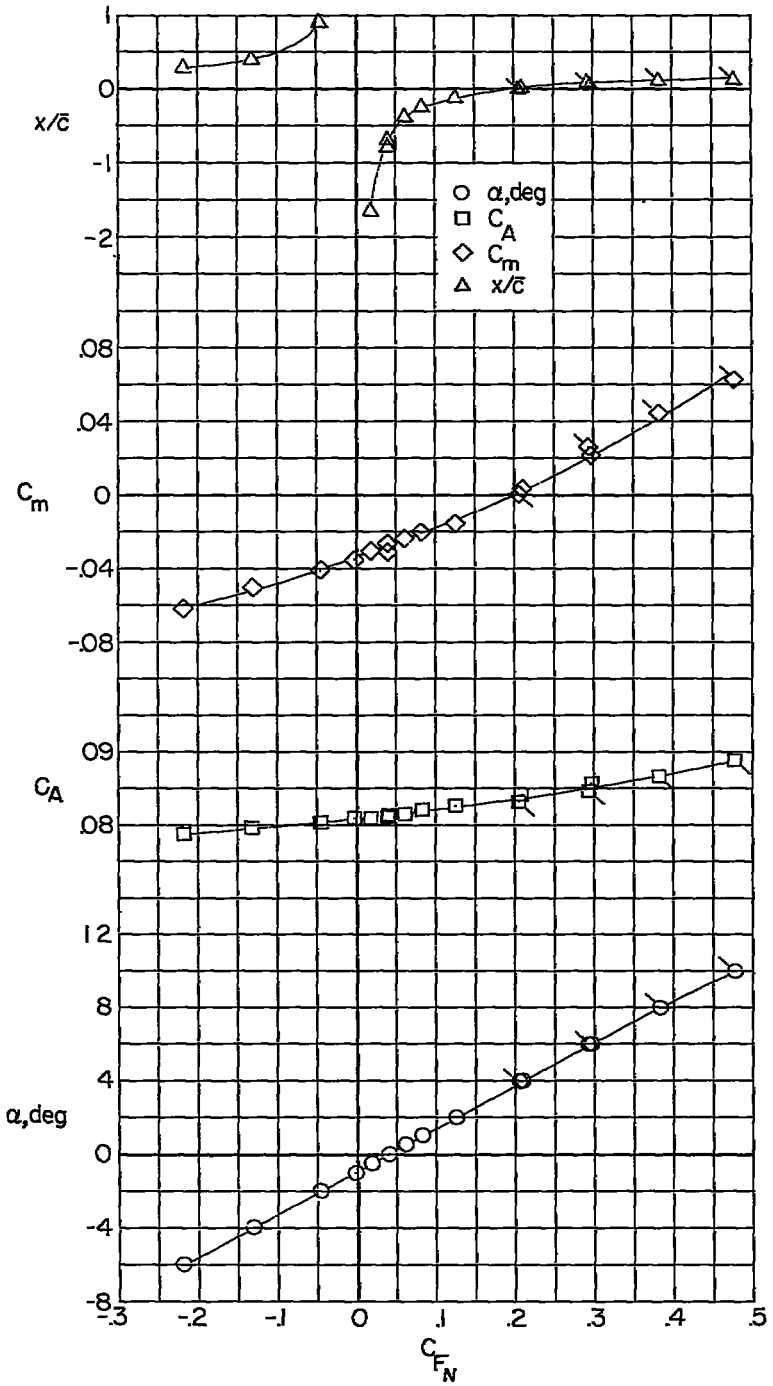

(a) Longitudinal characteristics in body-axis system at $\beta = 0^\circ$.

Figure 4.- Wing-body configuration at M = 2.22.

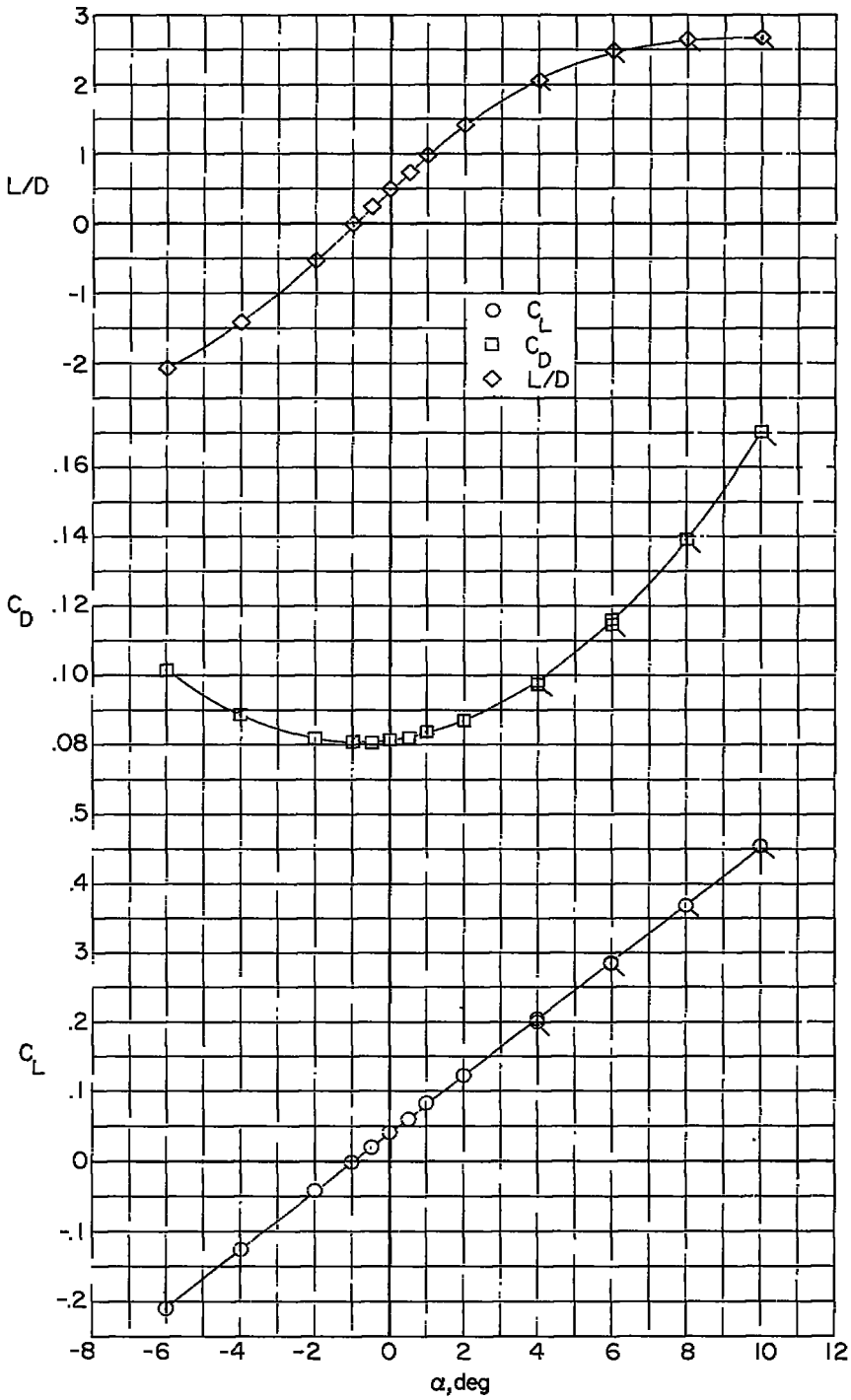

(b) Longitudinal force characteristics in stability-axis system at $\beta = 0^{\circ}$.

Figure 4.- Wing-body configuration at $M = 2.22$. Continued.

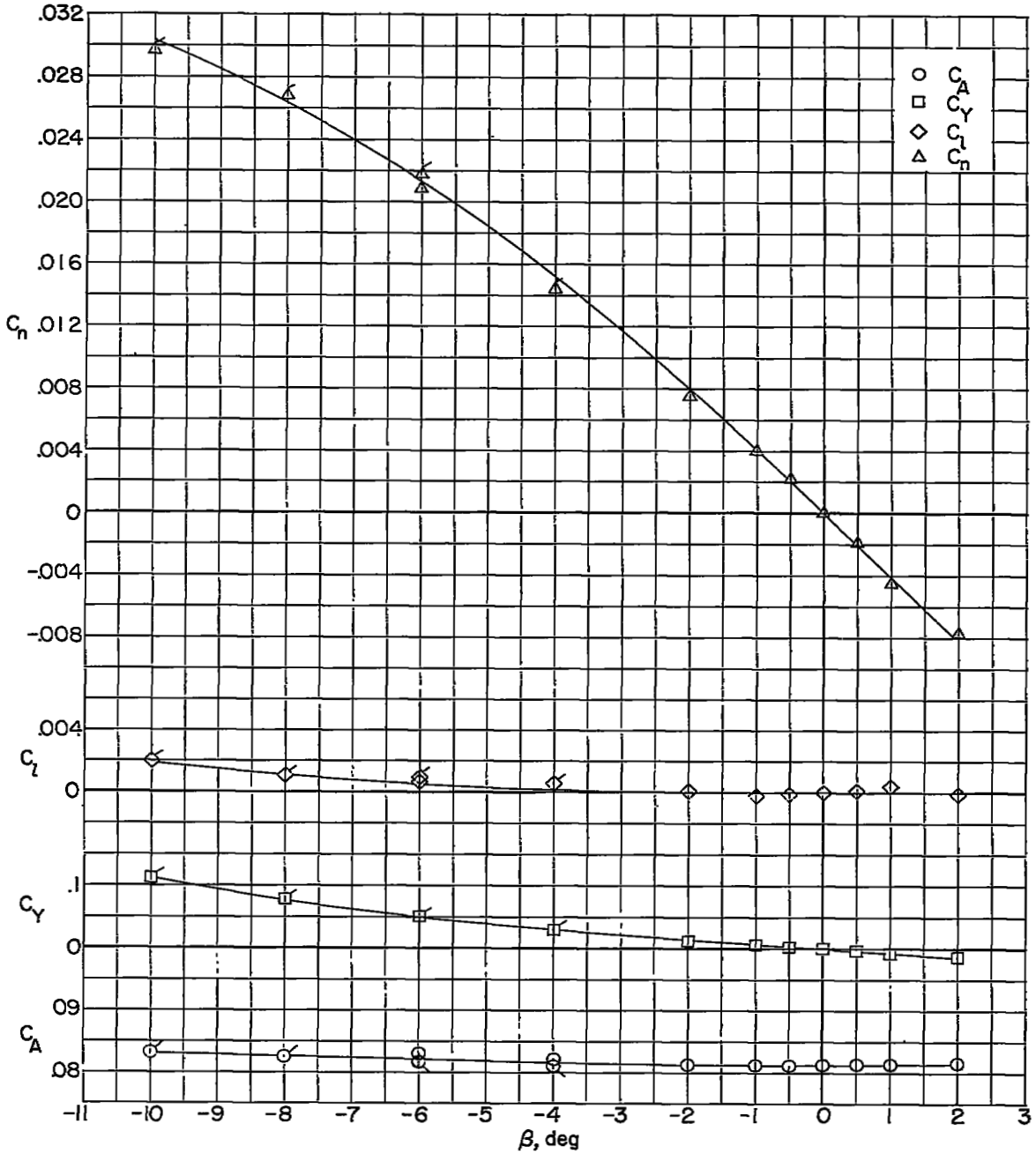

(c) Lateral characteristics in body-axis system at $\alpha = 0^{\circ}$.

Figure 4.- Wing-body configuration at M = 2.22. Concluded.

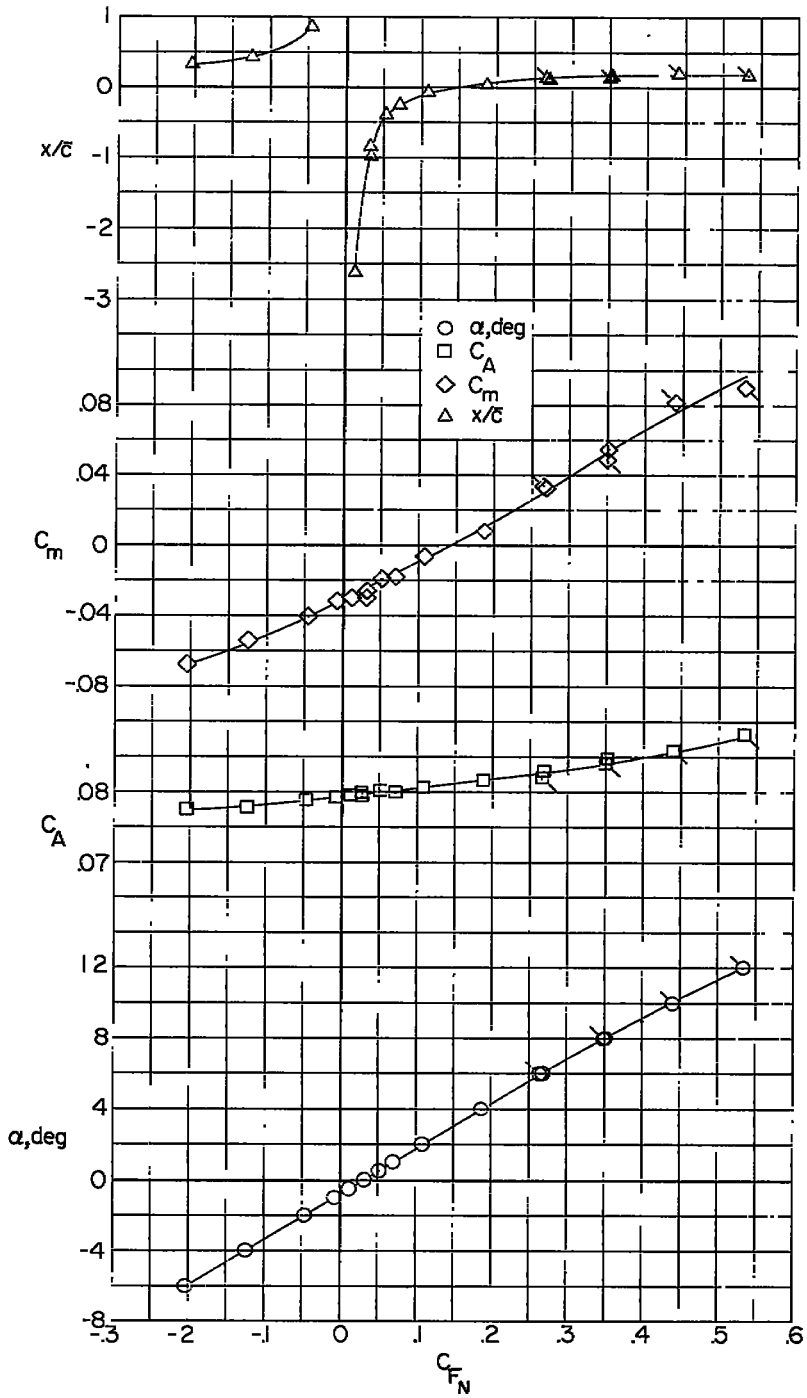

(a) Longitudinal characteristics in body-axis system at $\beta = 0^{\circ}$.

Figure 5.- Wing-body configuration at $M = 2.40$.

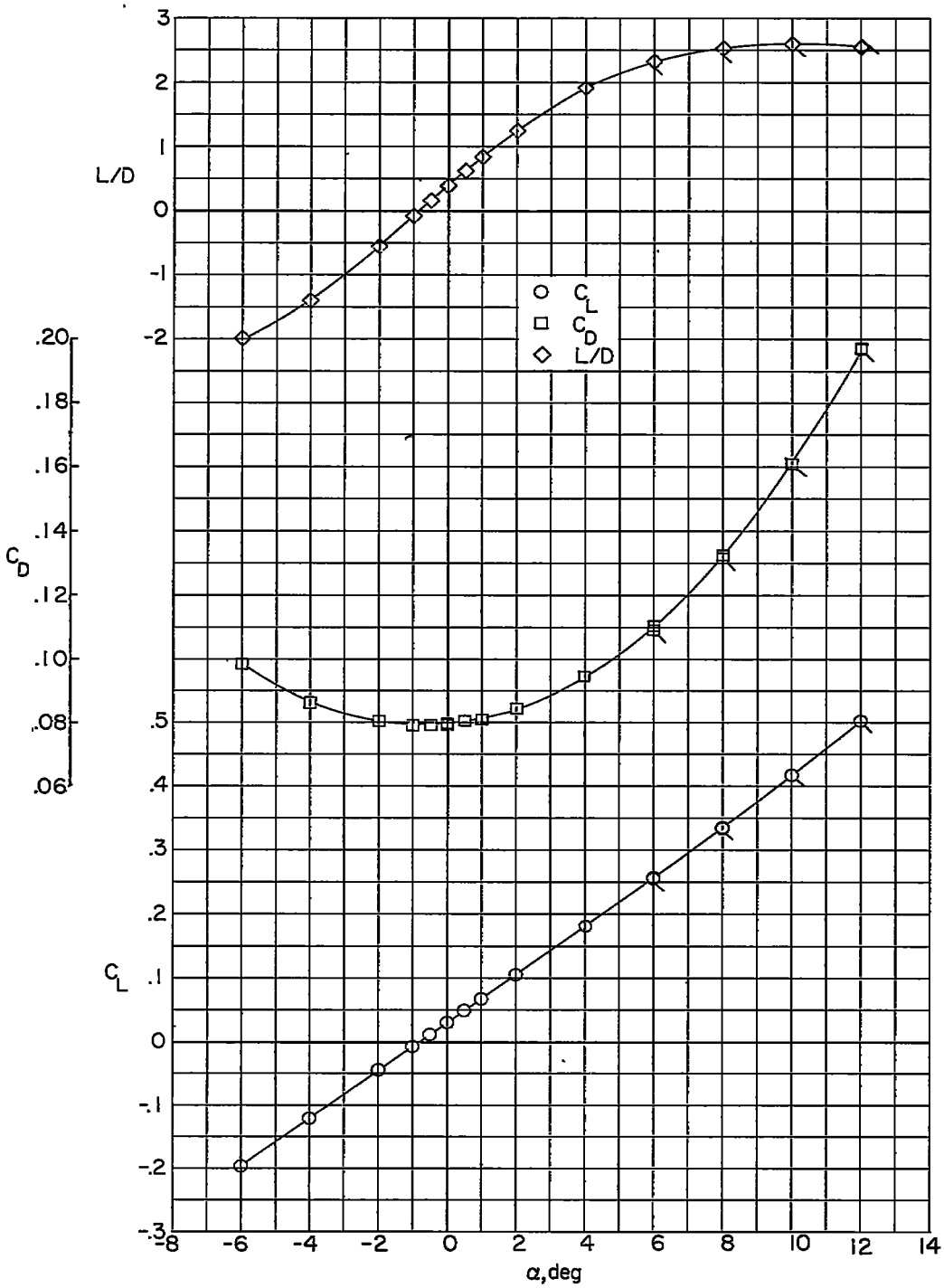

(b) Longitudinal force characteristics in stability-axis system at $\beta = 0^{\circ}$.

Figure 5.- Wing-body configuration at M = 2.40. Continued.

[redacted]

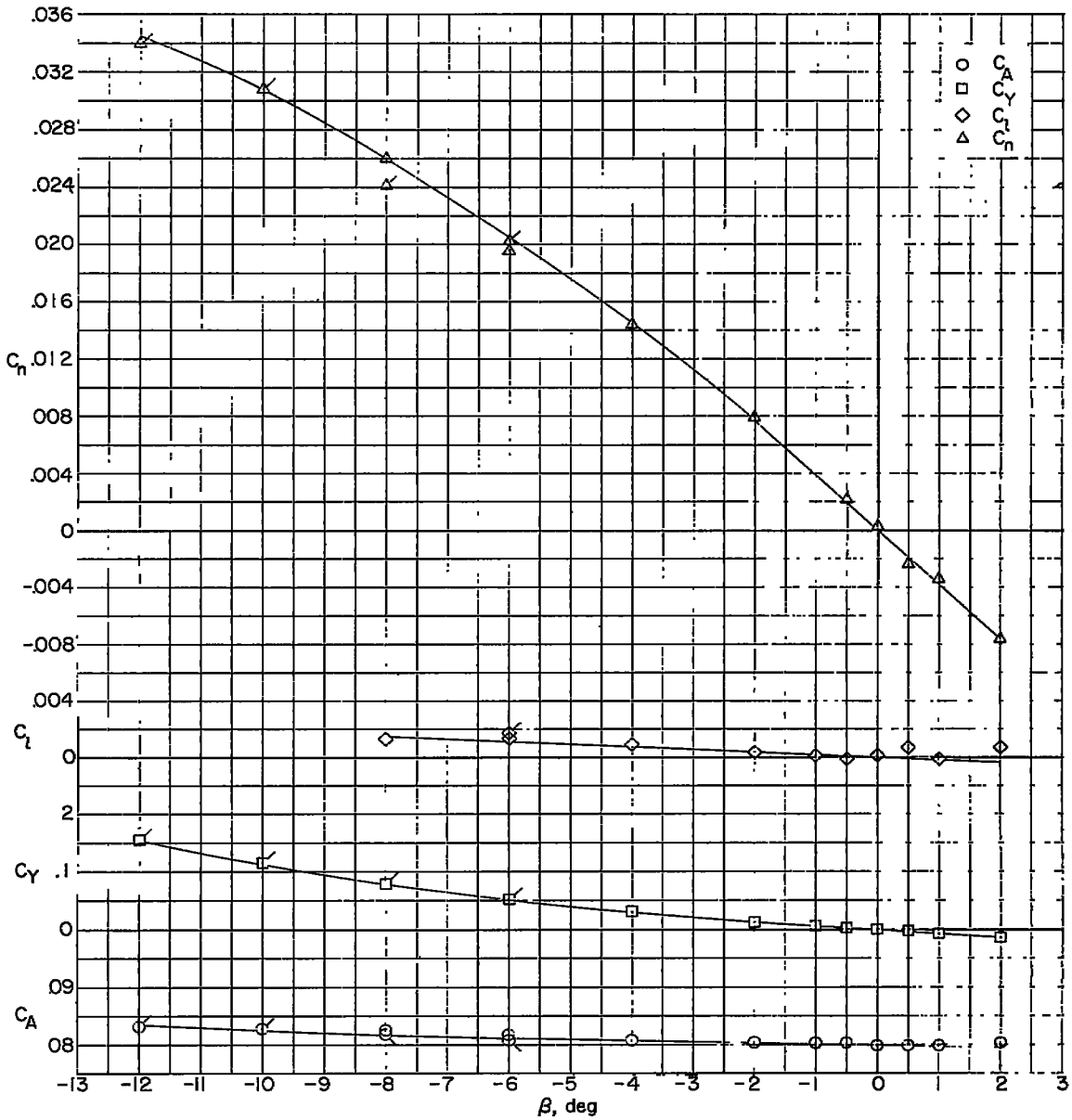

(c) Lateral characteristics in body-axis system at $\alpha = 0^{\circ}$.

Figure 5.- Wing-body configuration at M = 2.40. Concluded.

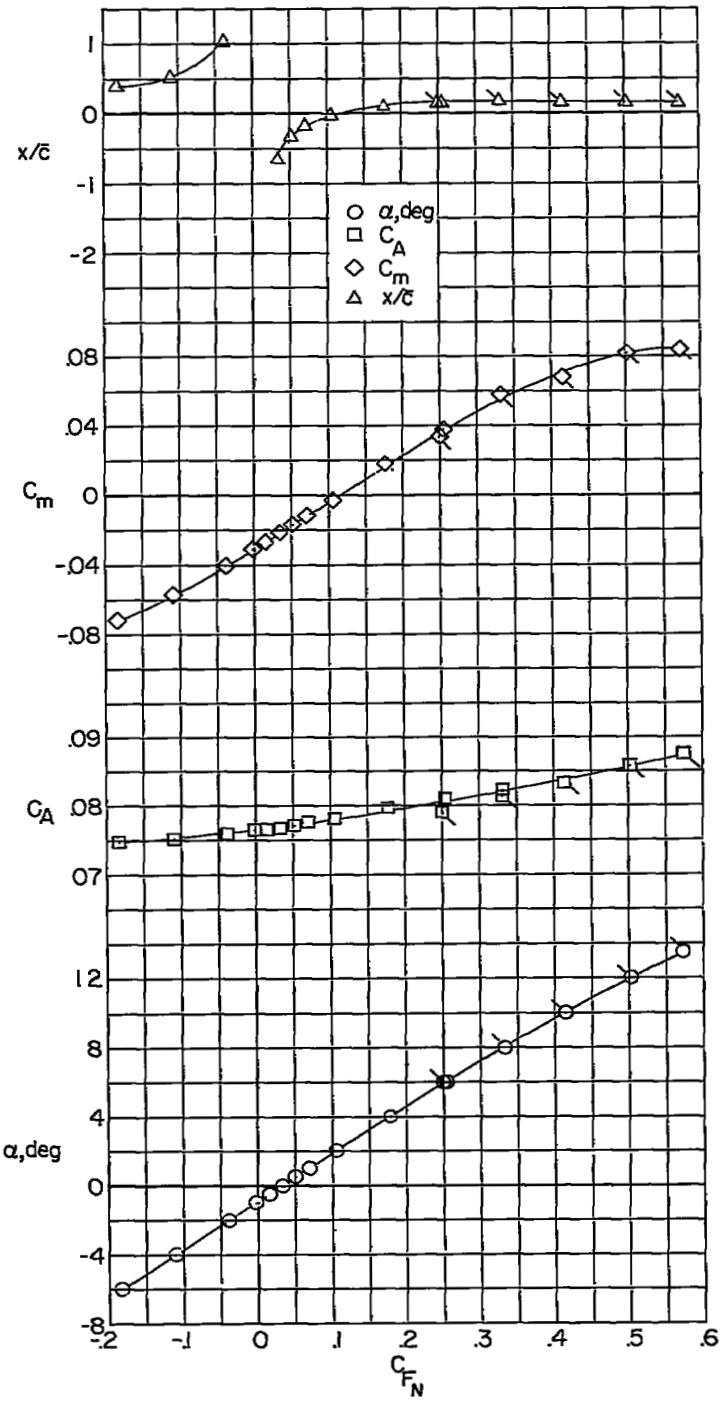

(a) Longitudinal characteristics in body-axis system at $\beta = 0^{\circ}$.

Figure 6.- Wing-body configuration at $M = 2.62$.

[redacted]

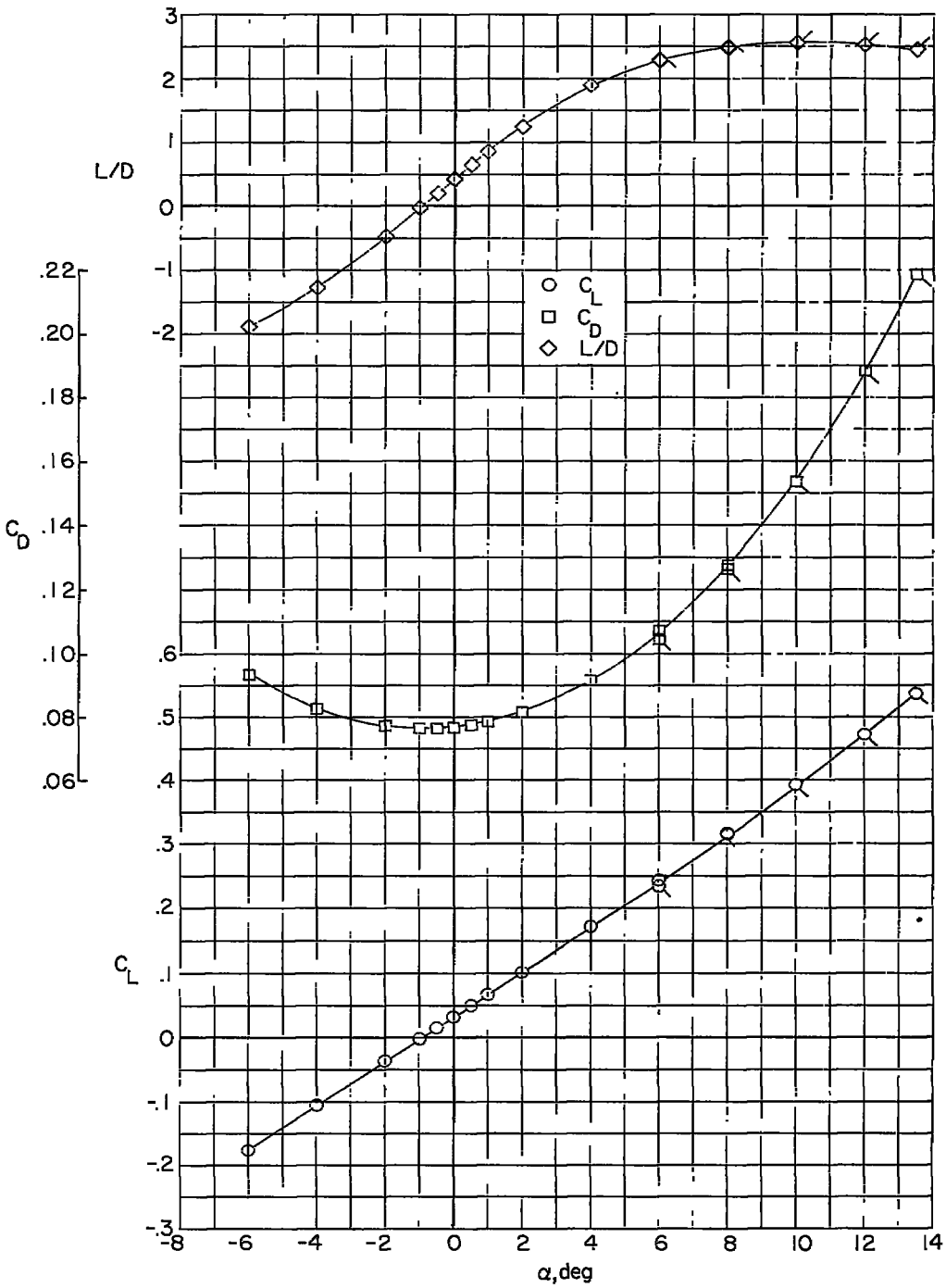

(b) Longitudinal force characteristics in stability-axis system at $\beta = 0^\circ$.

Figure 6.- Wing-body configuration at M = 2.62. Continued.

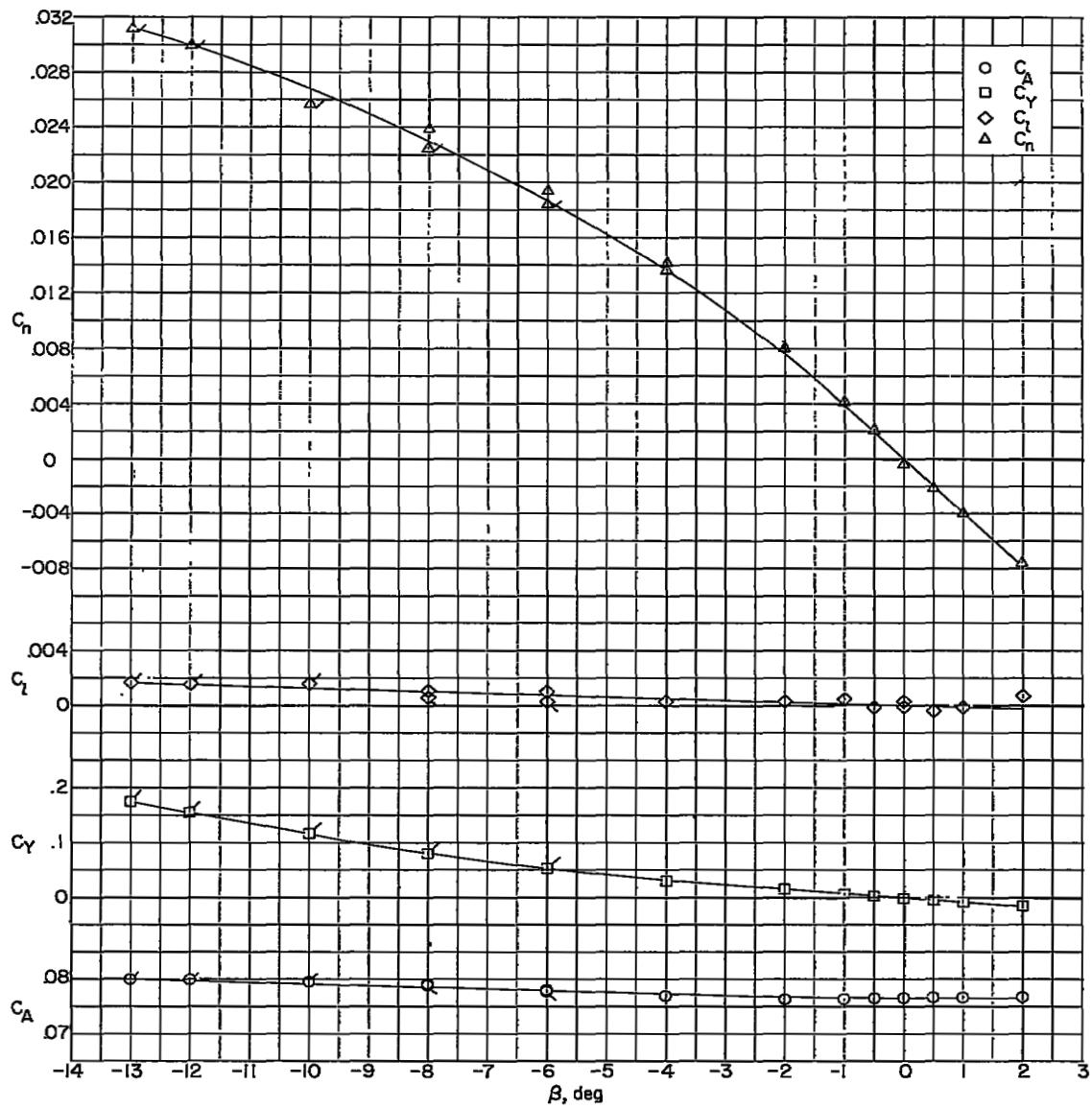

(c) Lateral characteristics in body-axis system at $\alpha = 0^{\circ}$.

Figure 6.- Wing-body configuration at M = 2.62. Concluded.

[redacted]

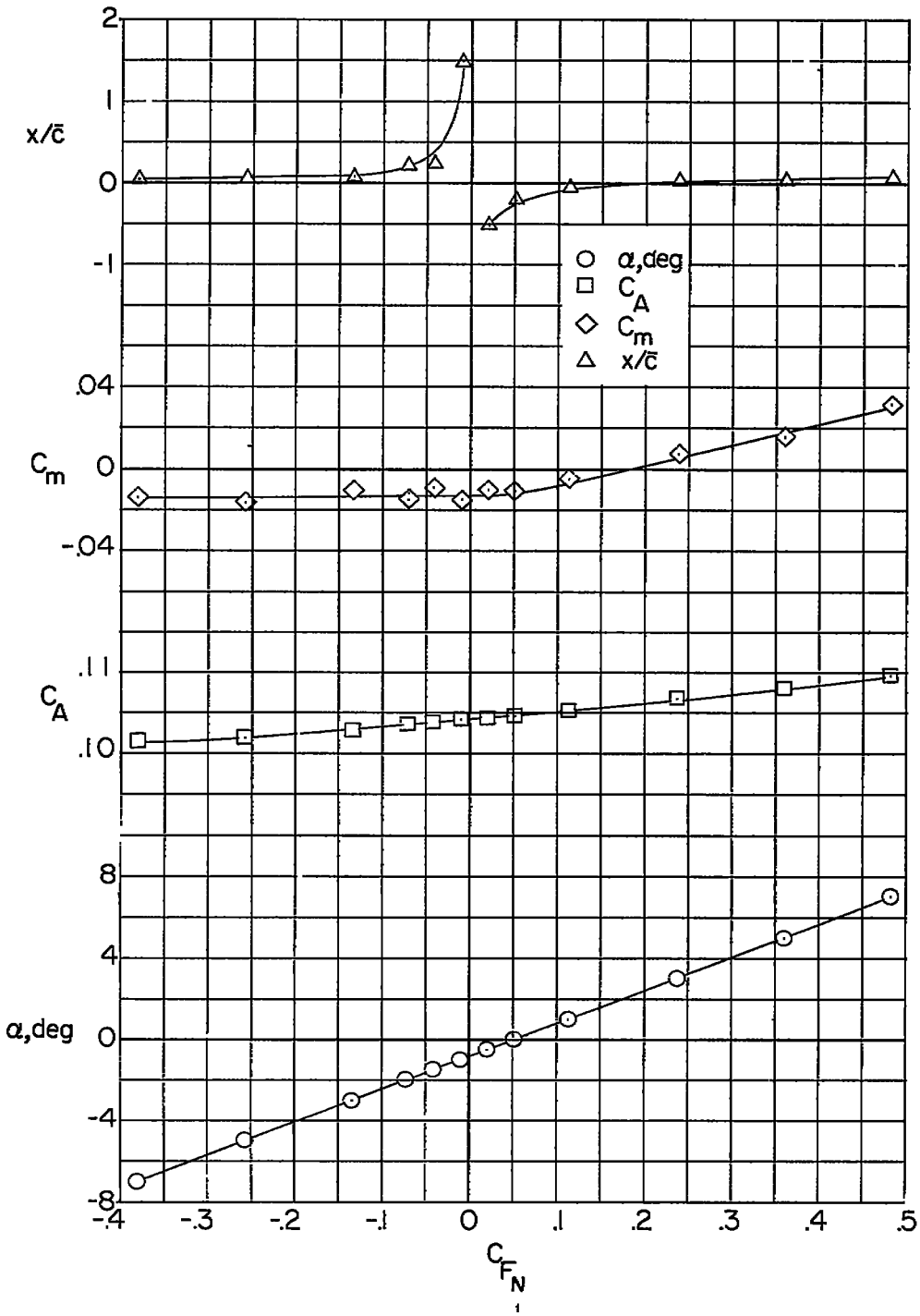

(a) Longitudinal characteristics in body-axis system at $\beta = 0^{\circ}$.

Figure 7.- Wing—body—vertical-tail configuration at M = 1.62.

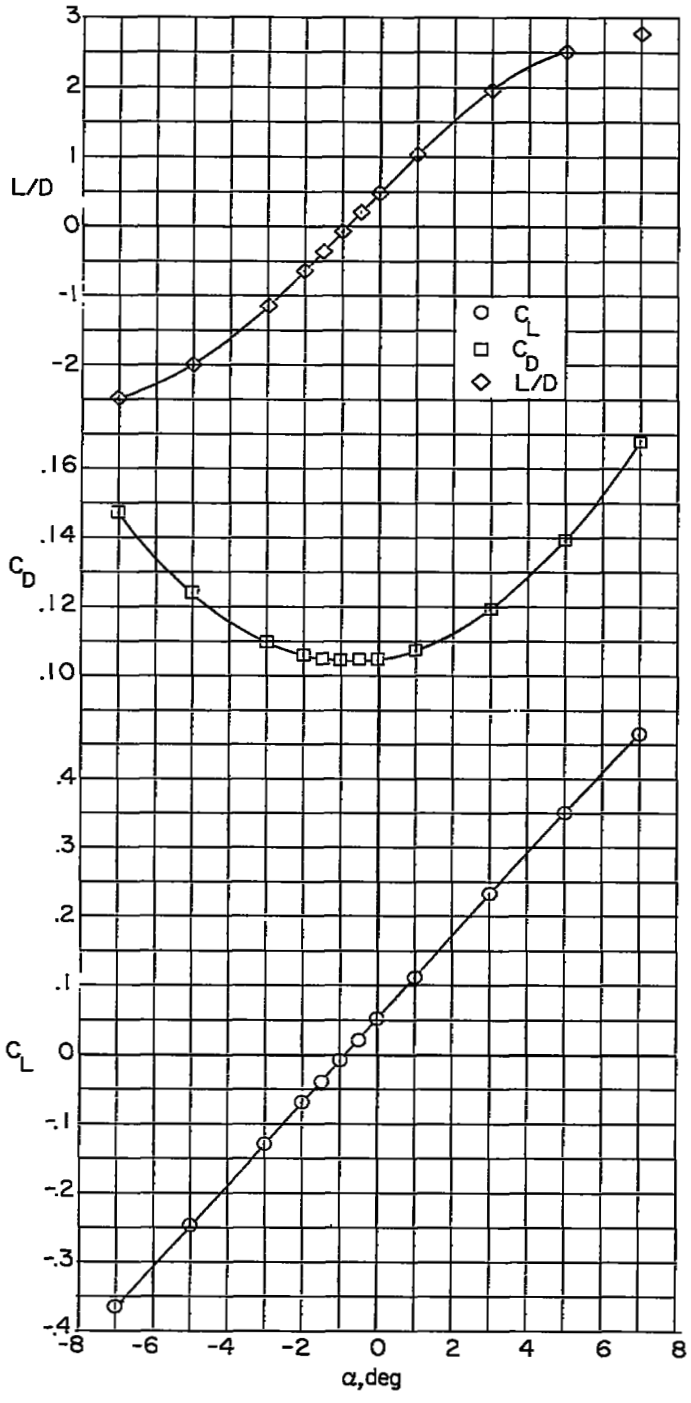

(b) Longitudinal force characteristics in stability-axis system at $\beta = 0^{\circ}$.

Figure 7.- Wing—body—vertical-tail configuration at $M = 1.62$. Continued.

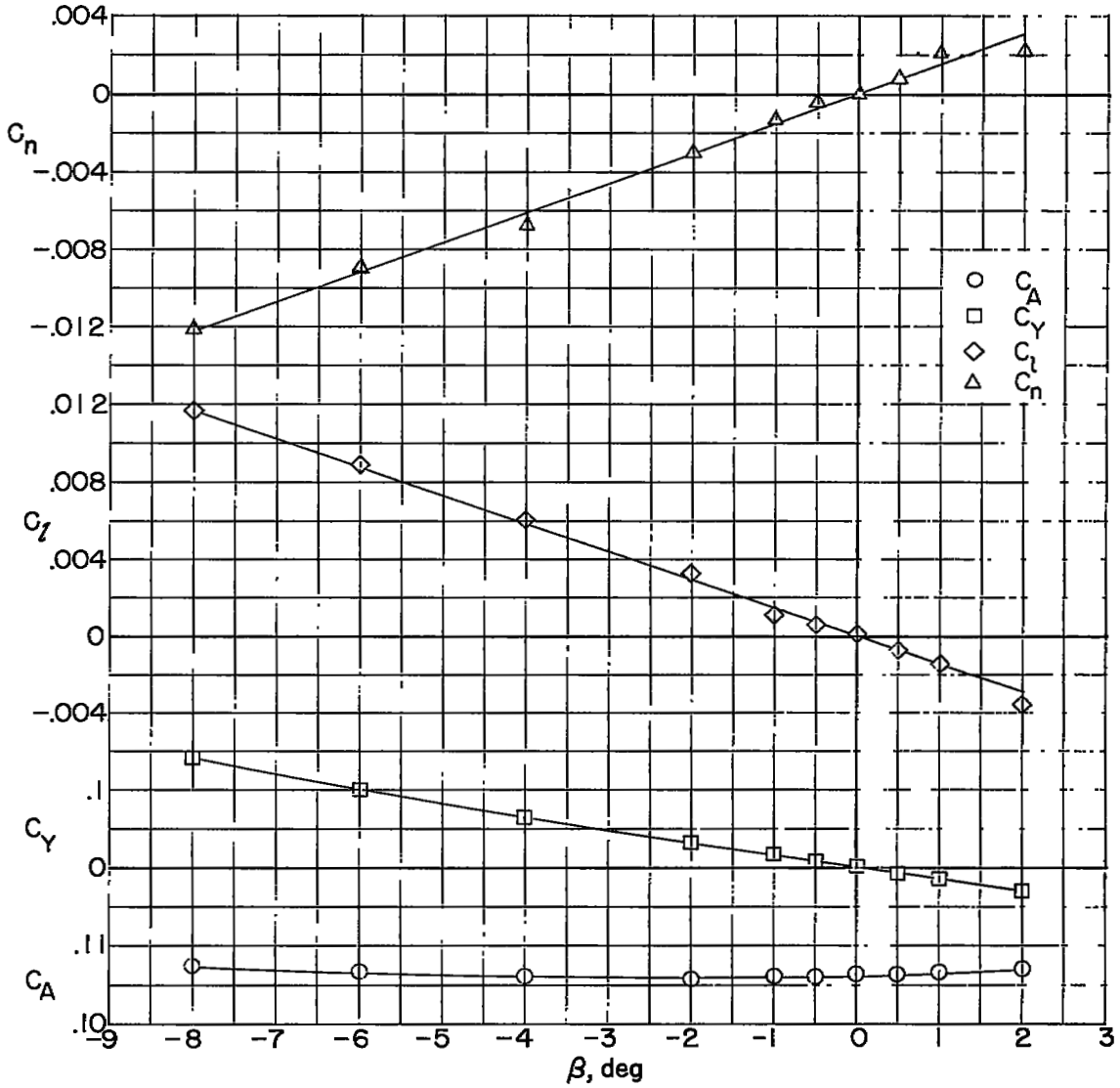

(c) Lateral characteristics in body-axis system at $\alpha = 0^\circ$.

Figure 7.- Wing—body—vertical-tail configuration at M = 1.62. Concluded.

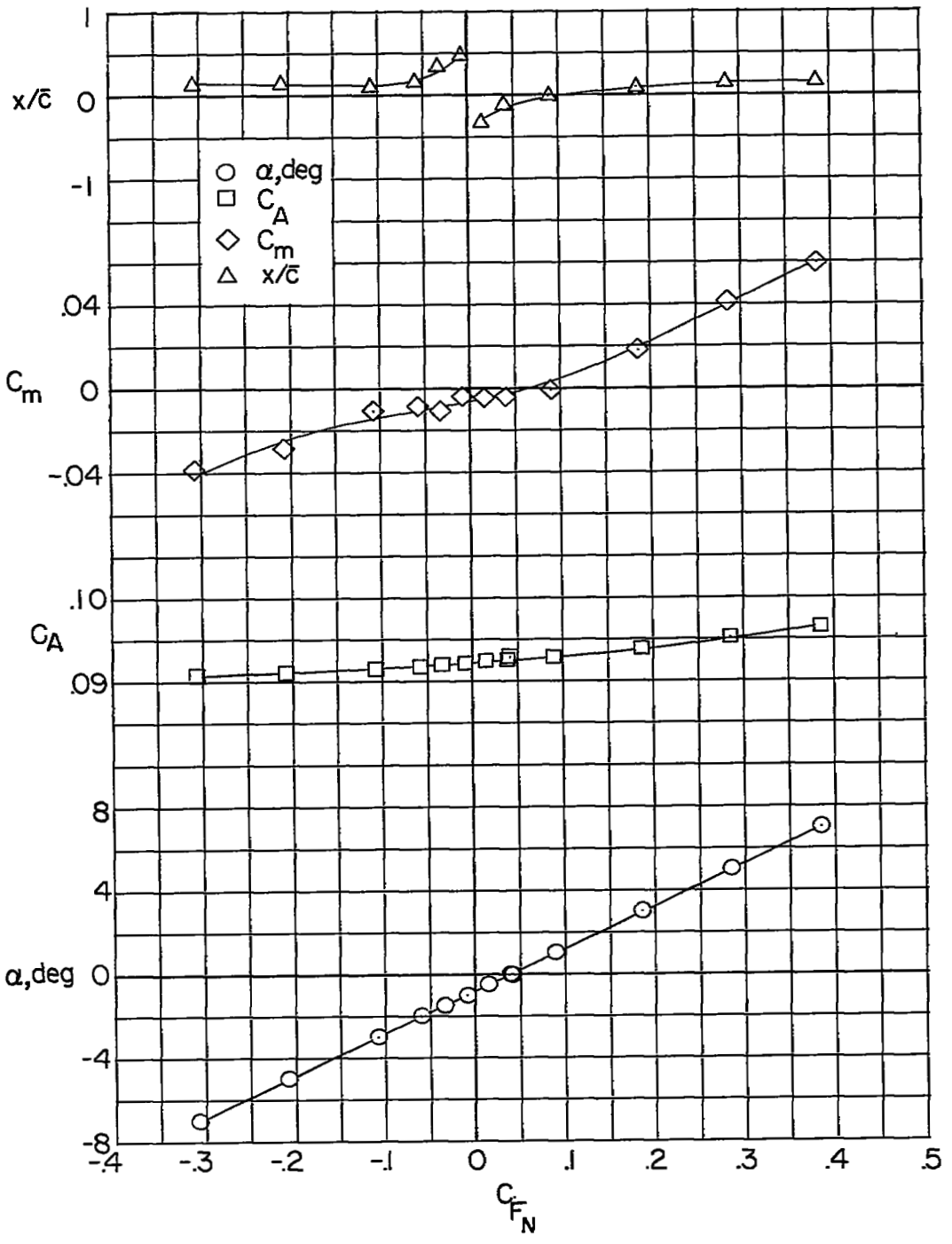

(a) Longitudinal characteristics in body-axis system at $\beta = 0^{\circ}$.

Figure 8.- Wing—body—vertical-tail configuration at $M = 1.94$.

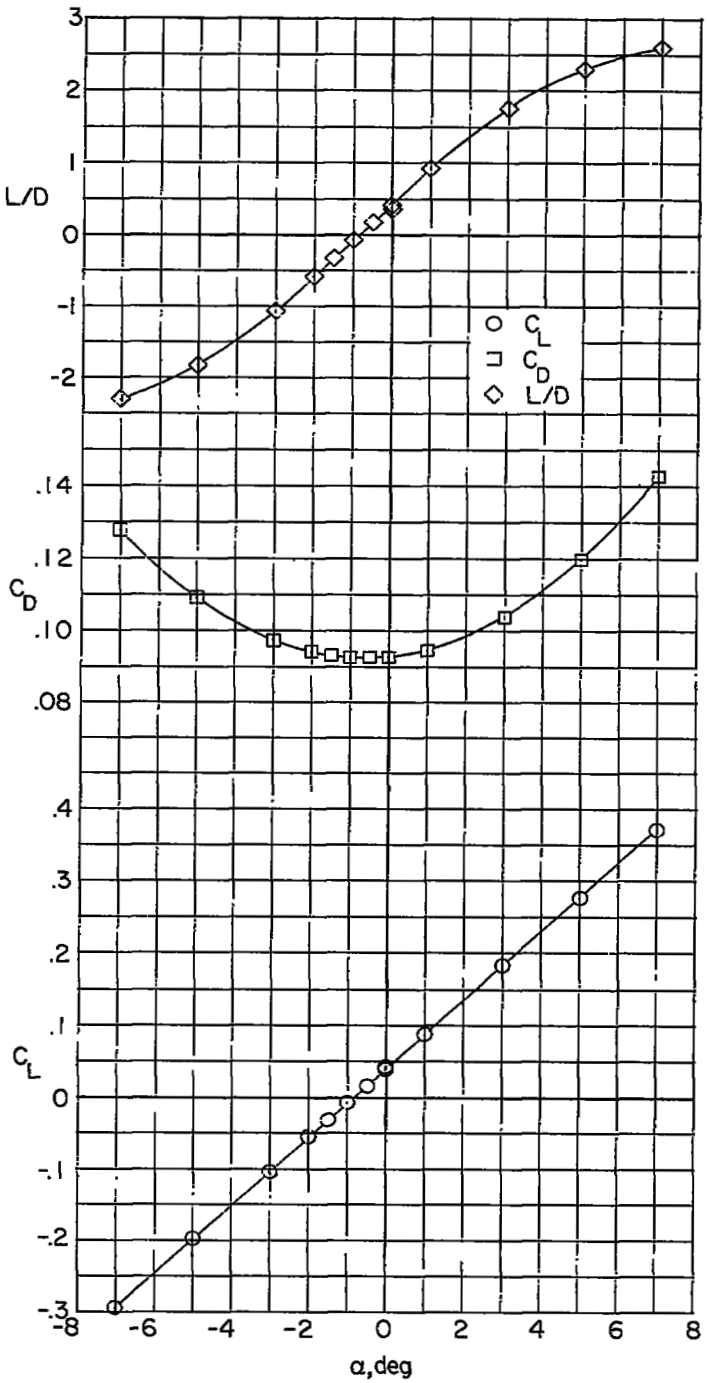

(b) Longitudinal force characteristics in stability-axis system at $\beta = 0^\circ$.

Figure 8.- Wing—body—vertical-tail configuration at $M = 1.94$. Continued.

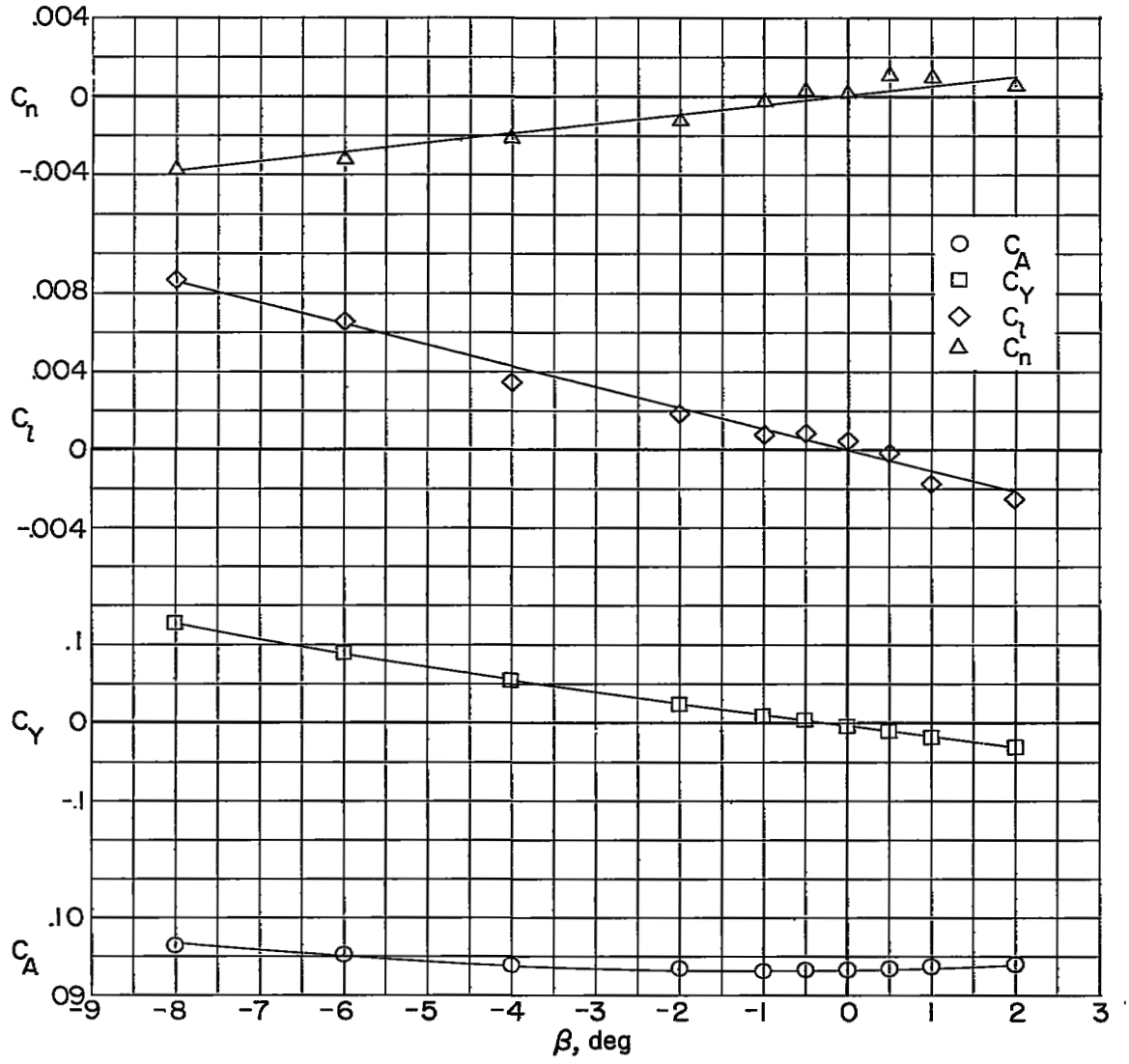

(c) Lateral characteristics in body-axis system at $\alpha = 0^\circ$.

Figure 8.- Wing—body—vertical-tail configuration at $M = 1.94$. Concluded.

[redacted]

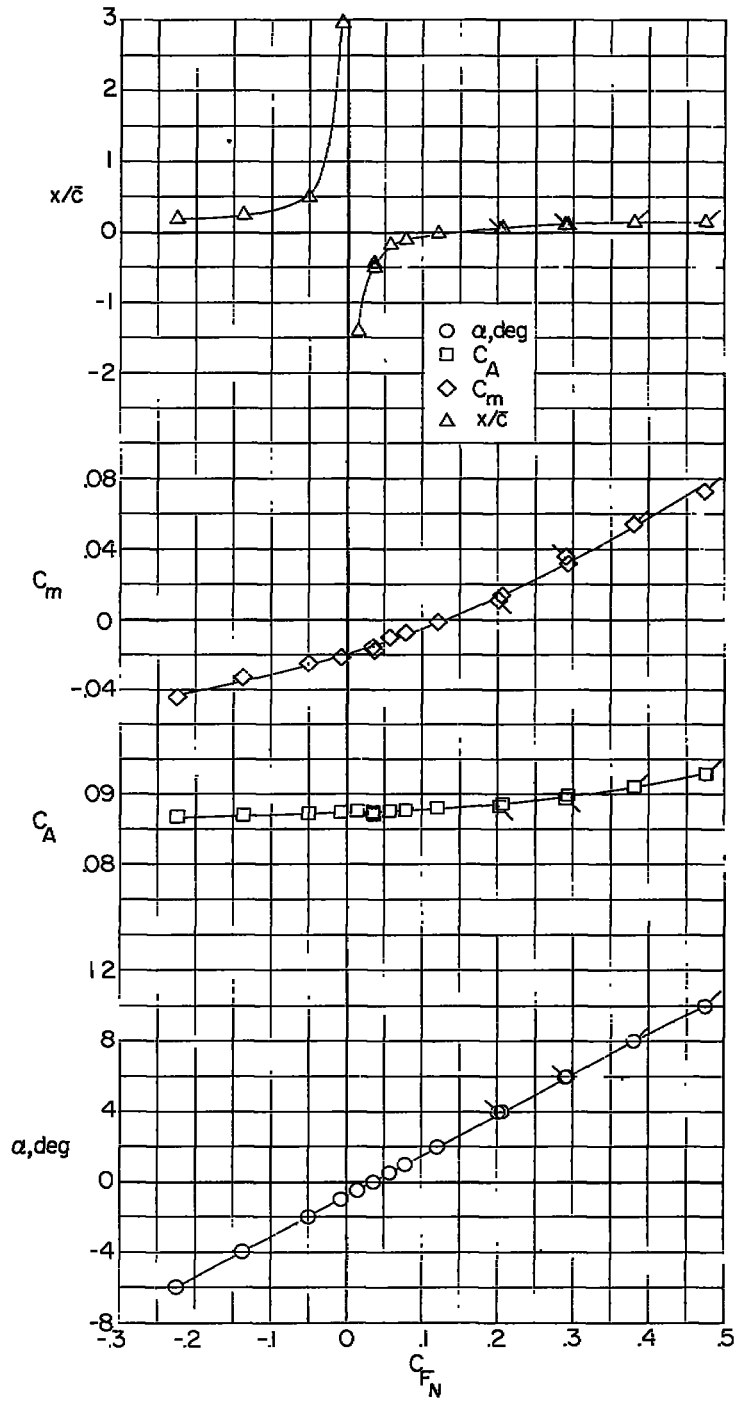

(a) Longitudinal characteristics in body-axis system at $\beta = 0^{\circ}$.

Figure 9.- Wing—body—vertical-tail configuration at $M = 2.22$.

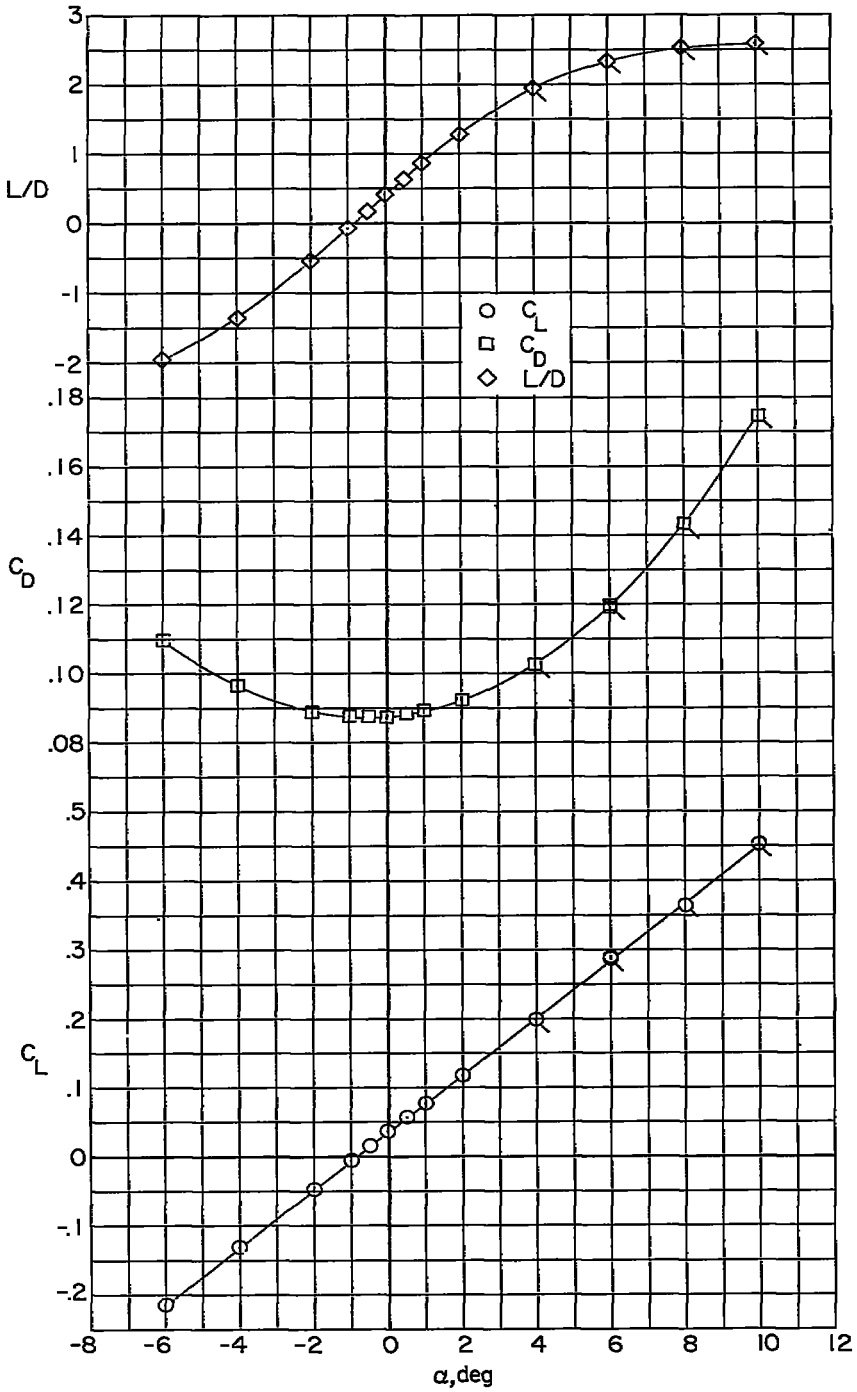

(b) Longitudinal force characteristics in stability-axis system at $\beta = 0^{\circ}$.

Figure 9.- Wing—body—vertical-tail configuration at M = 2.22. Continued.

[redacted]

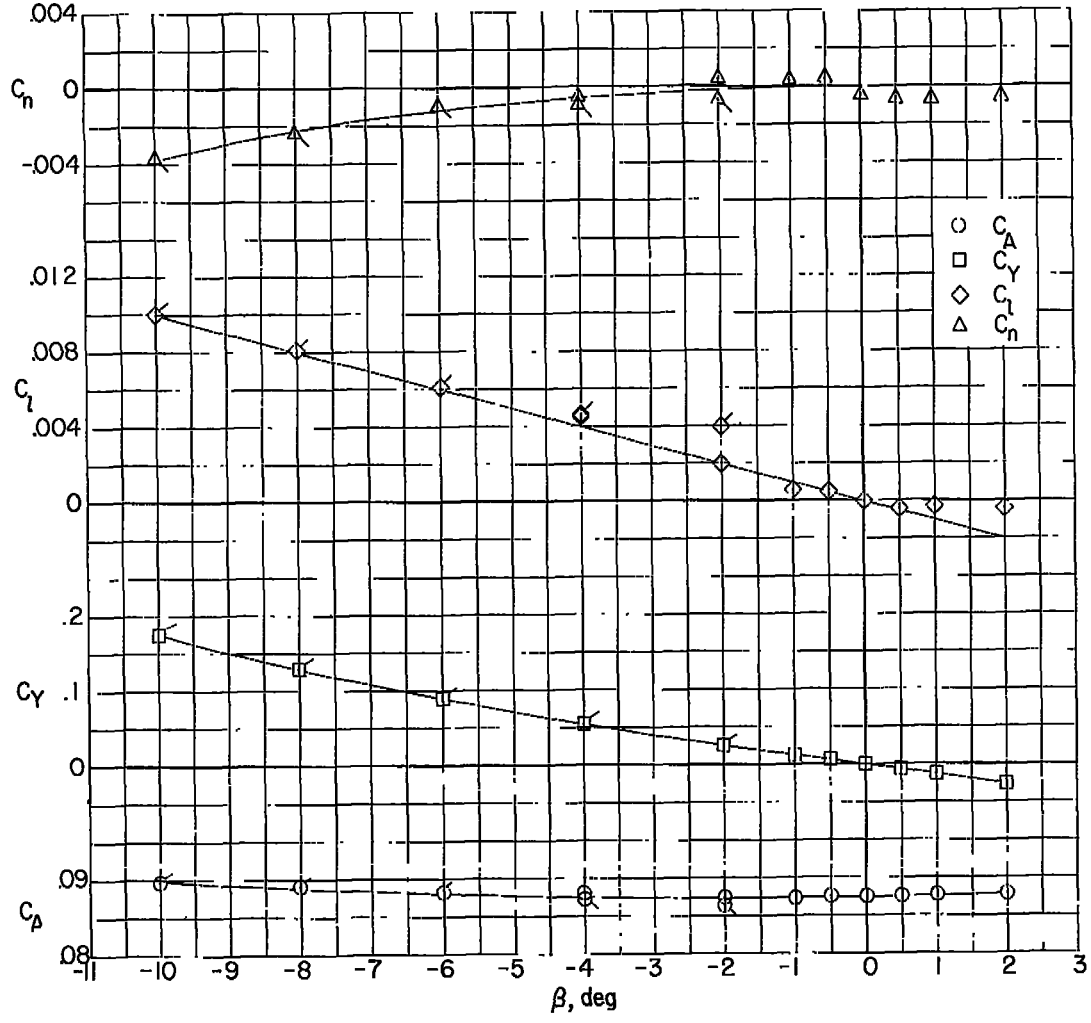

(c) Lateral characteristics in body-axis system at $\alpha = 0^{\circ}$.

Figure 9.- Wing—body—vertical-tail configuration at M = 2.22. Concluded.

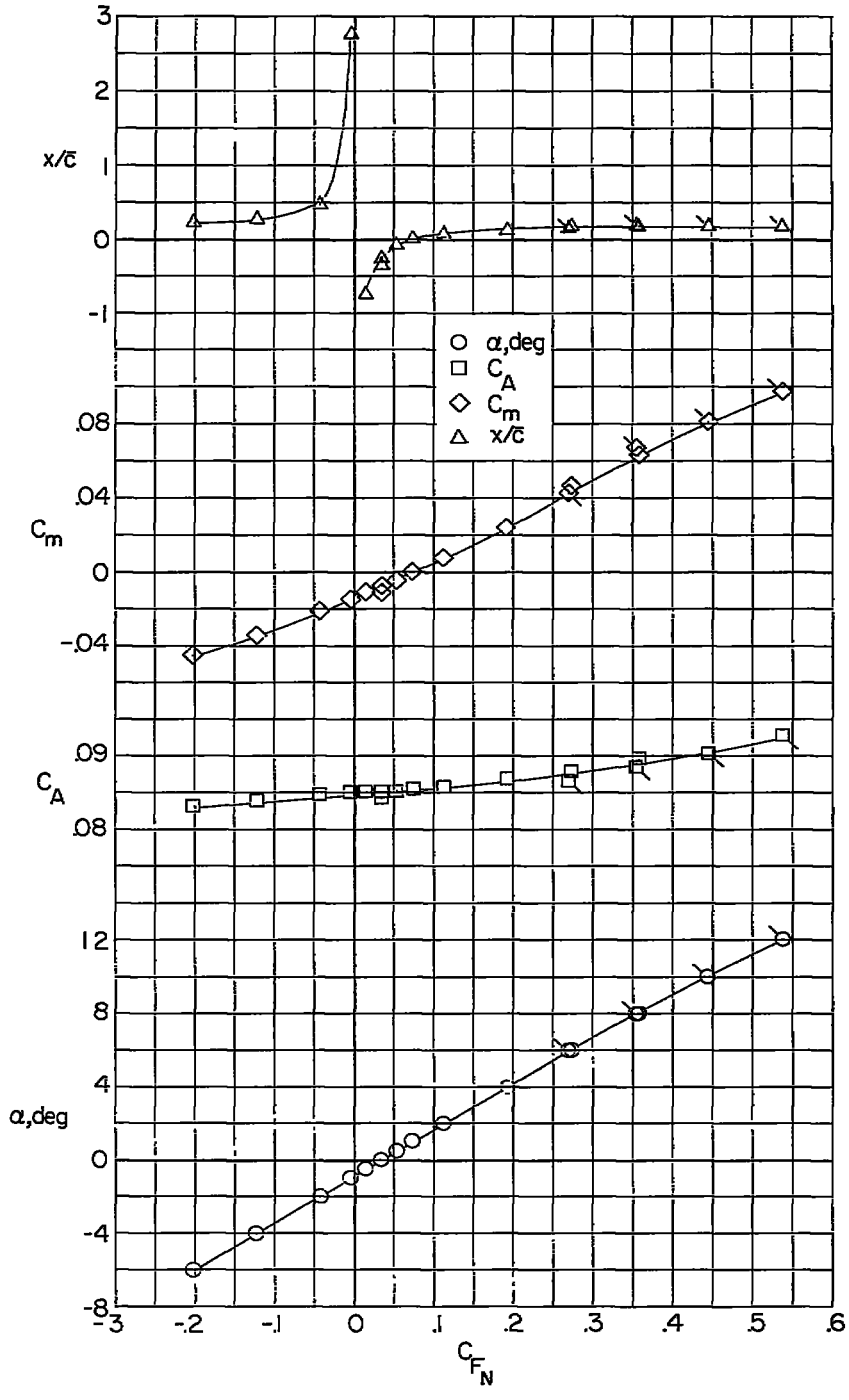

(a) Longitudinal characteristics in body-axis system at $\beta = 0^{\circ}$.

Figure 10.- Wing—body—vertical-tail configuration at $M = 2.40$.

[redacted]

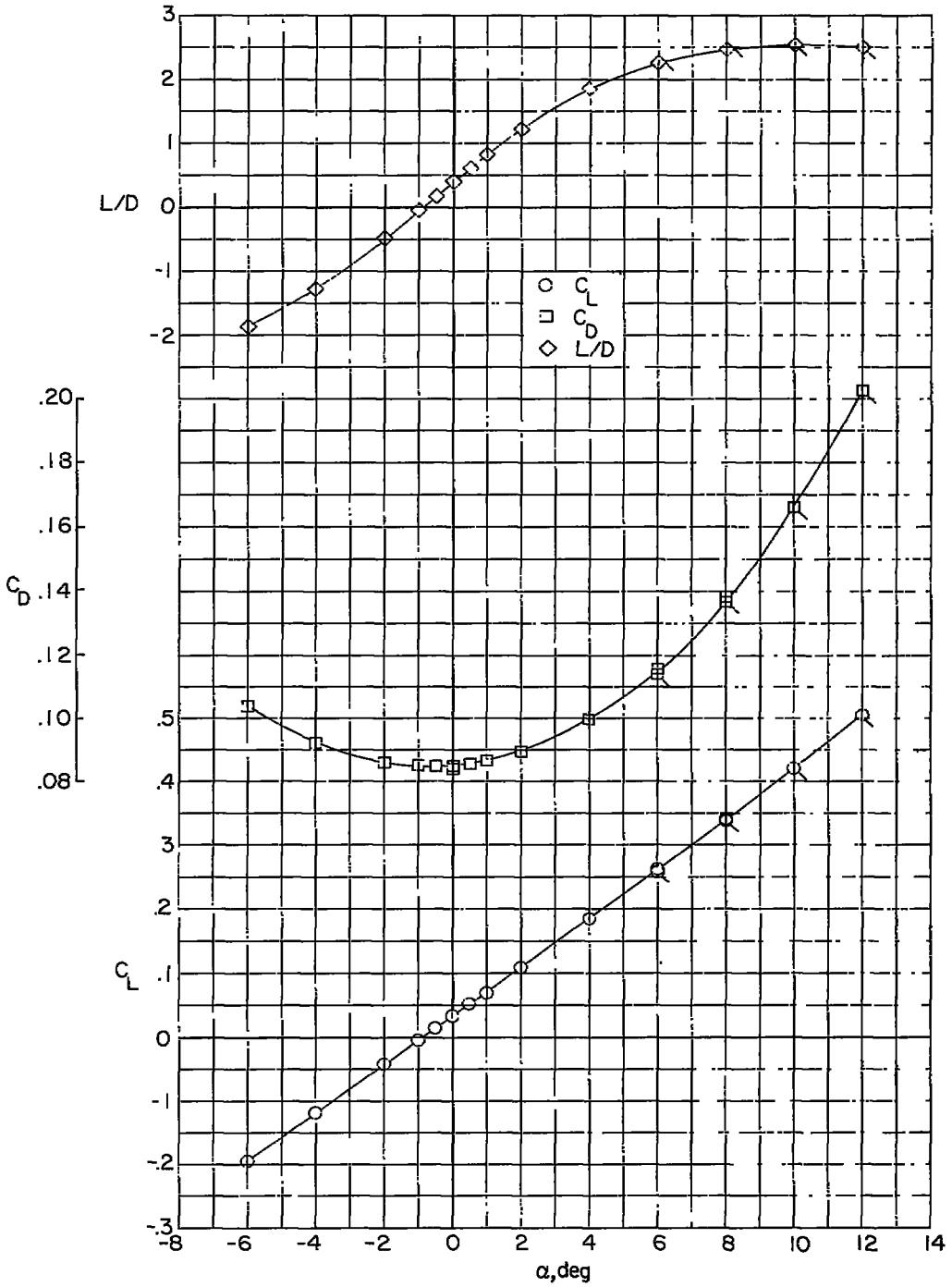

(b) Longitudinal force characteristics in stability-axis system at $\beta = 0^{\circ}$.

Figure 10.- Wing—body—vertical-tail configuration at M = 2.40. Continued.

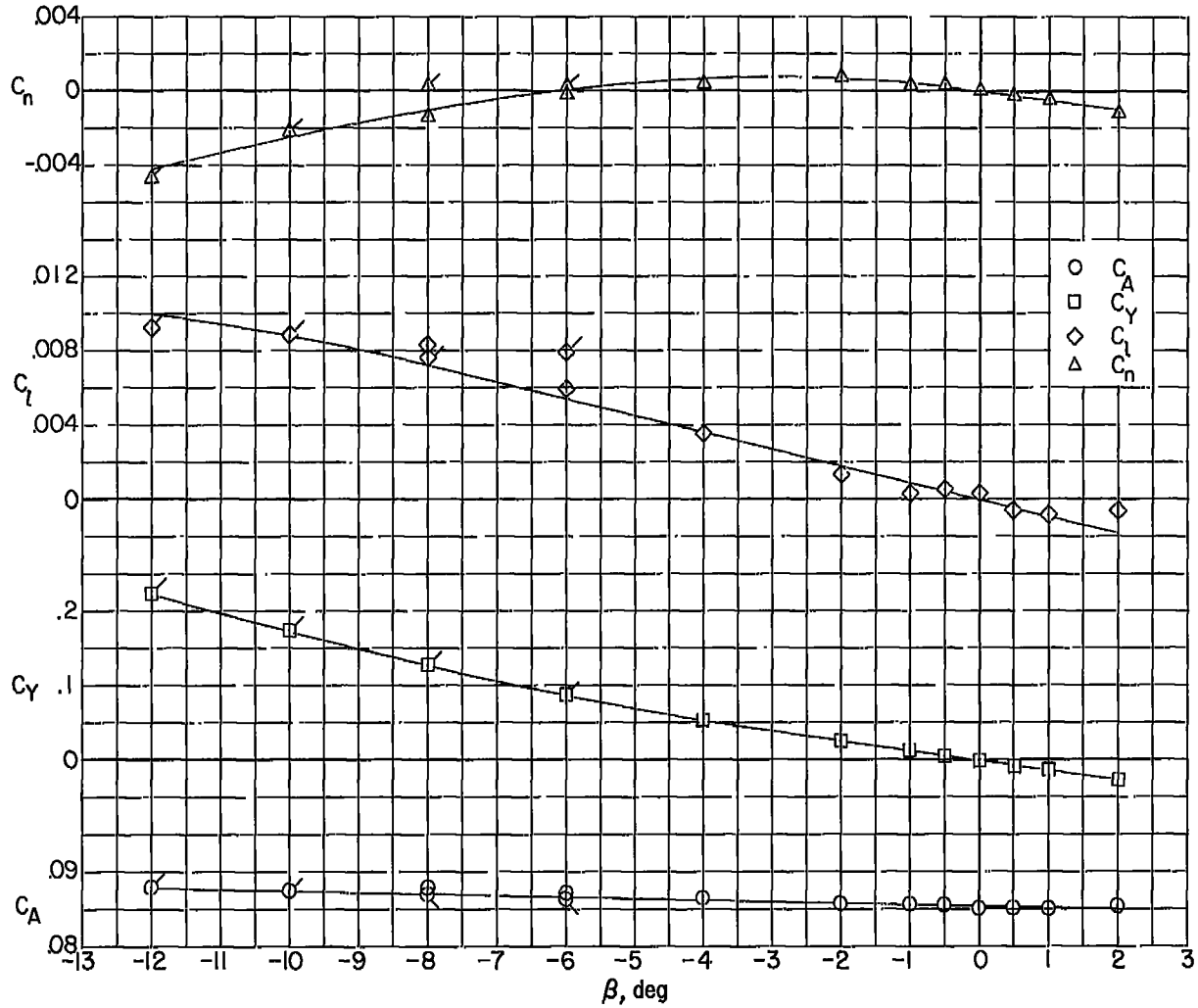

(c) Lateral characteristics in body-axis system at $\alpha = 0^\circ$.

Figure 10.- Wing—body—vertical-tail configuration at M = 2.40. Concluded.

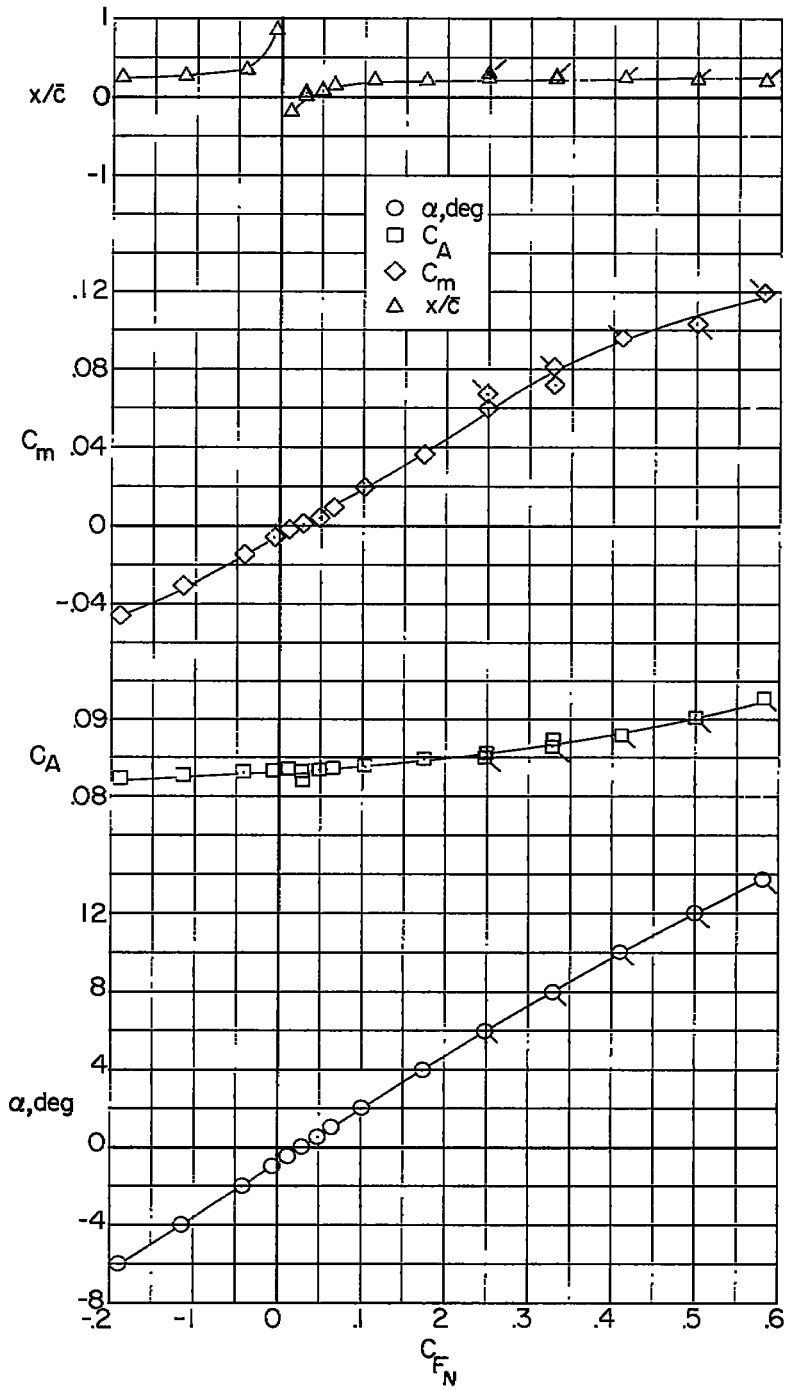

(a) Longitudinal characteristics in body-axis system at $\beta = 0^{\circ}$.

Figure 11.- Wing—body—vertical-tail configuration at $M = 2.62$.

[redacted]

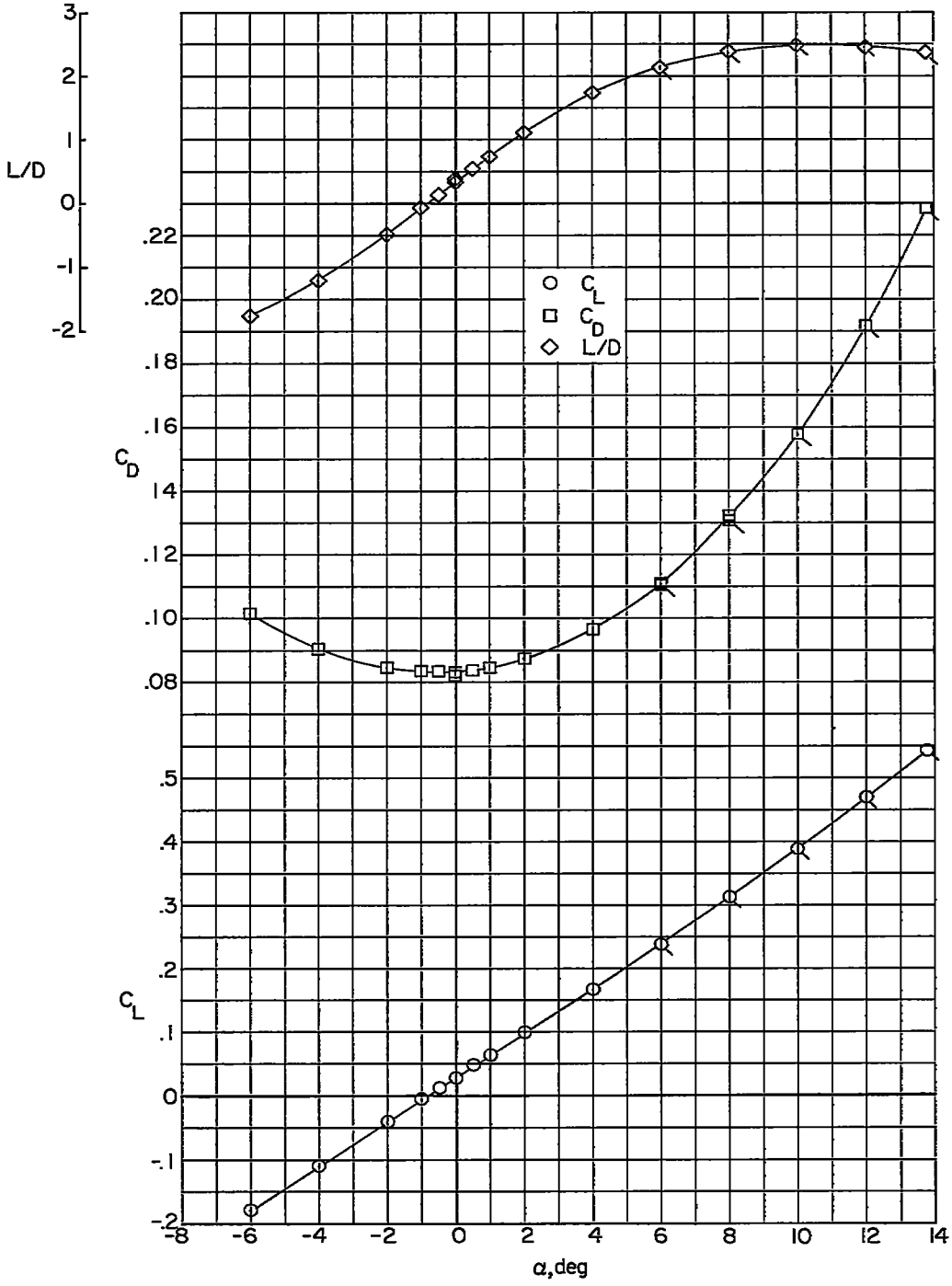

(b) Longitudinal force characteristics in stability-axis system at $\beta = 0^{\circ}$.

Figure 11.- Wing—body—vertical-tail configuration at M = 2.62. Continued.

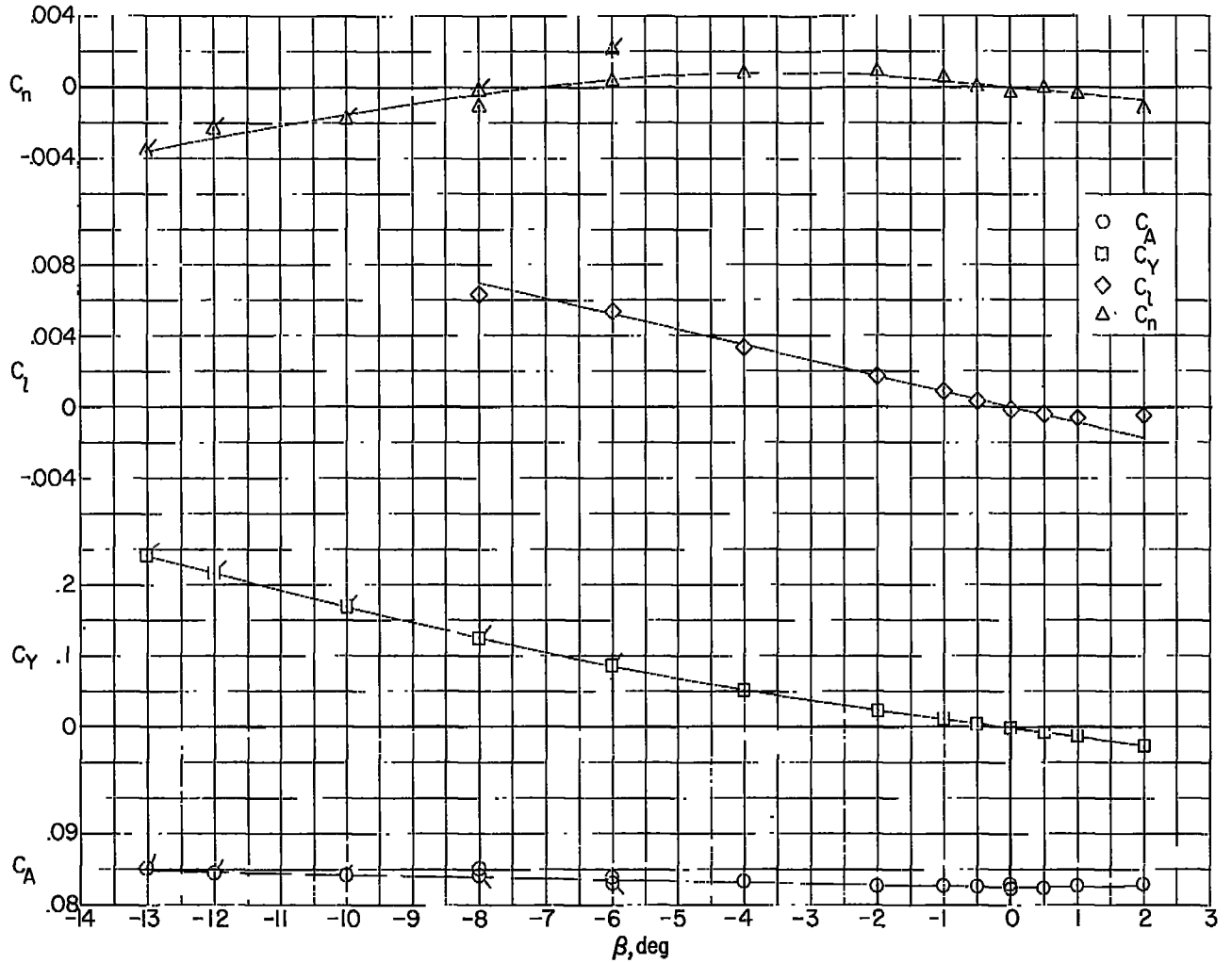

(c) Lateral characteristics in body-axis system at $\alpha = 0^{\circ}$.

Figure 11.- Wing—body—vertical-tail configuration at M = 2.62. Concluded.

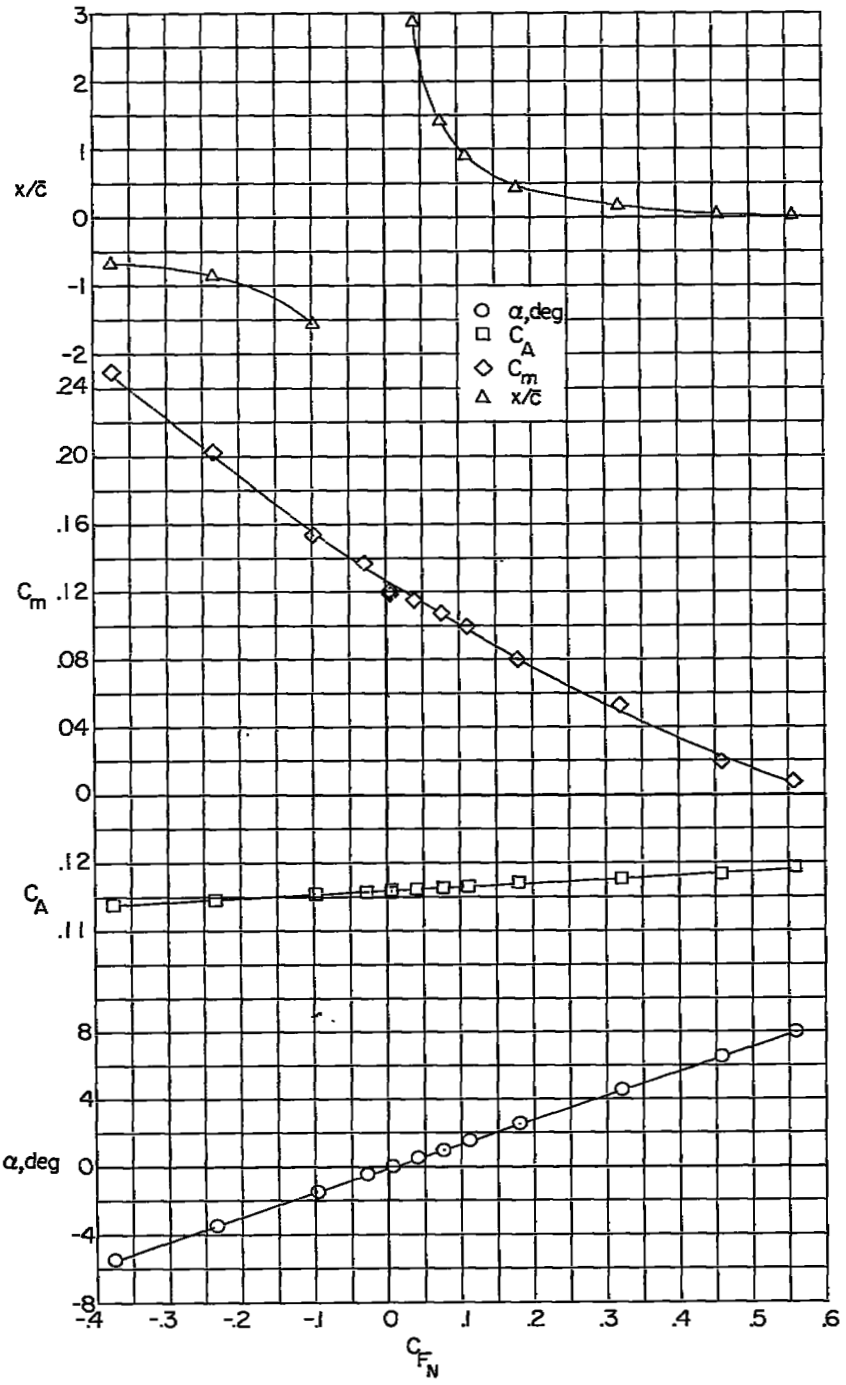

(a) Longitudinal characteristics in body-axis system at $\beta = 0^{\circ}$.

Figure 12.- Complete configuration with $i_t = 0^{\circ}$ at $M = 1.62$.

[redacted]

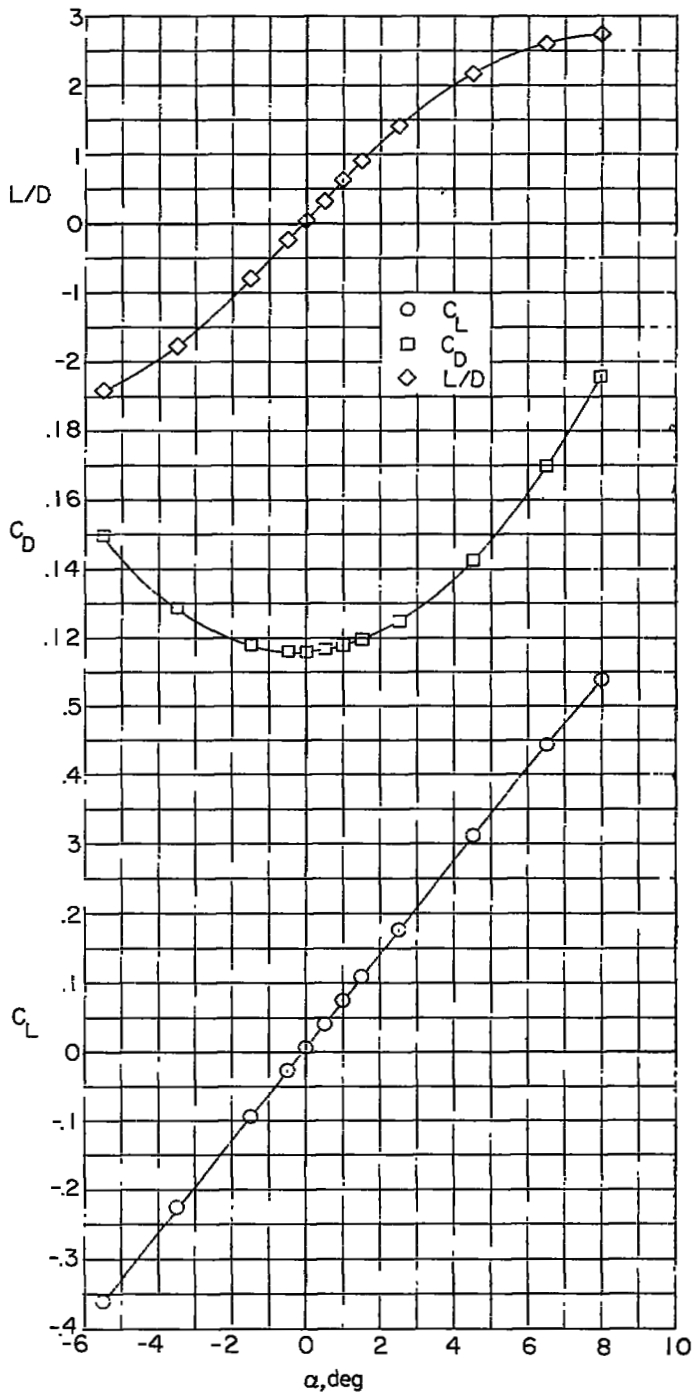

(b) Longitudinal force characteristics in stability-axis system at $\beta = 0^{\circ}$.

Figure 12.- Complete configuration with $i_t = 0^{\circ}$ at $M = 1.62$. Continued.

[redacted]

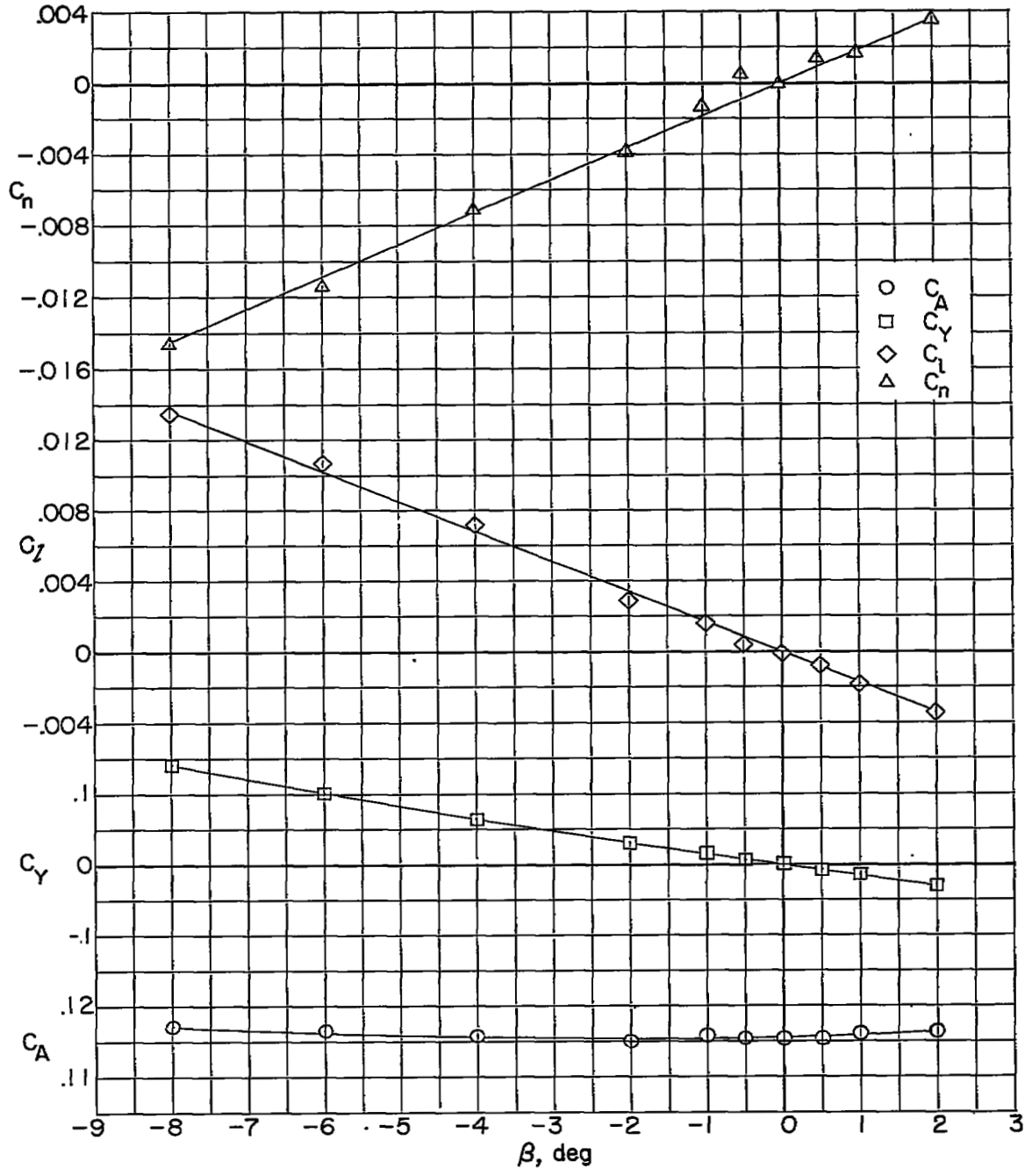

(c) Lateral characteristics in body-axis system at $\alpha = 0^\circ$.

Figure 12.- Complete configuration with $i_t = 0^\circ$ at $M = 1.62$. Concluded.

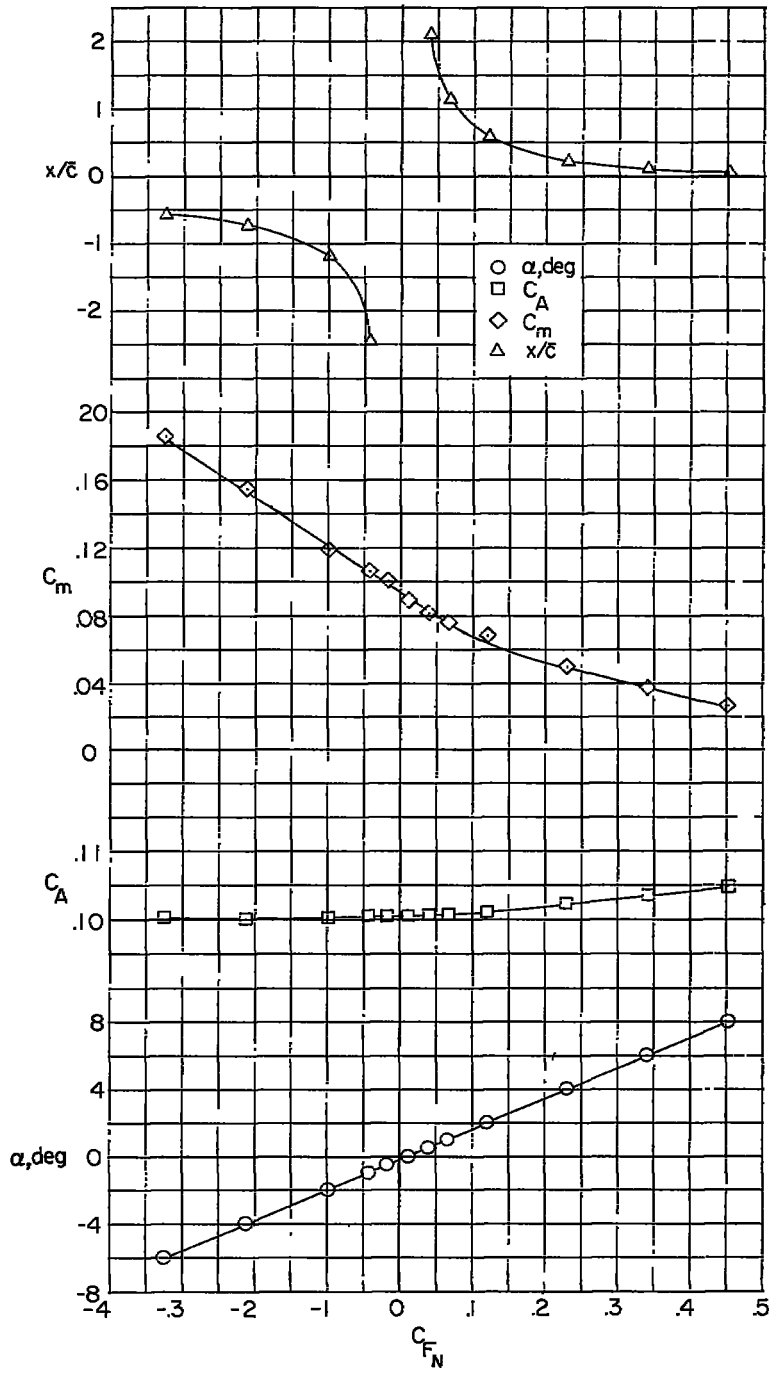

(a) Longitudinal characteristics in body-axis system at $\beta = 0^{\circ}$.

Figure 13.- Complete configuration with $i_t = 0^{\circ}$ at $M = 1.94$.

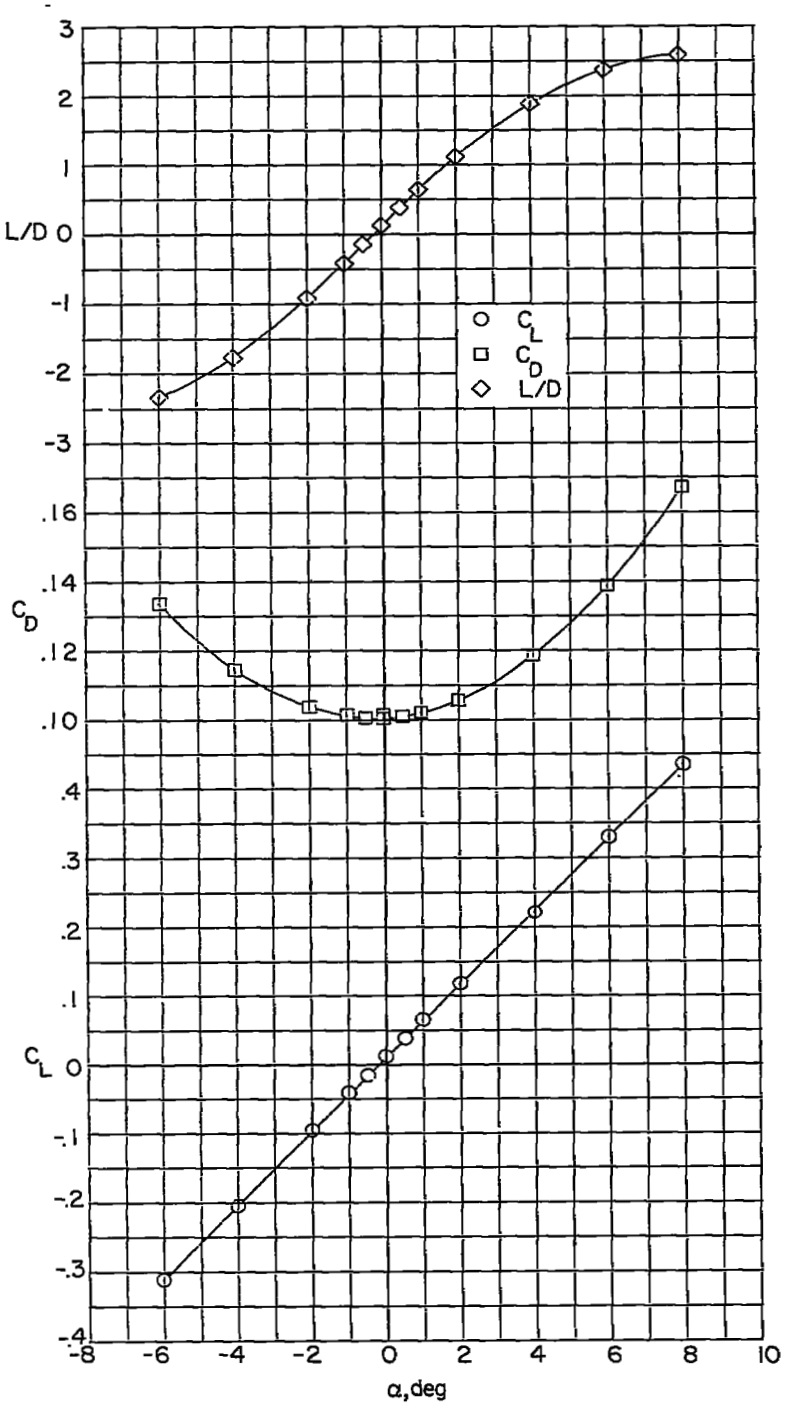

(b) Longitudinal force characteristics in stability-axis system at $\beta = 0^{\circ}$.

Figure 13.- Complete configuration with $i_t = 0^{\circ}$ at $M = 1.94$. Continued.

[redacted]

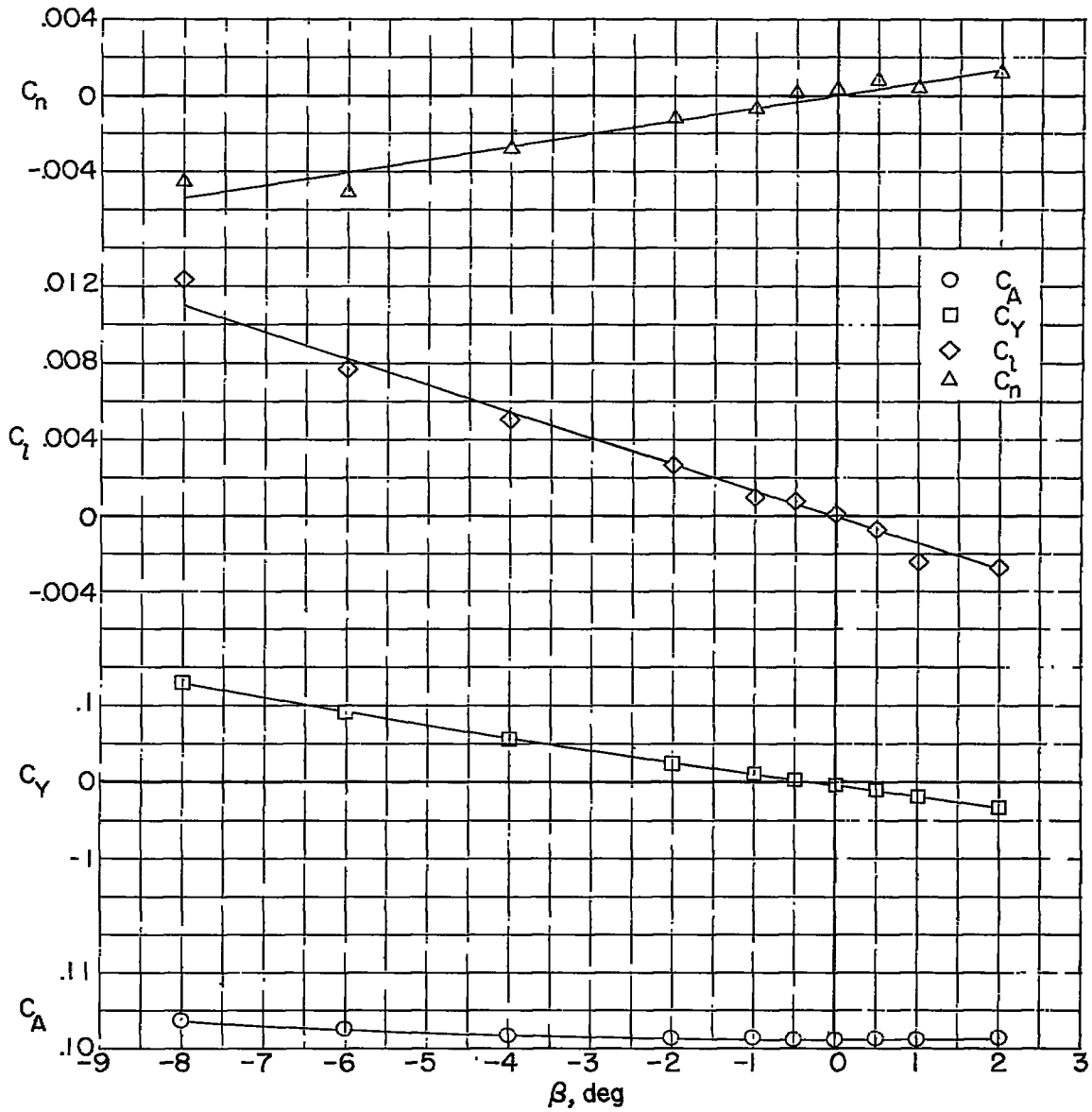

(c) Lateral characteristics in body-axis system at $\alpha = 0^\circ$.

Figure 13.- Complete configuration with $i_t = 0^\circ$ at $M = 1.94$. Concluded.

[redacted]

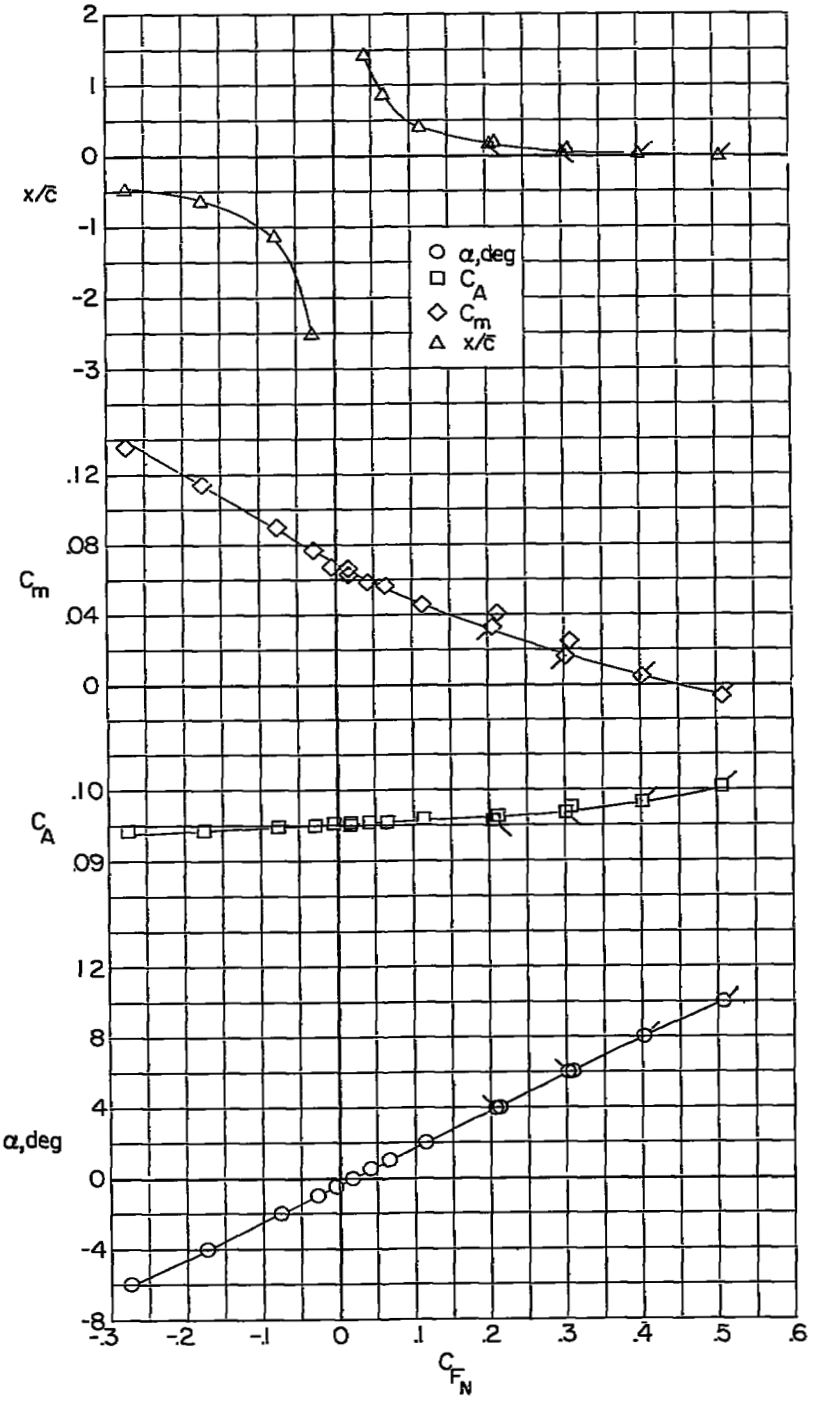

(a) Longitudinal characteristics in body-axis system at $\beta = 0^{\circ}$.

Figure 14.- Complete configuration with $i_t = 0^{\circ}$ at $M = 2.22$.

[redacted]

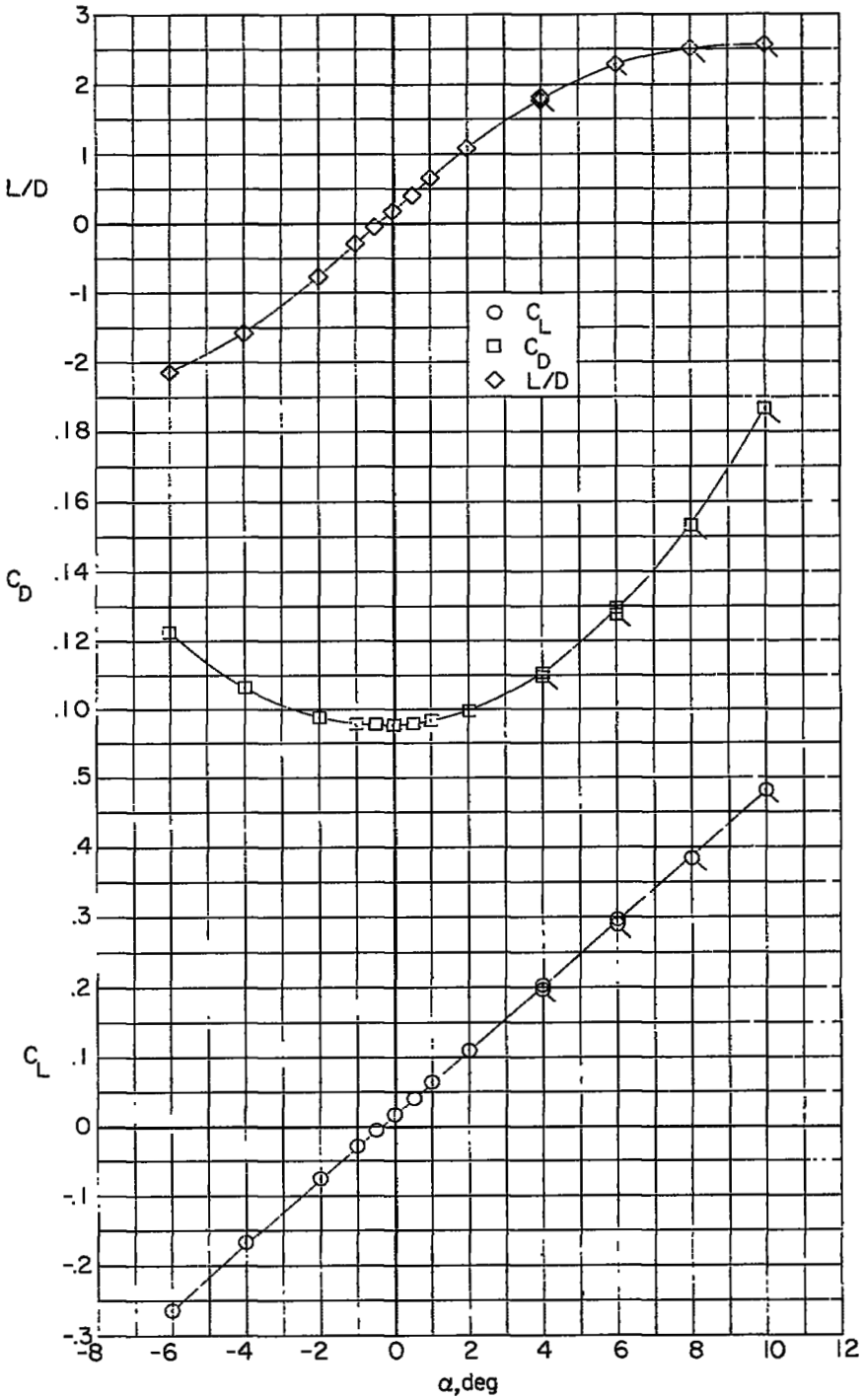

(b) Longitudinal force characteristics in stability-axis system at $\beta = 0^{\circ}$.

Figure 14.- Complete configuration with $i_t = 0^{\circ}$ at $M = 2.22$. Continued.

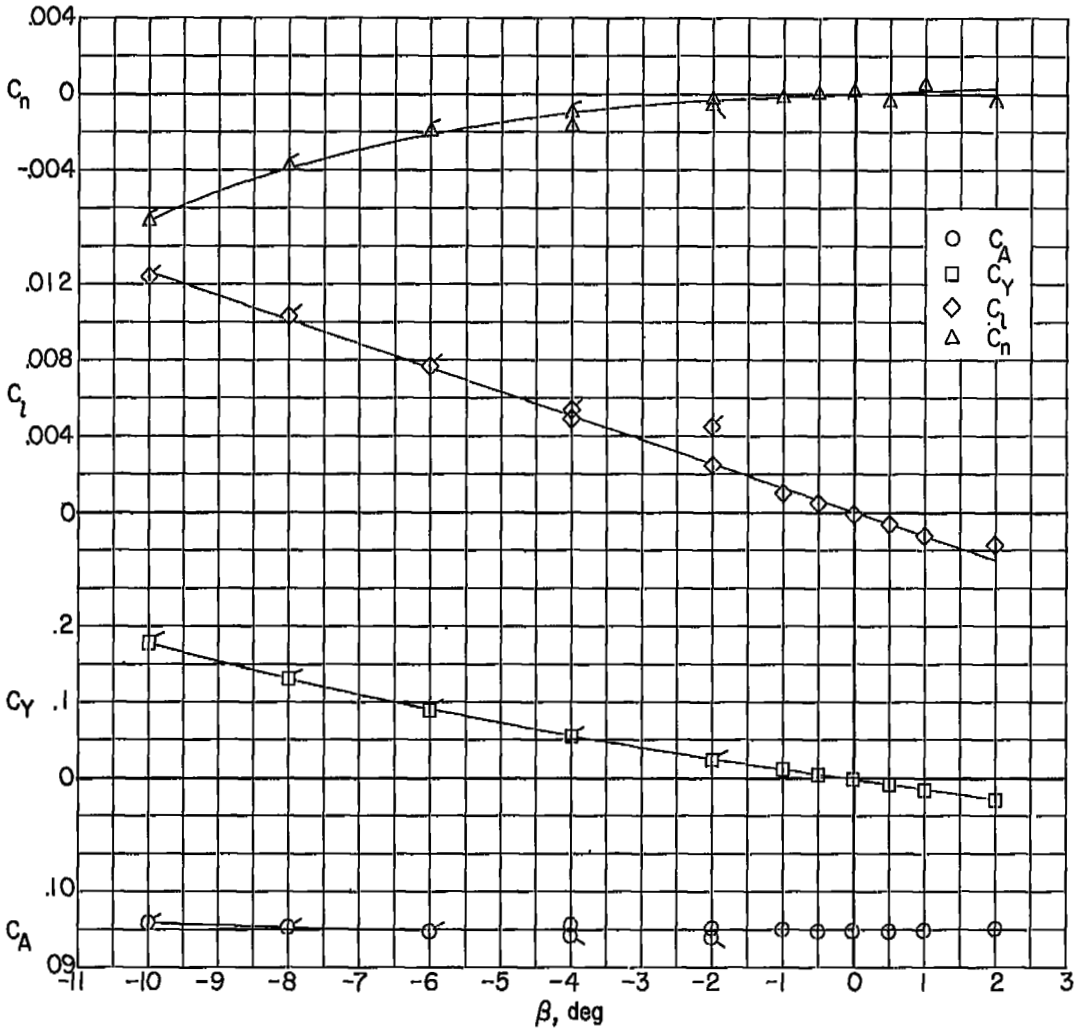

(c) Lateral characteristics in body-axis system at $\alpha = 0^{\circ}$.

Figure 14.- Complete configuration with $i_t = 0^{\circ}$ at $M = 2.22$. Concluded.

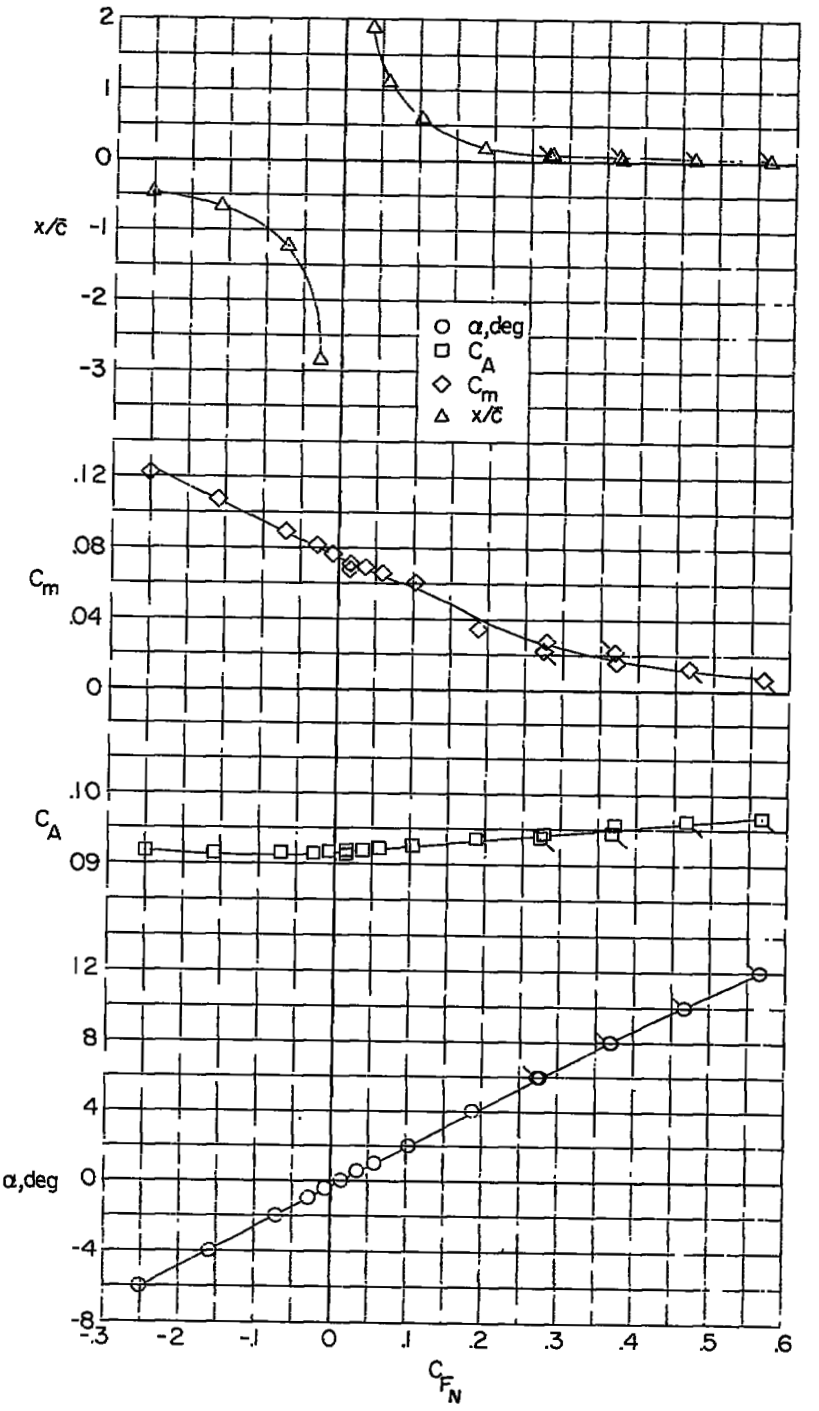

(a) Longitudinal characteristics in body-axis system at $\beta = 0^{\circ}$.

Figure 15.- Complete configuration with $i_t = 0^{\circ}$ at $M = 2.40$.

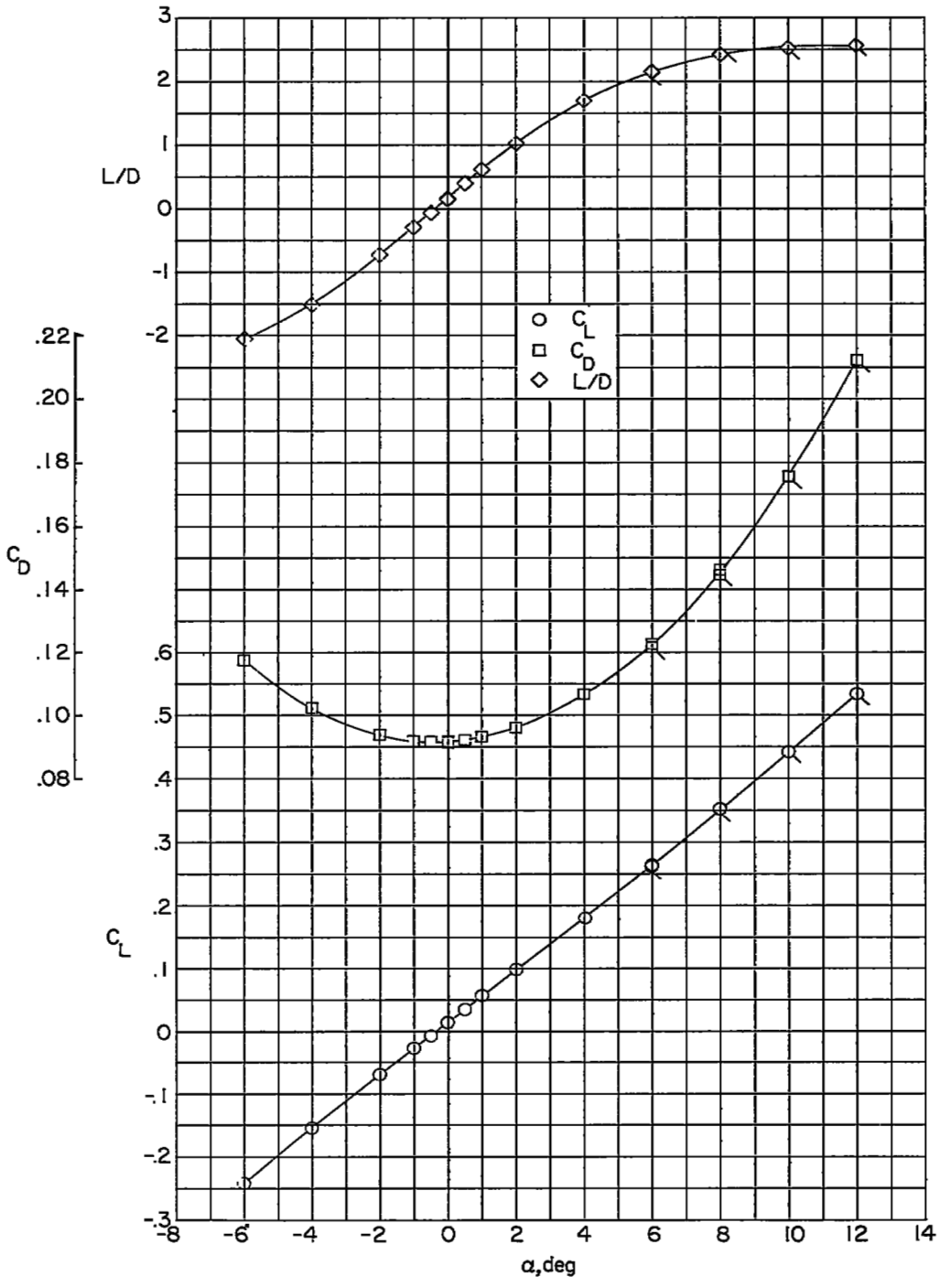

(b) Longitudinal force characteristics in stability-axis system at $\beta = 0^{\circ}$.

Figure 15.- Complete configuration with $i_t = 0^{\circ}$ at $M = 2.40$. Continued.

[redacted]

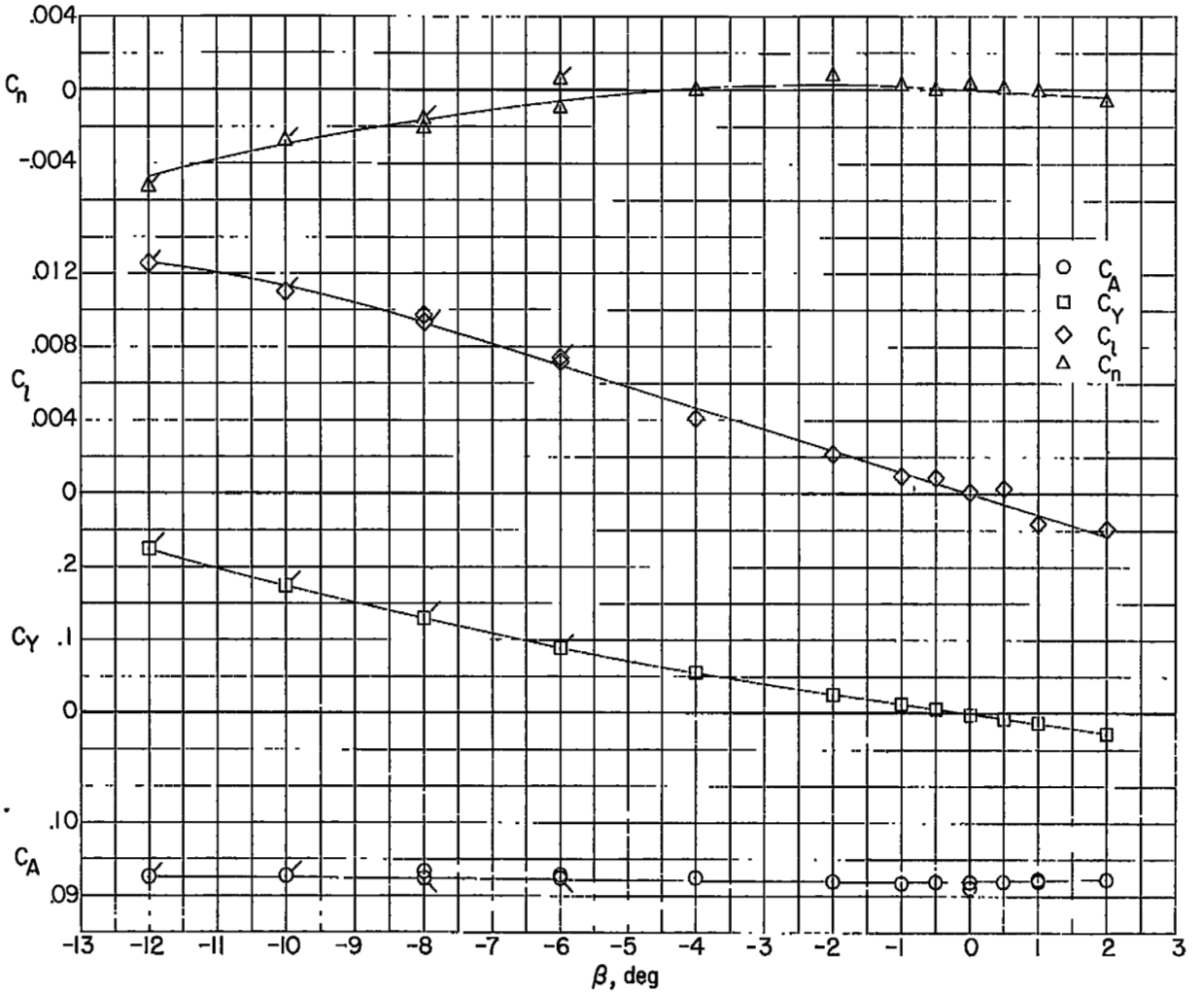

(c) Lateral characteristics in body-axis system at $\alpha = 0^\circ$.

Figure 15.- Complete configuration with $i_t = 0^\circ$ at $M = 2.40$. Concluded.

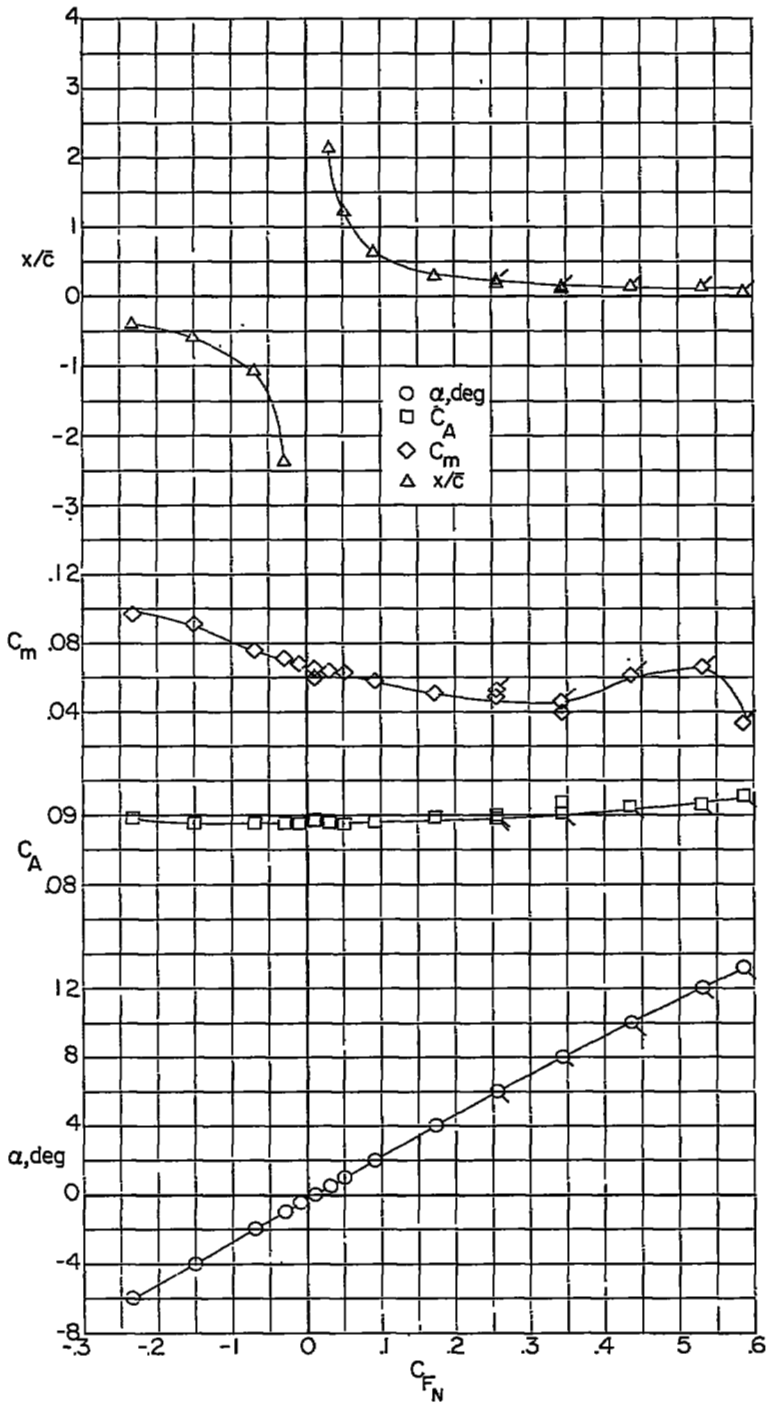

(a) Longitudinal characteristics in body-axis system at $\beta = 0^{\circ}$.

Figure 16.- Complete configuration with $i_t = 0^{\circ}$ at $M = 2.62$.

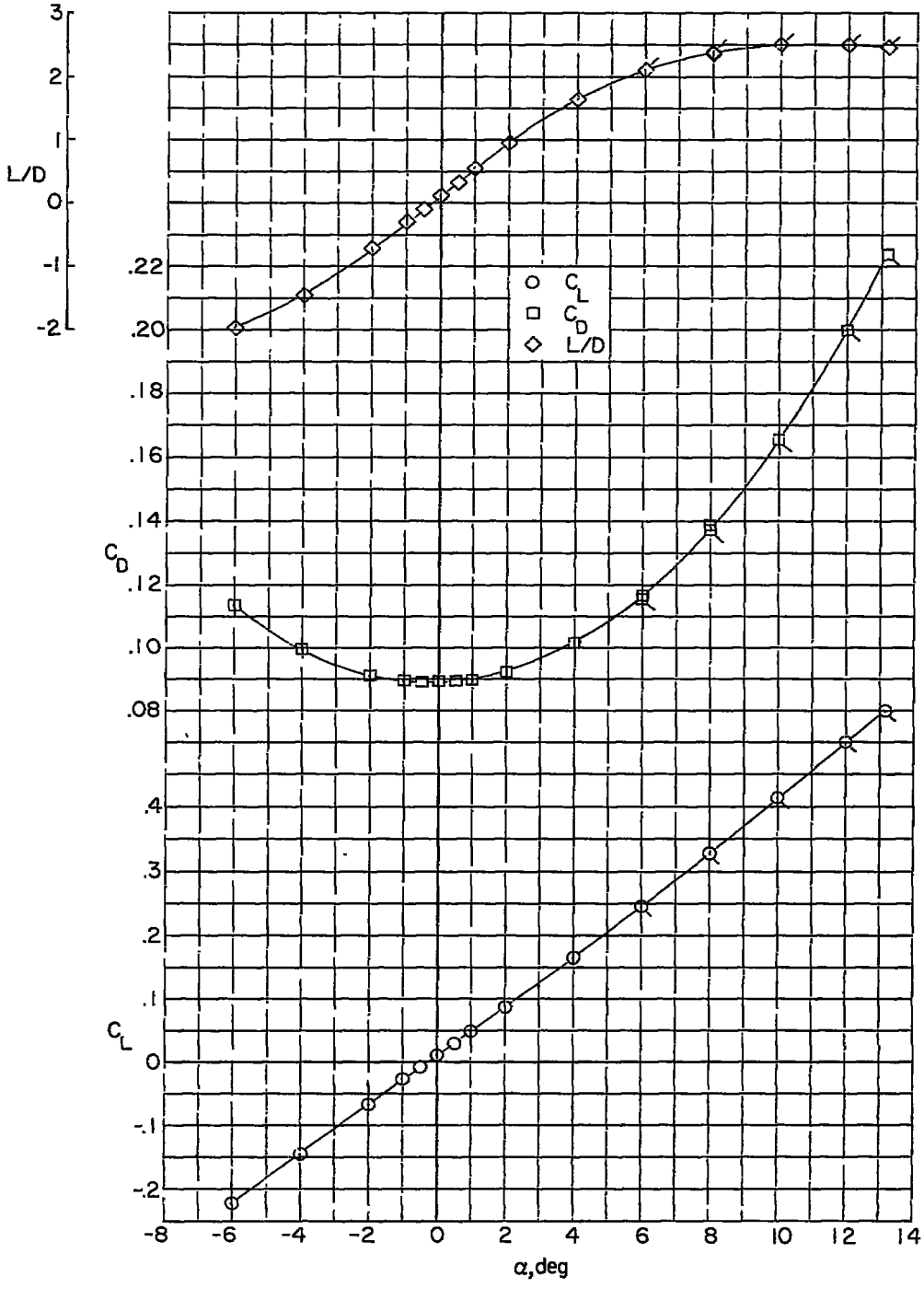

(b) Longitudinal force characteristics in stability-axis system at $\beta = 0^\circ$.

Figure 16.- Complete configuration with $i_t = 0^\circ$ at $M = 2.62$. Continued.

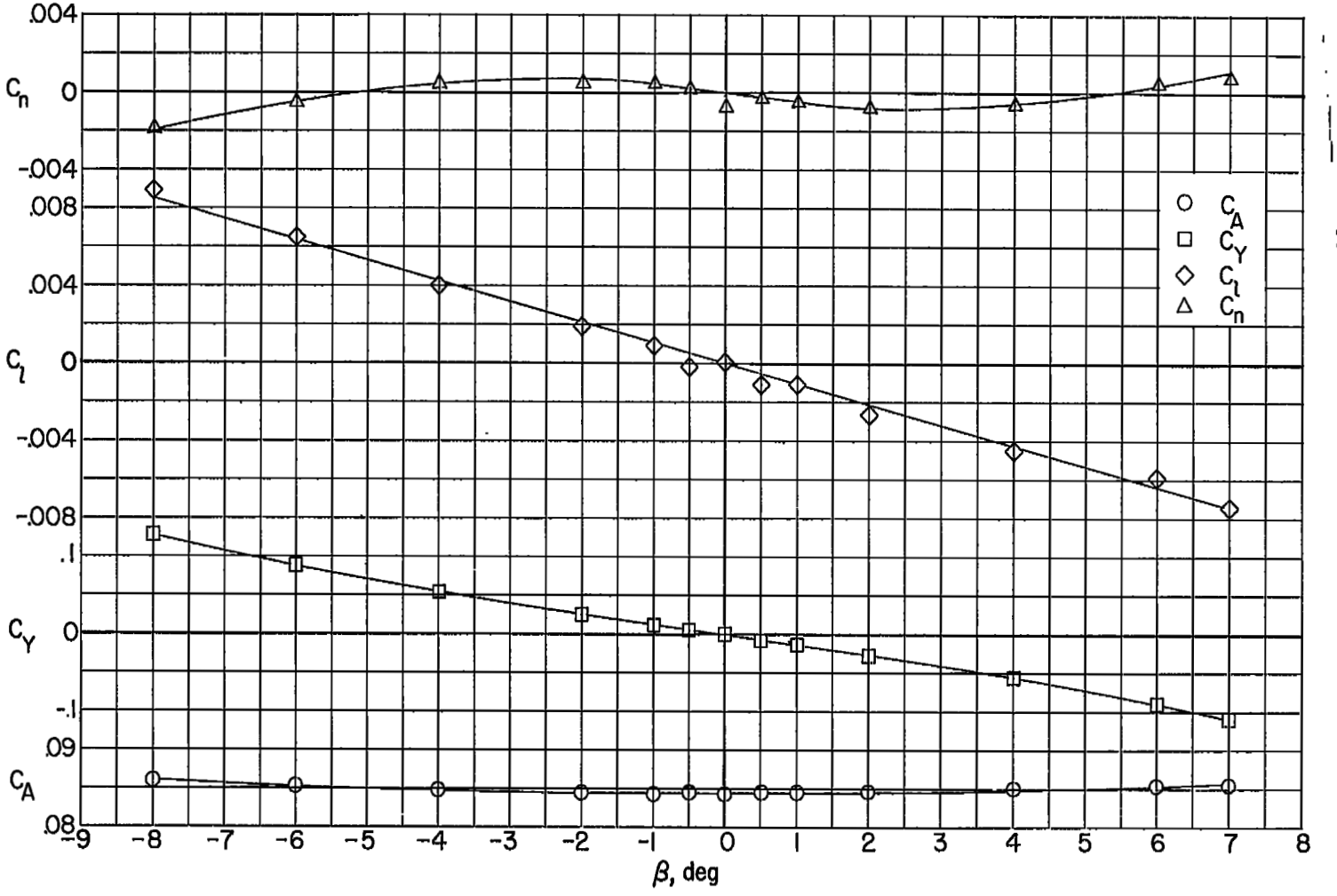

(c) Lateral characteristics in body-axis system at $\alpha = 0^\circ$.

Figure 16.- Complete configuration with $i_t = 0^\circ$ at $M = 2.62$. Concluded.

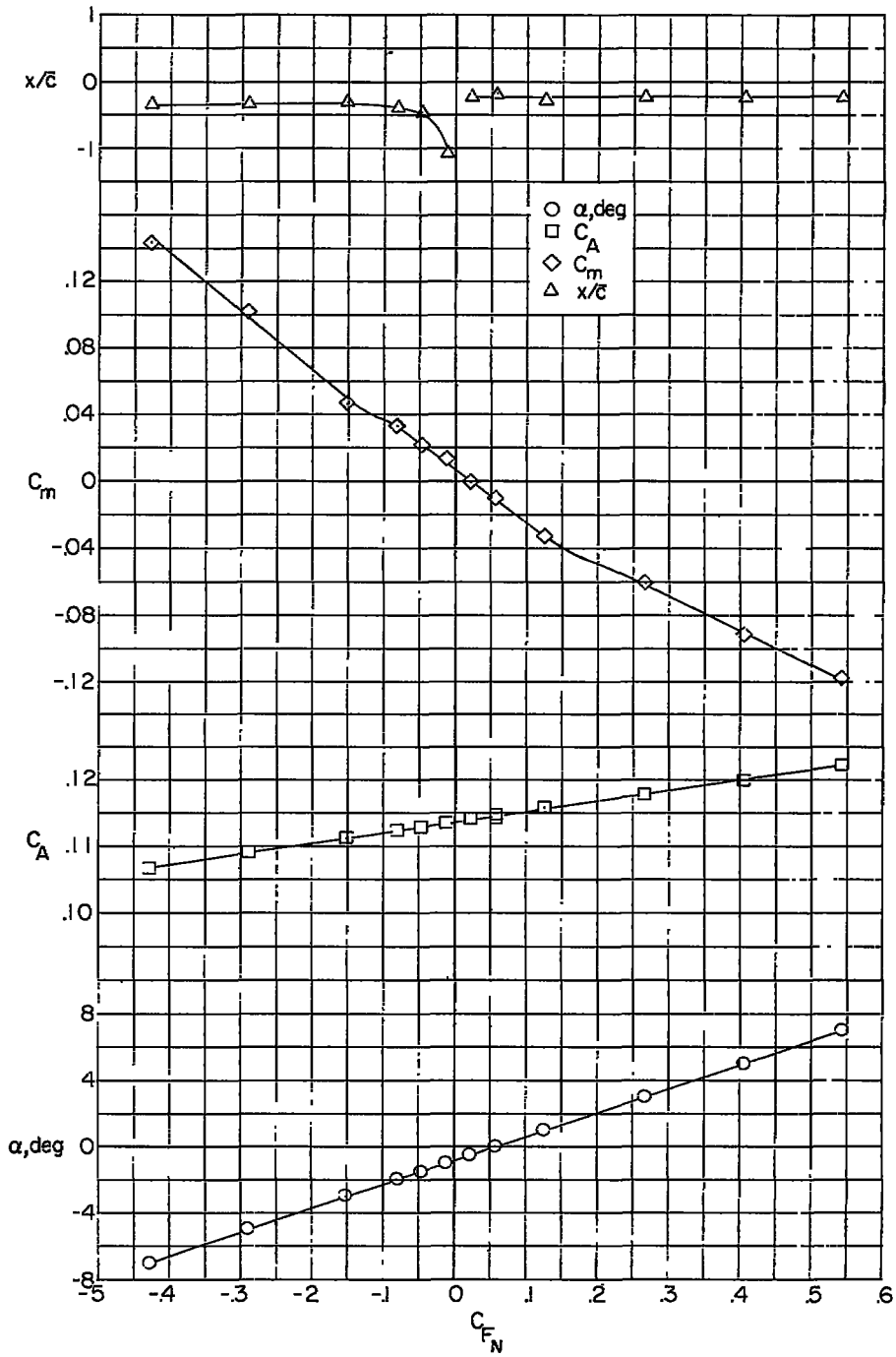

(a) Longitudinal characteristics in body-axis system at $\beta = 0^{\circ}$.

Figure 17.- Complete configuration with $i_t = 5^{\circ}$ at $M = 1.62$.

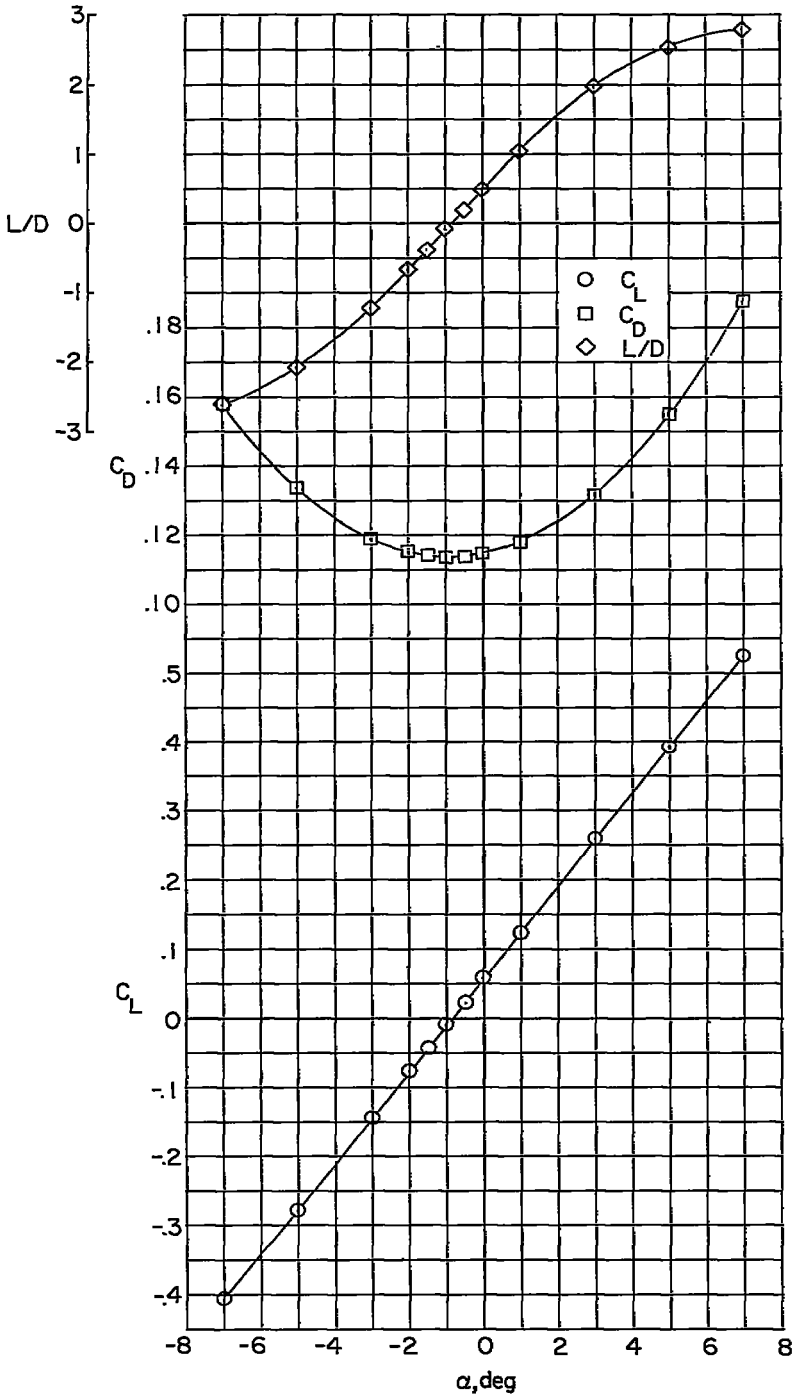

(b) Longitudinal force characteristics in stability-axis system at $\beta = 0^\circ$.

Figure 17.- Complete configuration with $i_t = 5^\circ$ at $M = 1.62$. Continued.

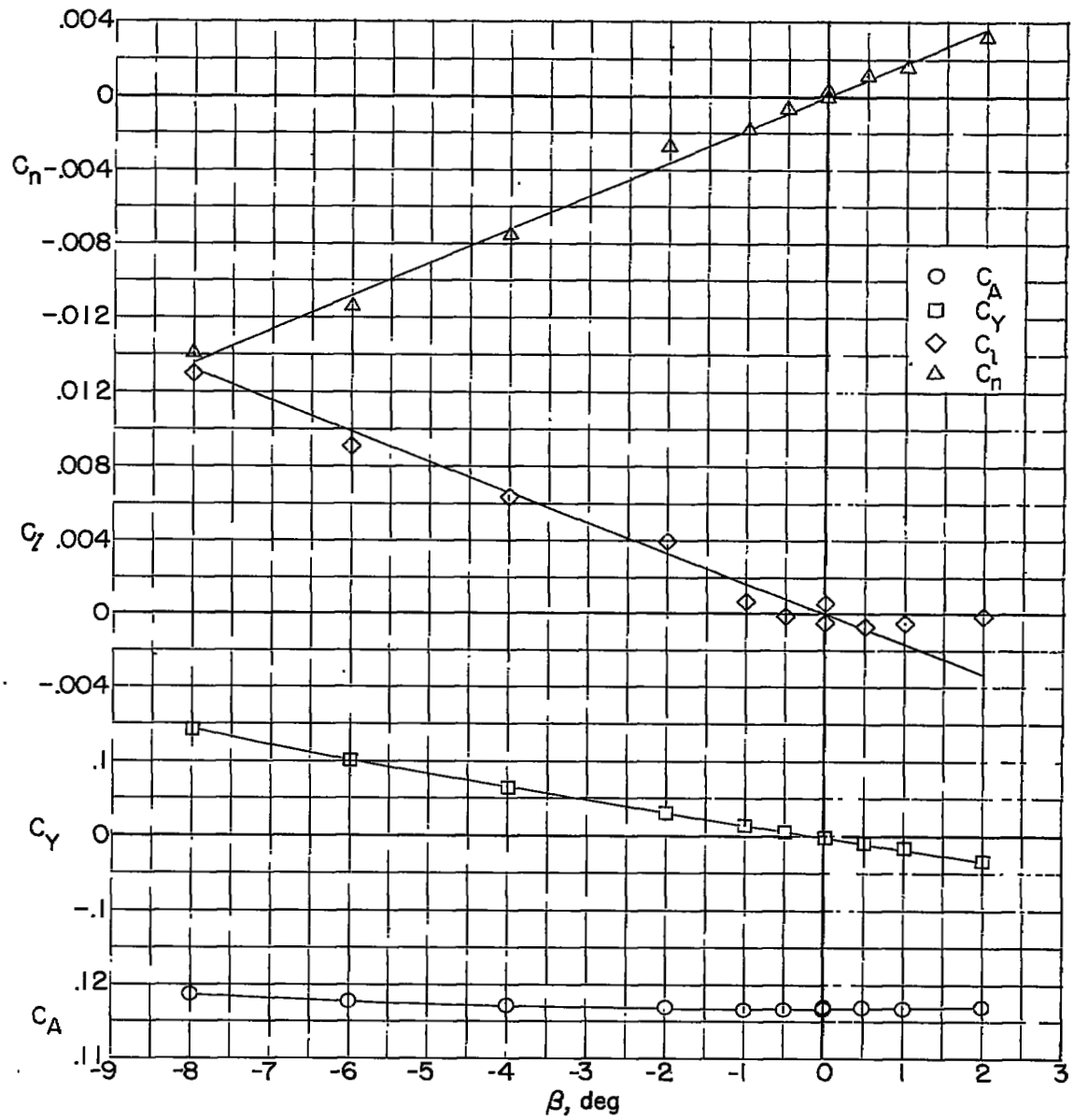

(c) Lateral characteristics in body-axis system at $\alpha = 0^\circ$.

Figure 17.- Complete configuration with $i_t = 5^\circ$ at $M = 1.62$. Concluded.

[redacted]

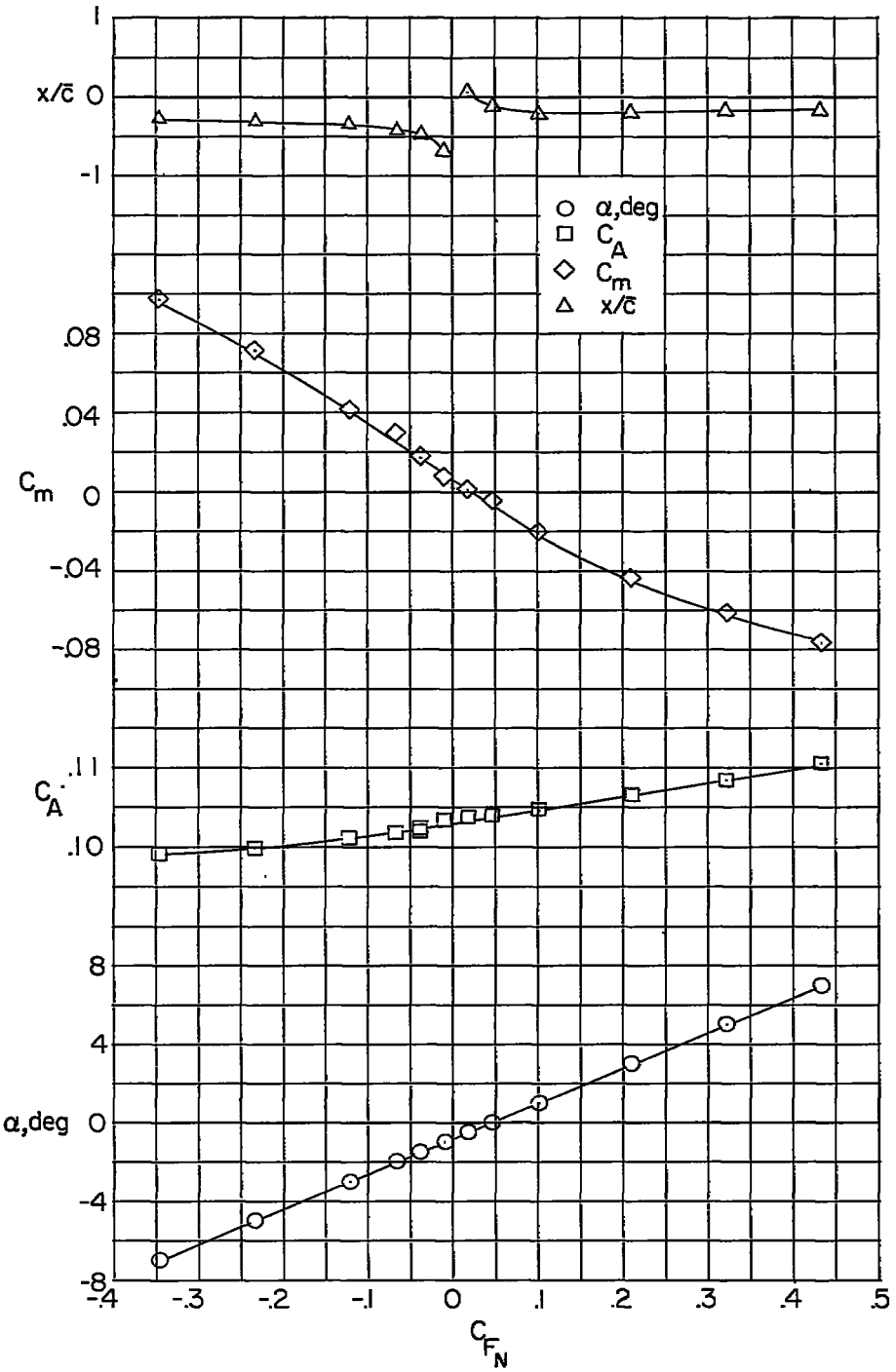

(a) Longitudinal characteristics in body-axis system at $\beta = 0^{\circ}$.

Figure 18.- Complete configuration with $i_t = 5^{\circ}$ at $M = 1.94$.

[redacted]

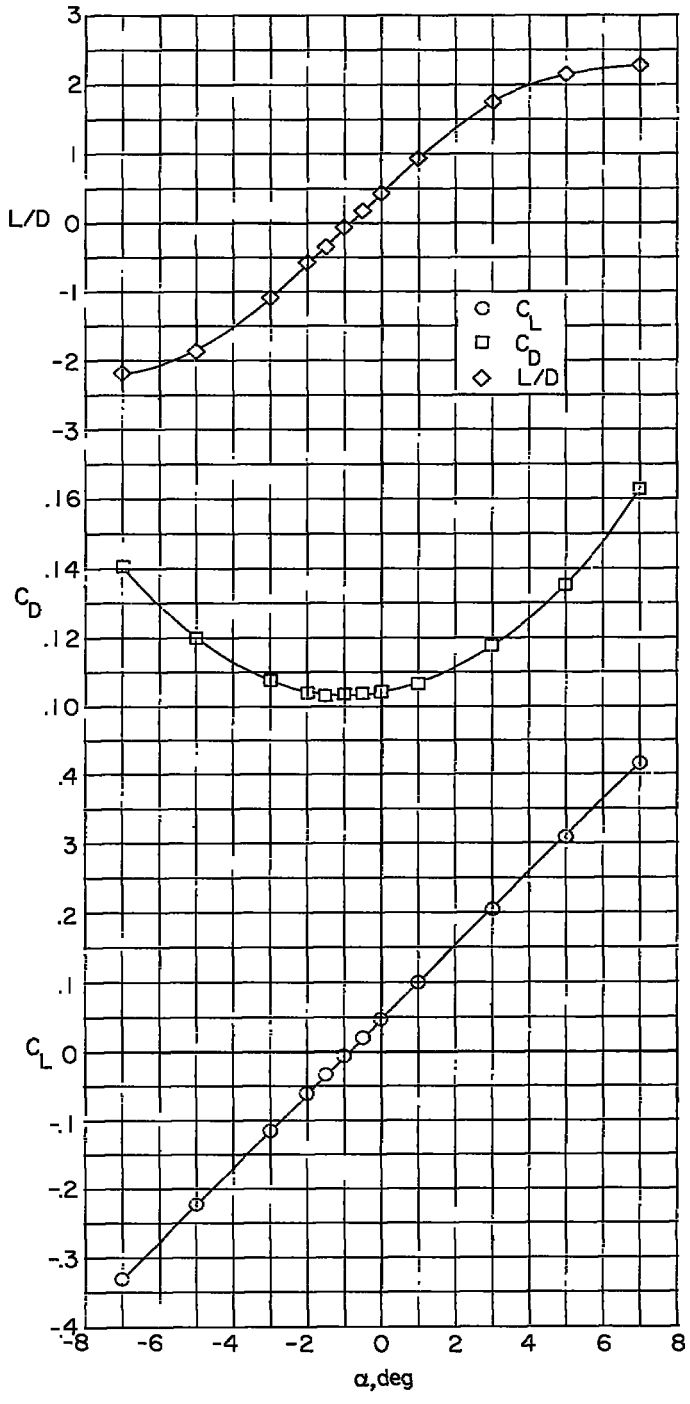

(b) Longitudinal force characteristics in stability-axis system at $\beta = 0^\circ$.

Figure 18.- Complete configuration with $i_t = 5^\circ$ at $M = 1.94$. Continued.

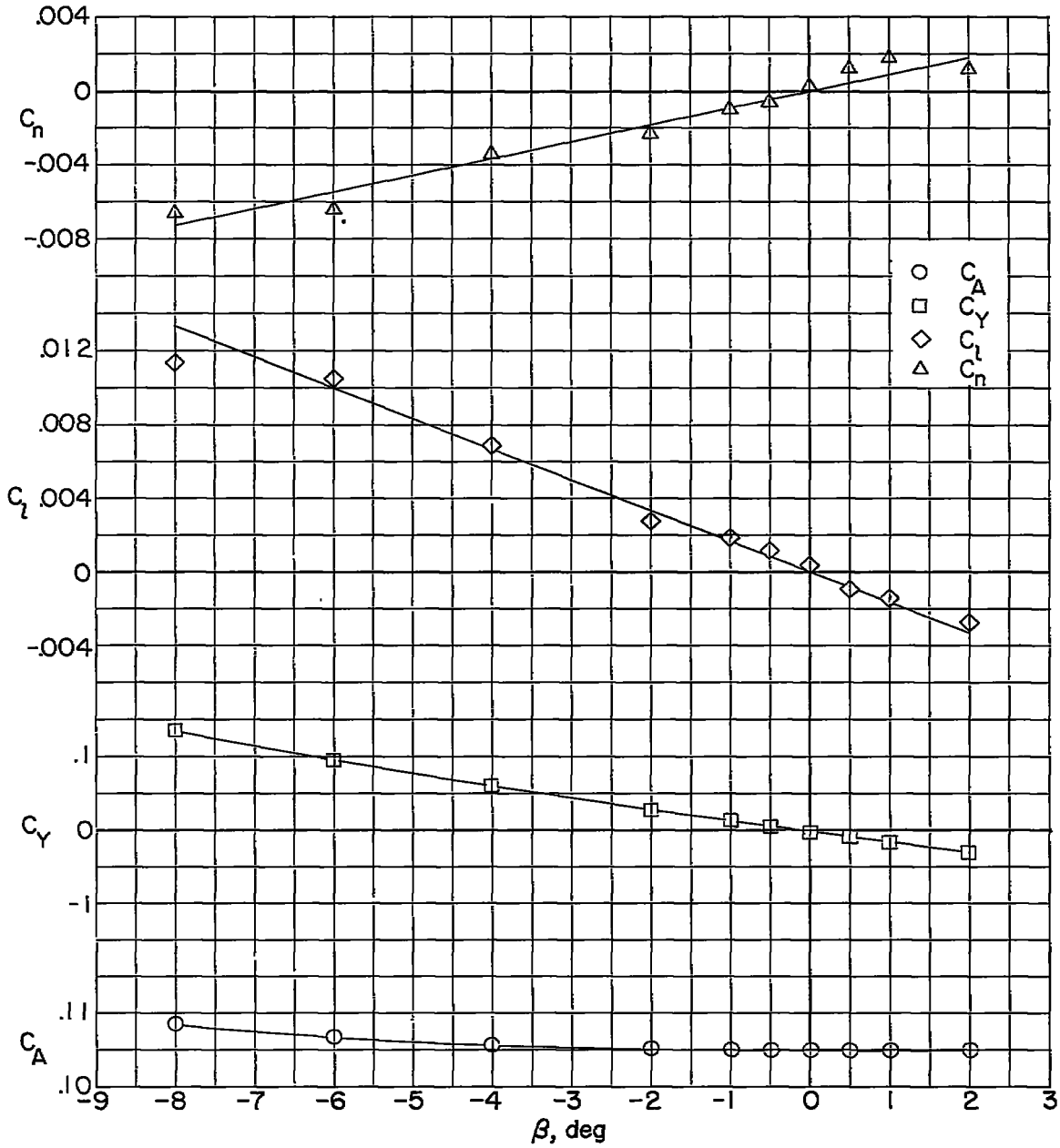

(c) Lateral characteristics in body-axis system at $\alpha = 0^\circ$.

Figure 18.- Complete configuration with $i_t = 5^\circ$ at $M = 1.94$. Concluded.

[redacted]

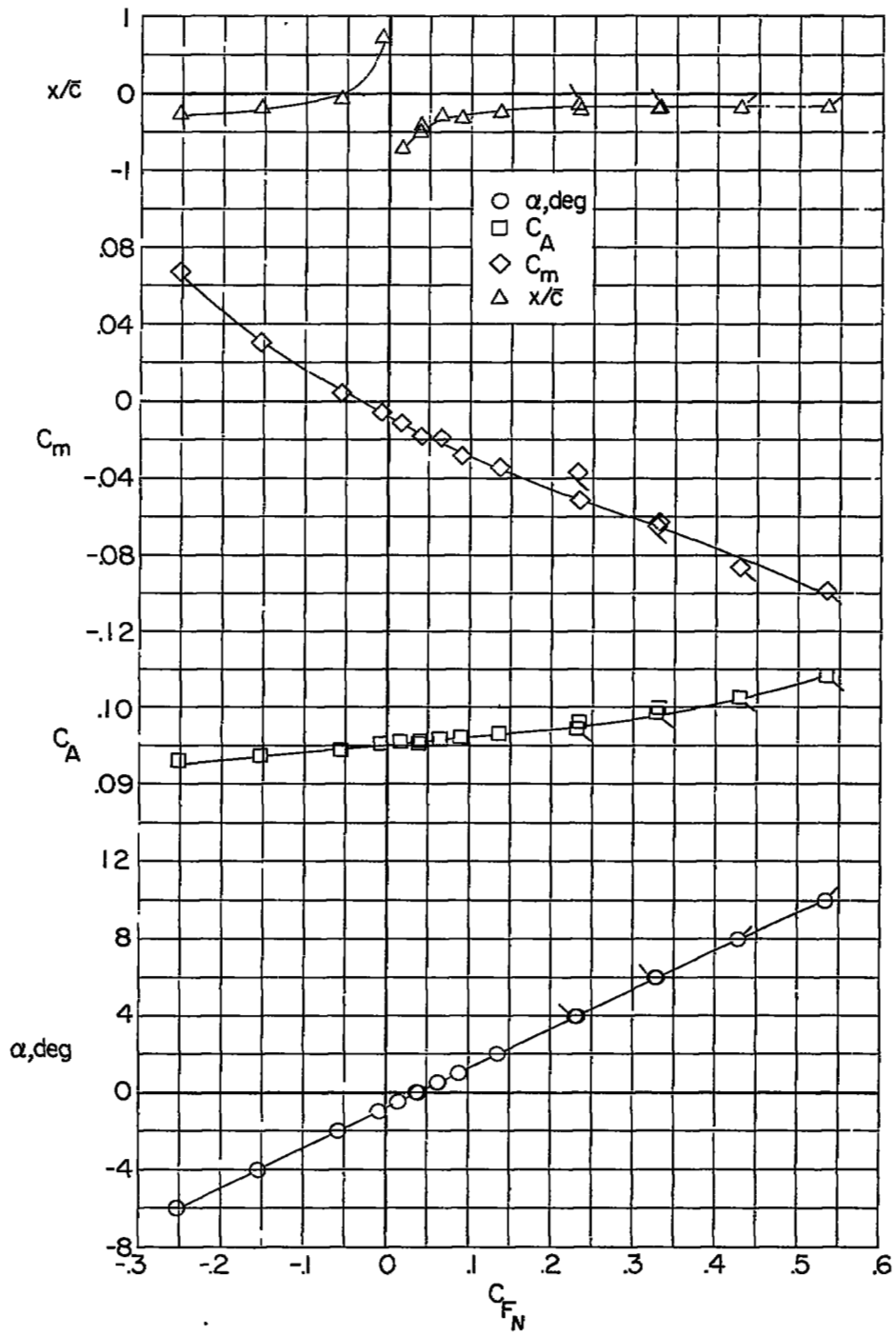

(a) Longitudinal characteristics in body-axis system at $\beta = 0^{\circ}$.

Figure 19.- Complete configuration with $i_t = 5^{\circ}$ at $M = 2.22$.

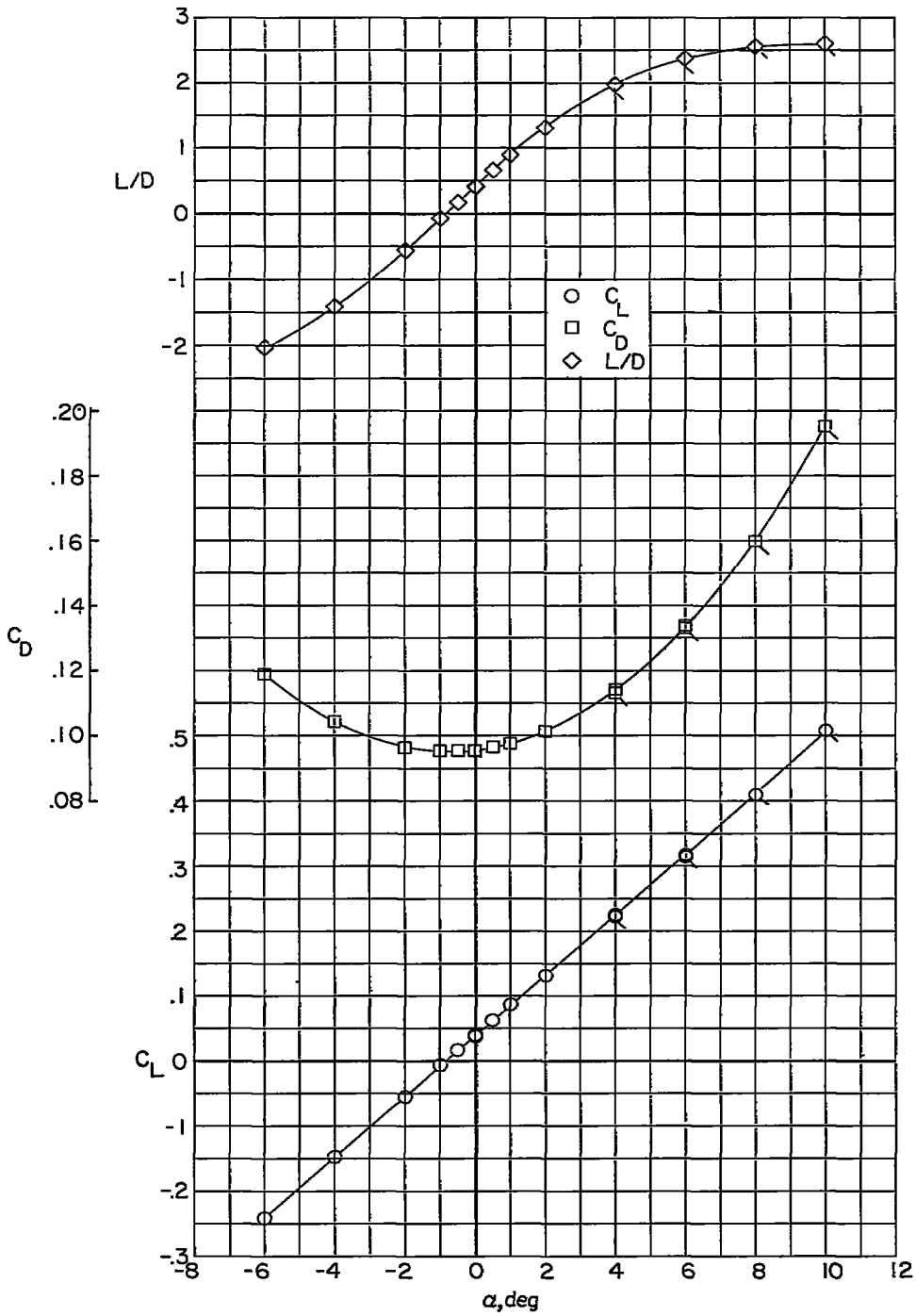

(b) Longitudinal force characteristics in stability-axis system at $\beta = 0^{\circ}$.

Figure 19.- Complete configuration with $i_t = 5^{\circ}$ at $M = 2.22$. Continued.

[redacted]

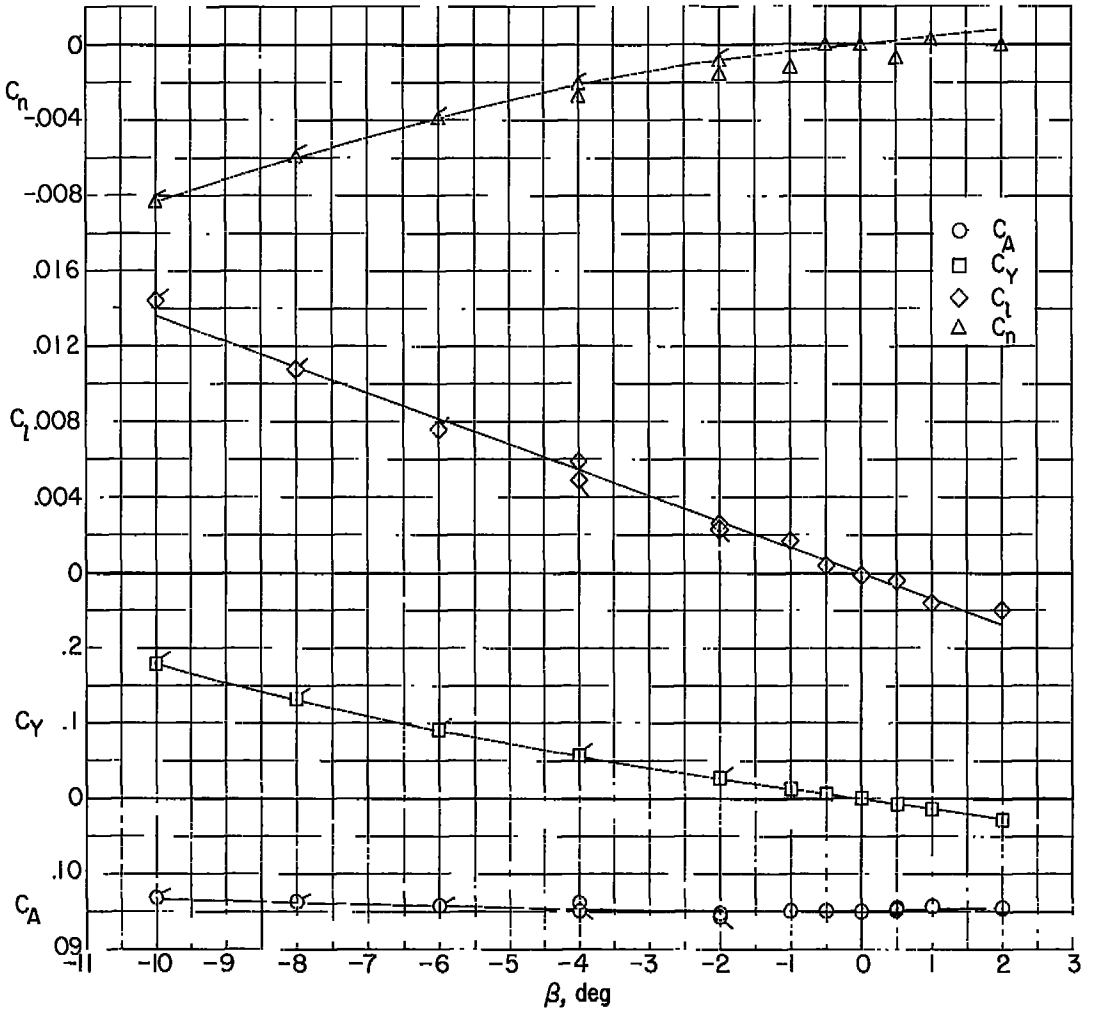

(c) Lateral characteristics in body-axis system at $\alpha = 0^\circ$.

Figure 19.- Complete configuration with $i_t = 5^\circ$ at M = 2.22. Concluded.

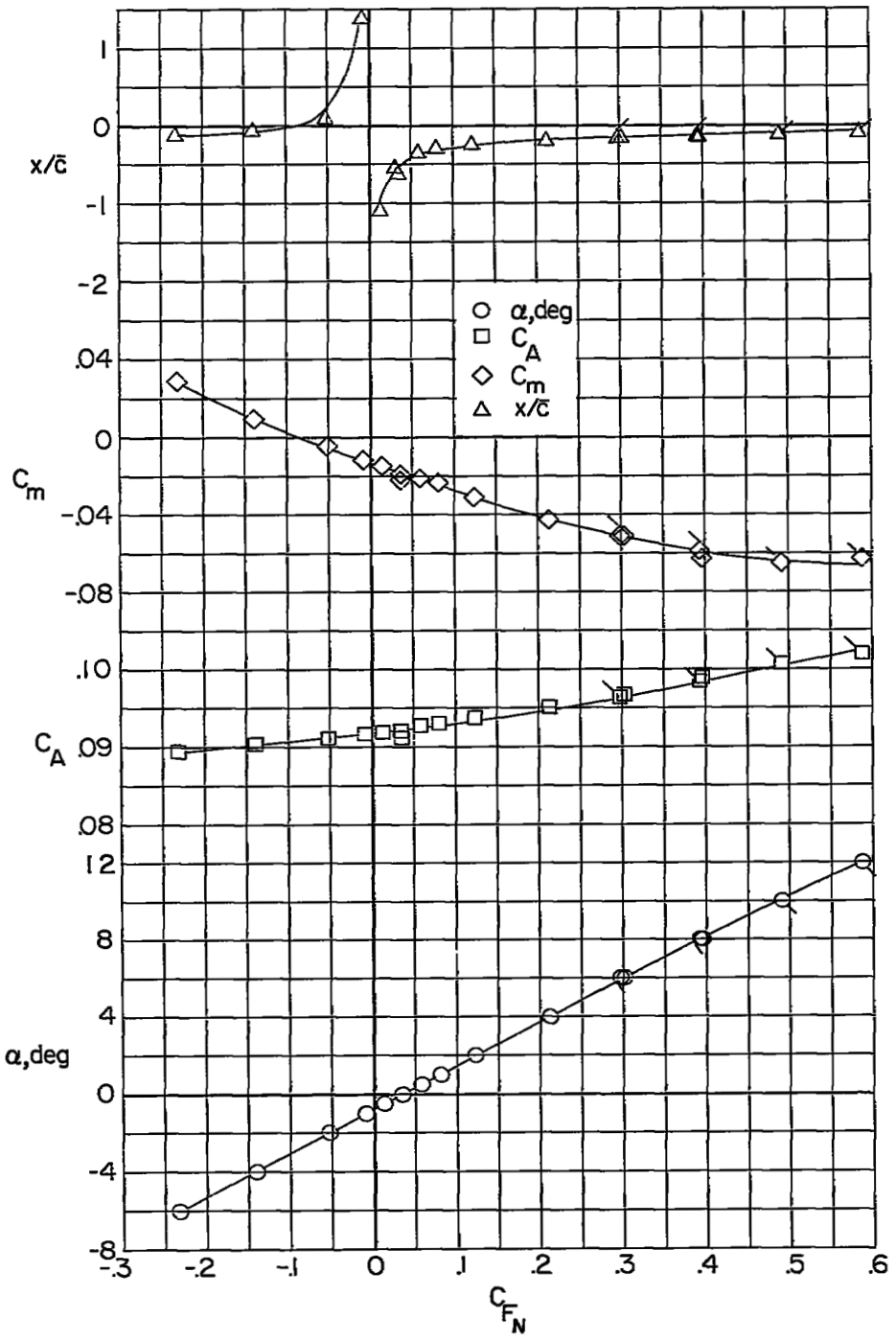

(a) Longitudinal characteristics in body-axis system at $\beta = 0^{\circ}$.

Figure 20.- Complete configuration with $i_t = 5^{\circ}$ at $M = 2.40$.

[redacted]

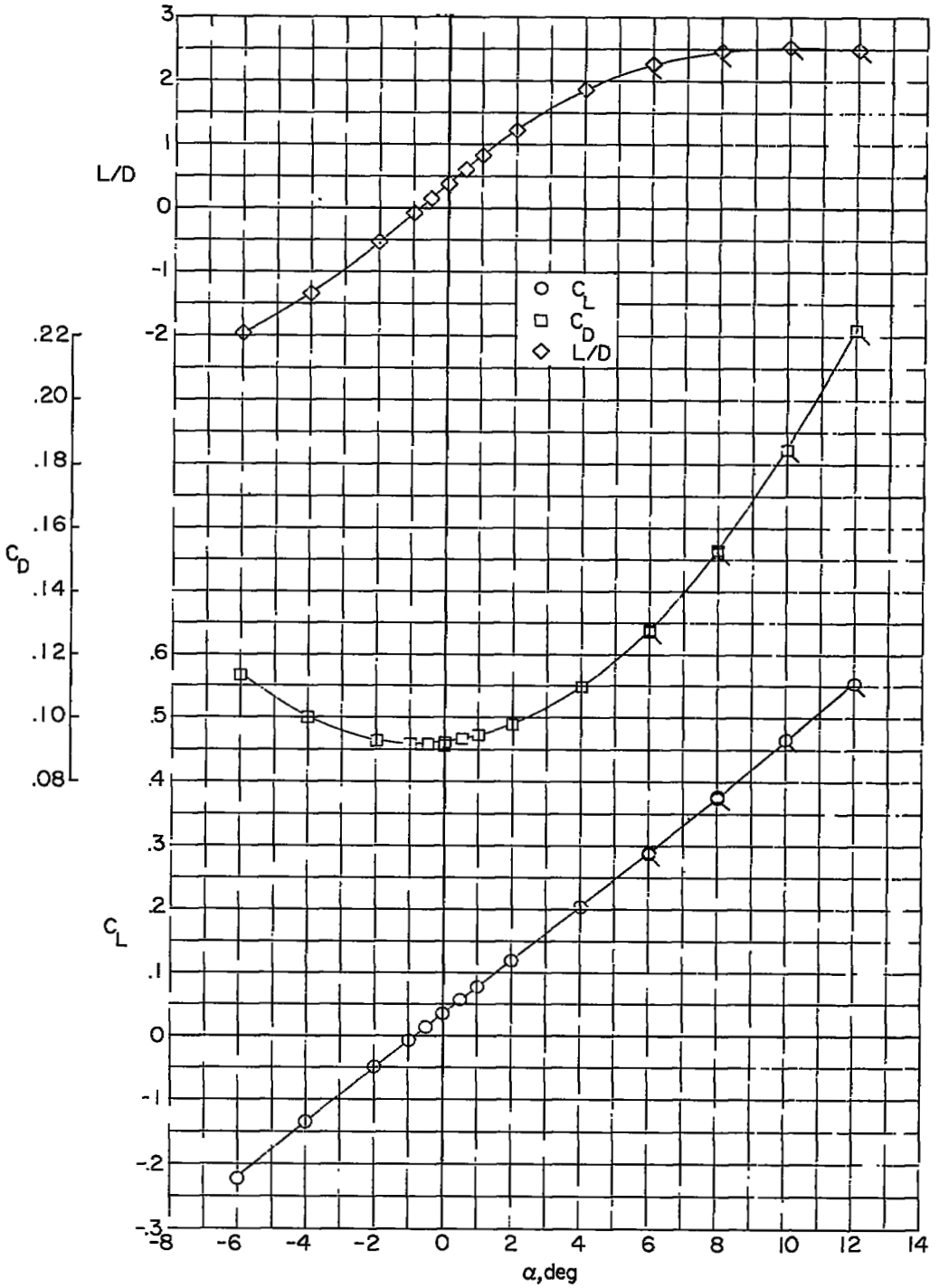

(b) Longitudinal force characteristics in stability-axis system at $\beta = 0^{\circ}$.

Figure 20.- Complete configuration with $i_t = 5^{\circ}$ at $M = 2.40$. Continued.

[redacted]

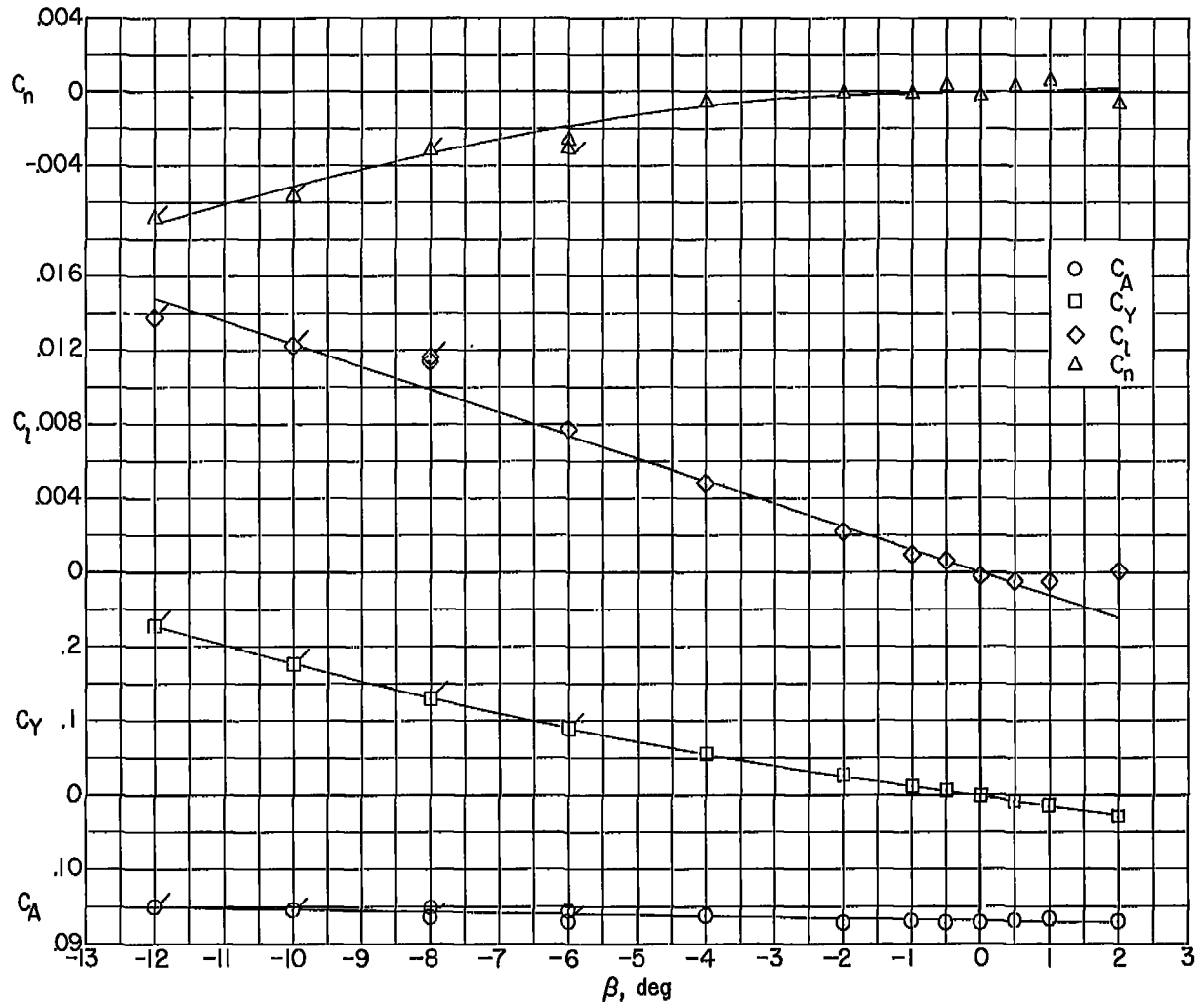

(c) Lateral characteristics in body-axis system at $\alpha = 0^\circ$.

Figure 20.- Complete configuration with $i_t = 5^\circ$ at $M = 2.40$. Concluded.

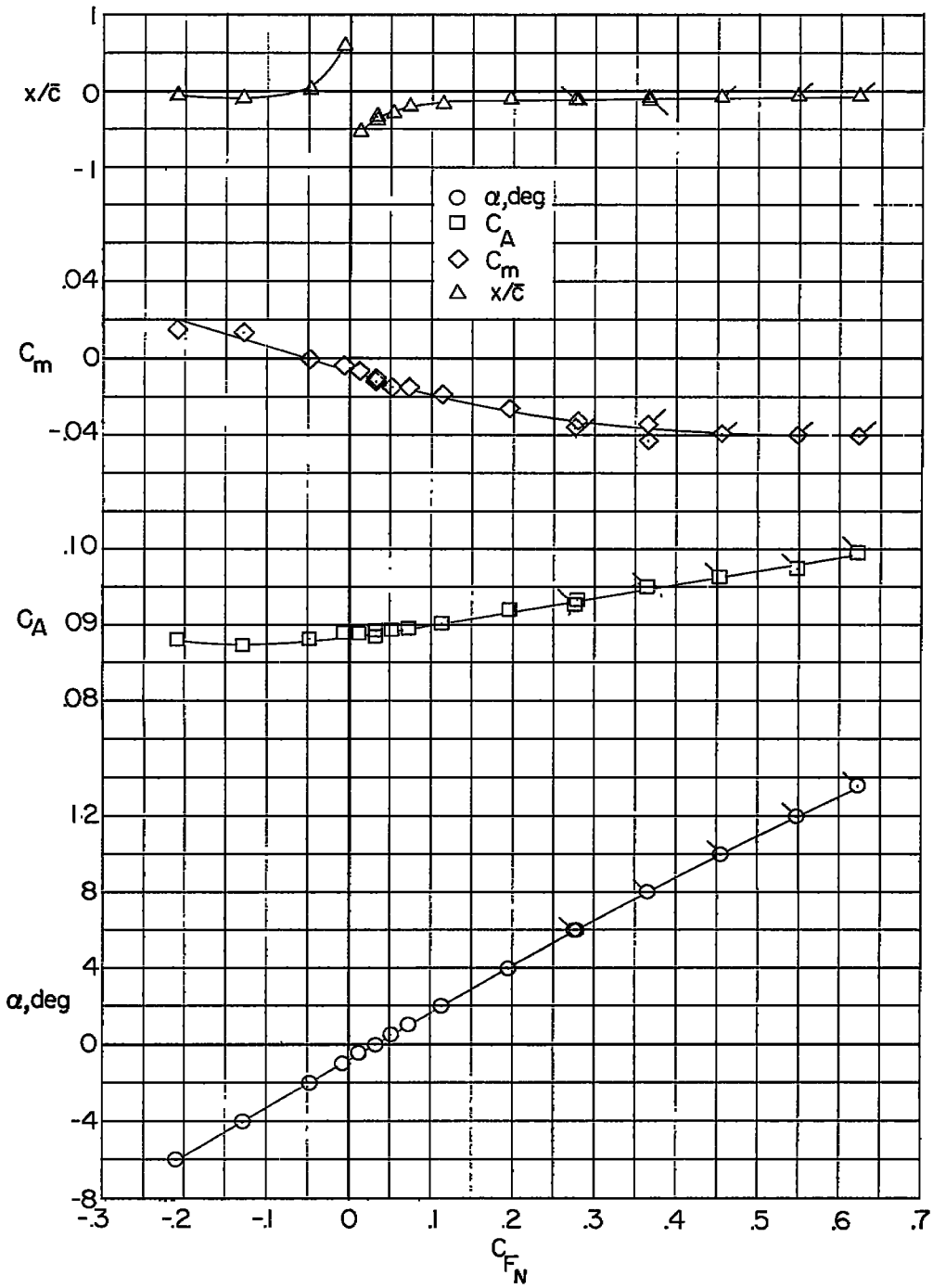

(a) Longitudinal characteristics in body-axis system at $\beta = 0^{\circ}$.

Figure 21.- Complete configuration with $i_t = 5^{\circ}$ at $M = 2.62$.

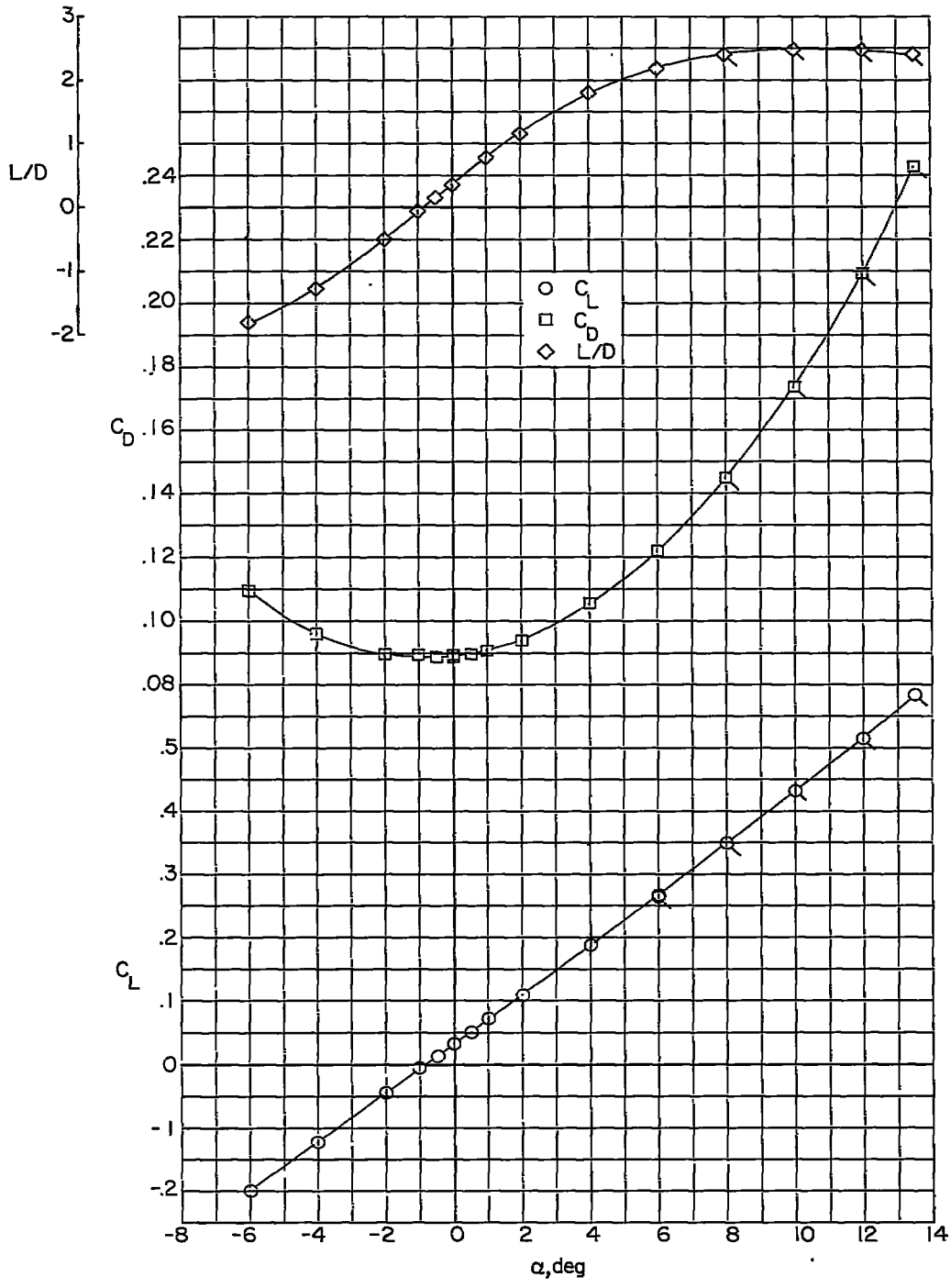

(b) Longitudinal force characteristics in stability-axis system at $\beta = 0^{\circ}$.

Figure 21.- Complete configuration with $i_t = 5^{\circ}$ at $M = 2.62$. Continued.

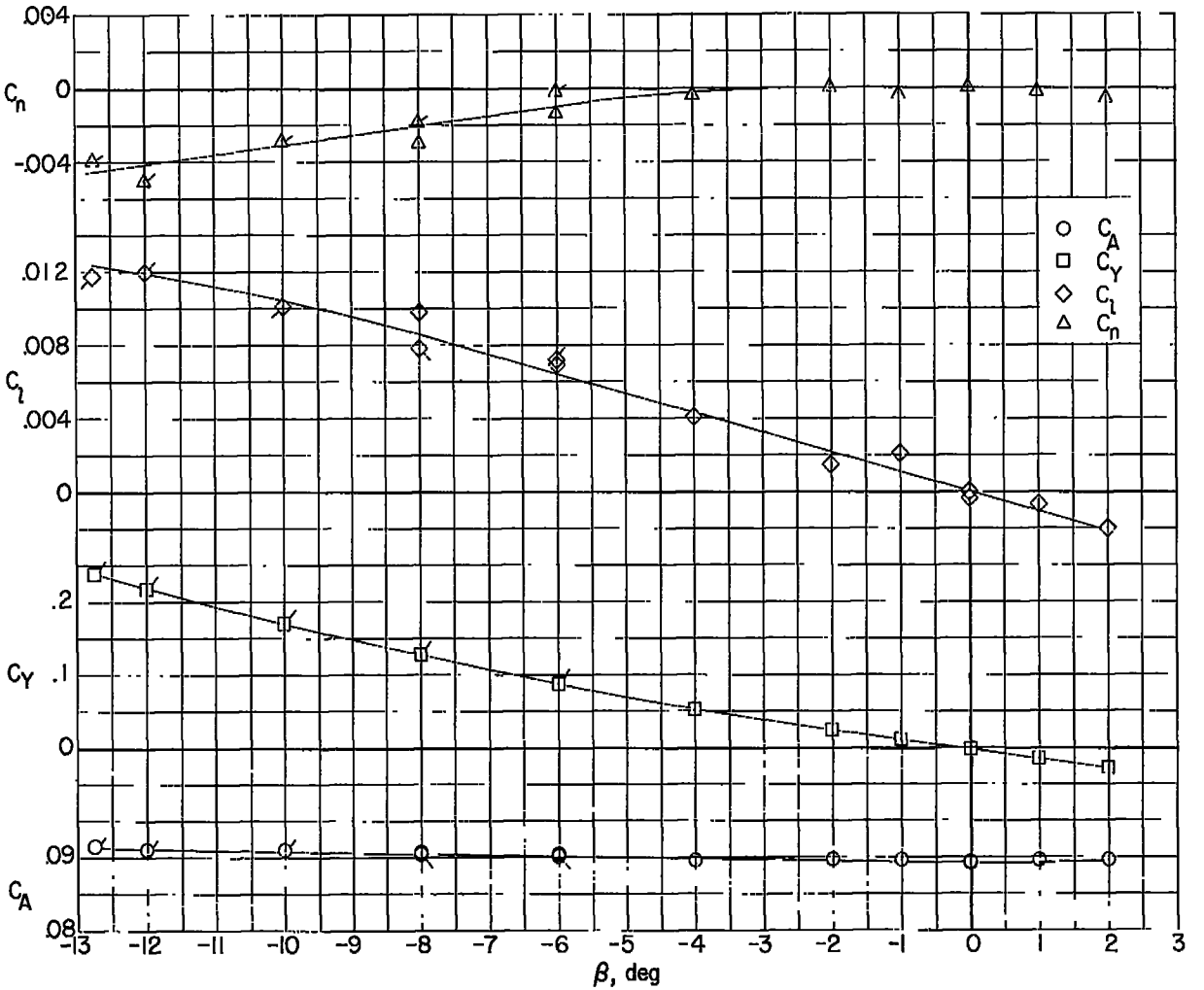

(c) Lateral characteristics in body-axis system at $\alpha = 0^{\circ}$.

Figure 21.- Complete configuration with $i_t = 5^{\circ}$ at M = 2.62. Concluded.

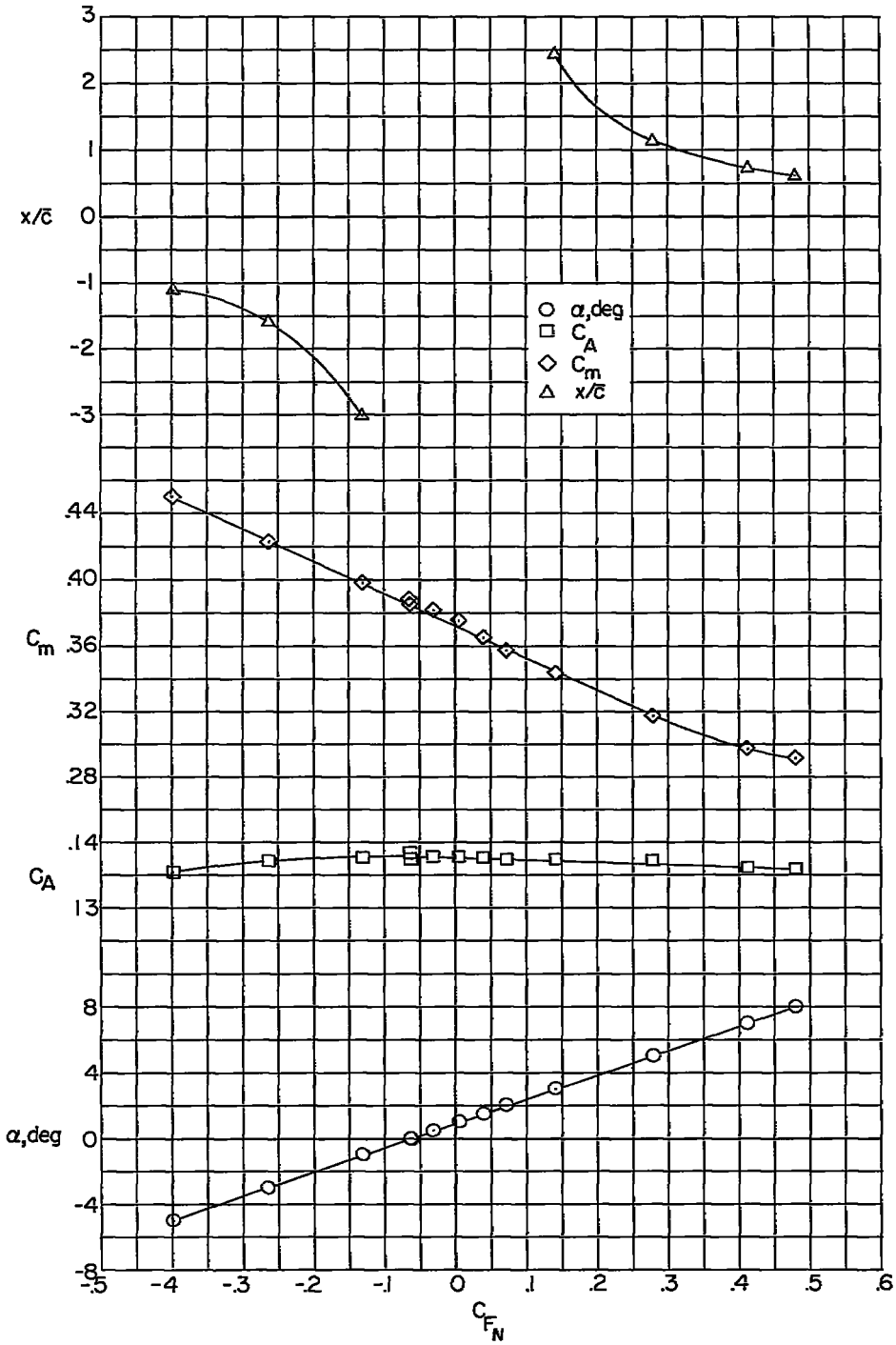

(a) Longitudinal characteristics in body-axis system at $\beta = 0^{\circ}$.

Figure 22.- Complete configuration with $i_t = -10^{\circ}$ at $M = 1.62$.

[redacted]

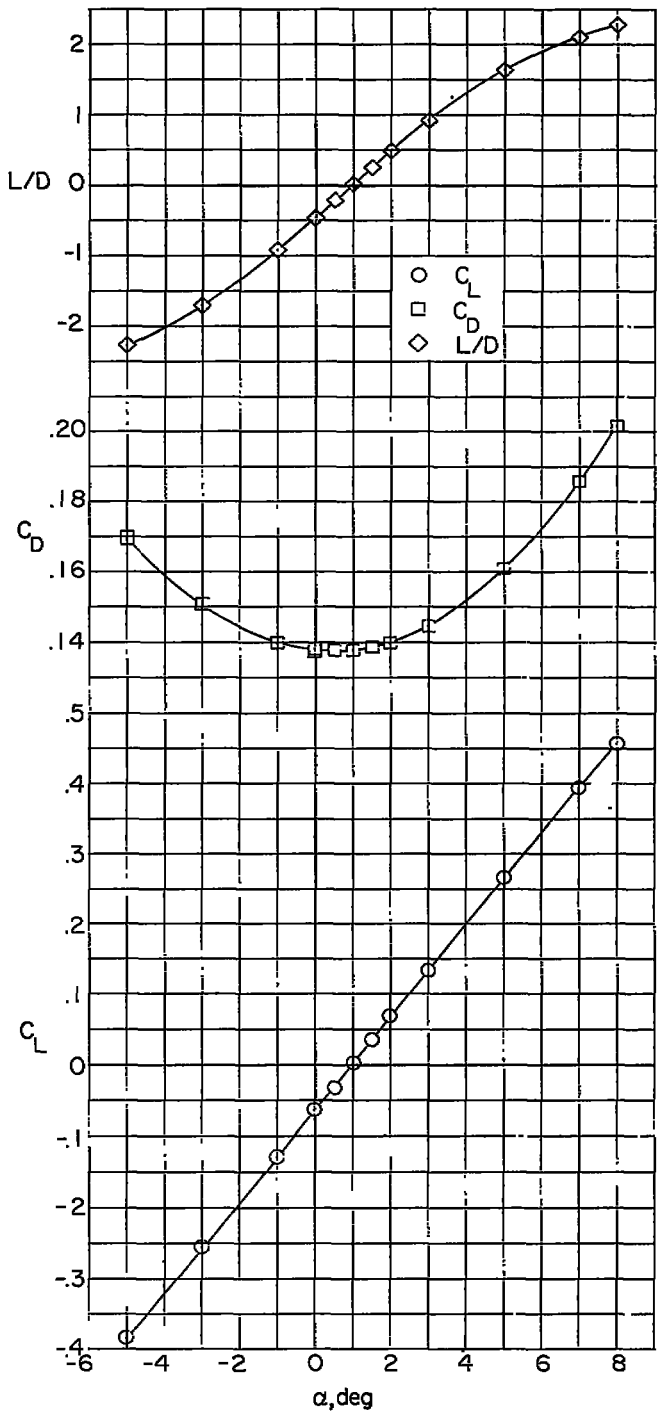

(b) Longitudinal force characteristics in stability-axis system at $\beta = 0^\circ$.

Figure 22.- Complete configuration with $i_t = -10^\circ$ at $M = 1.62$. Continued.

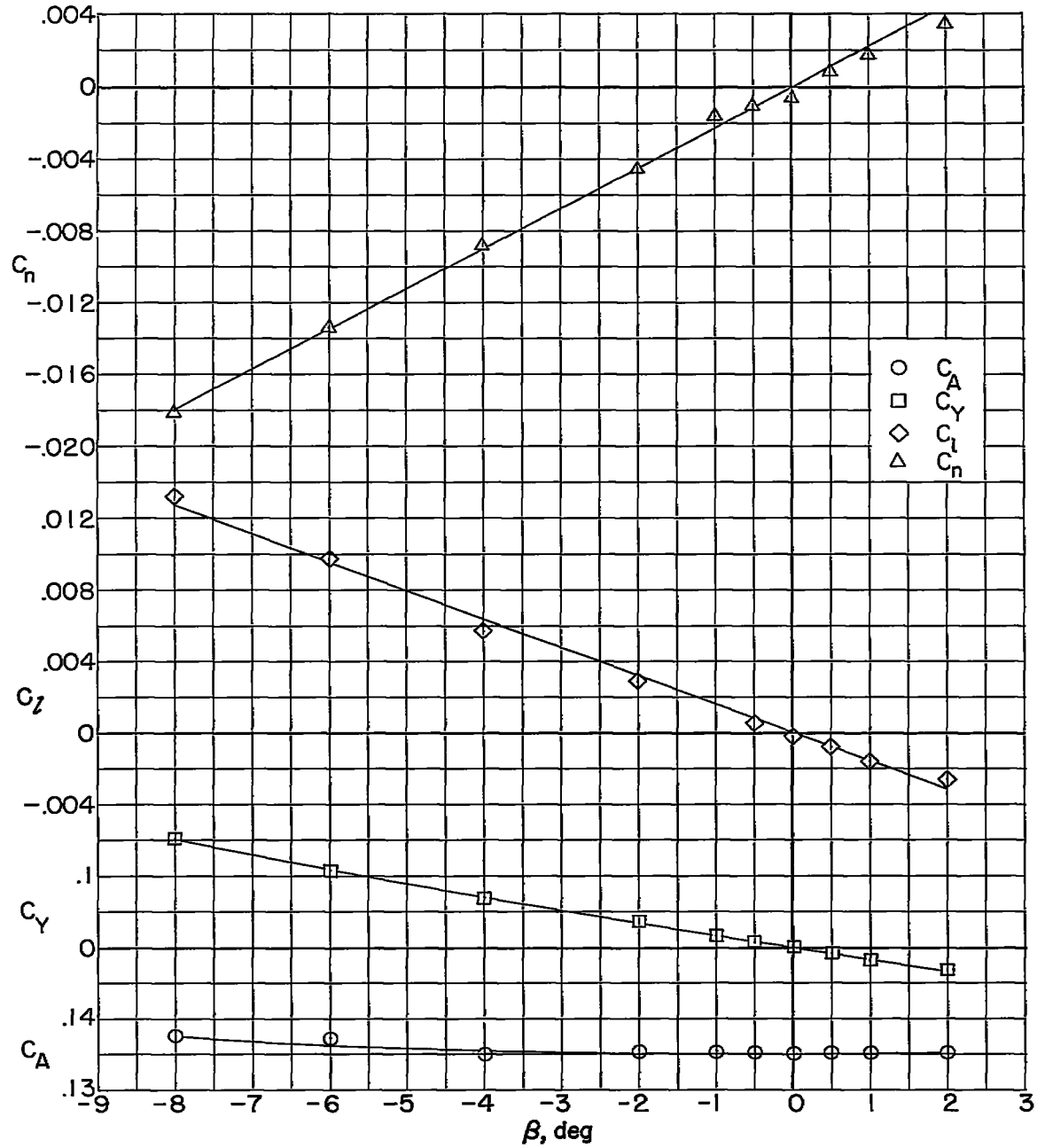

(c) Lateral characteristics in body-axis system at $\alpha = 0^\circ$.

Figure 22.- Complete configuration with $i_t = -10^\circ$ at $M = 1.62$. Concluded.

[redacted]

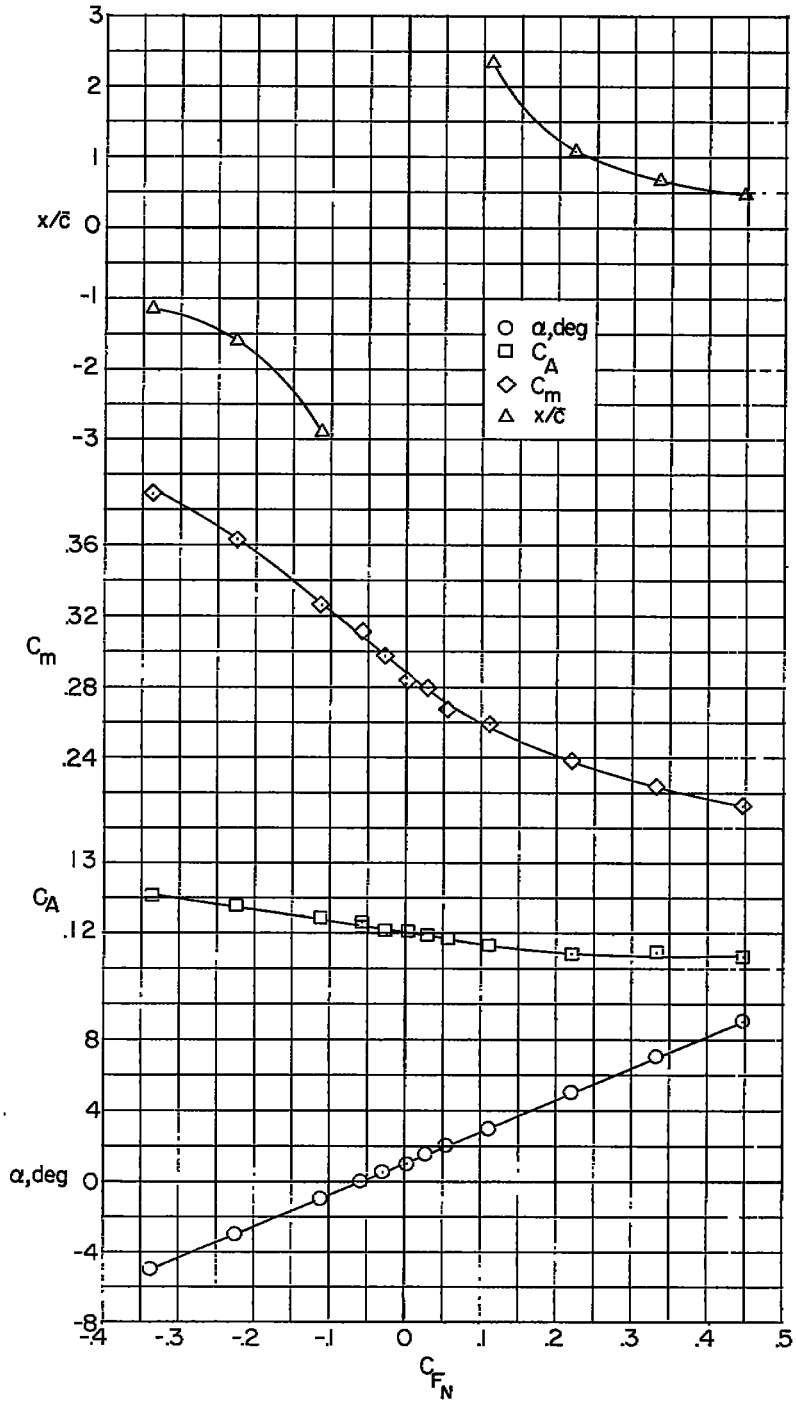

(a) Longitudinal characteristics in body-axis system at $\beta = 0^\circ$.

Figure 23.- Complete configuration with $i_t = -10^\circ$ at $M = 1.94$.

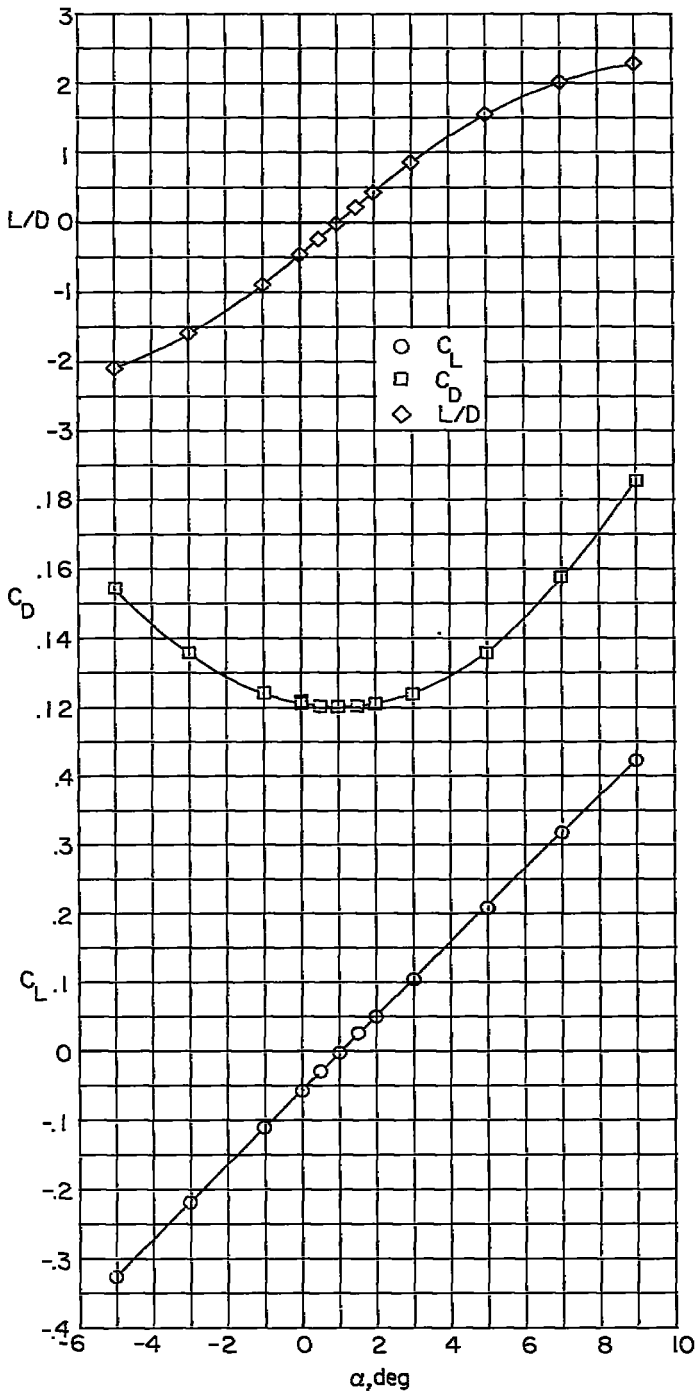

(b) Longitudinal force characteristics in stability-axis system at $\beta = 0^{\circ}$.

Figure 23.- Complete configuration with $i_t = -10^{\circ}$ at $M = 1.94$. Continued.

[redacted]

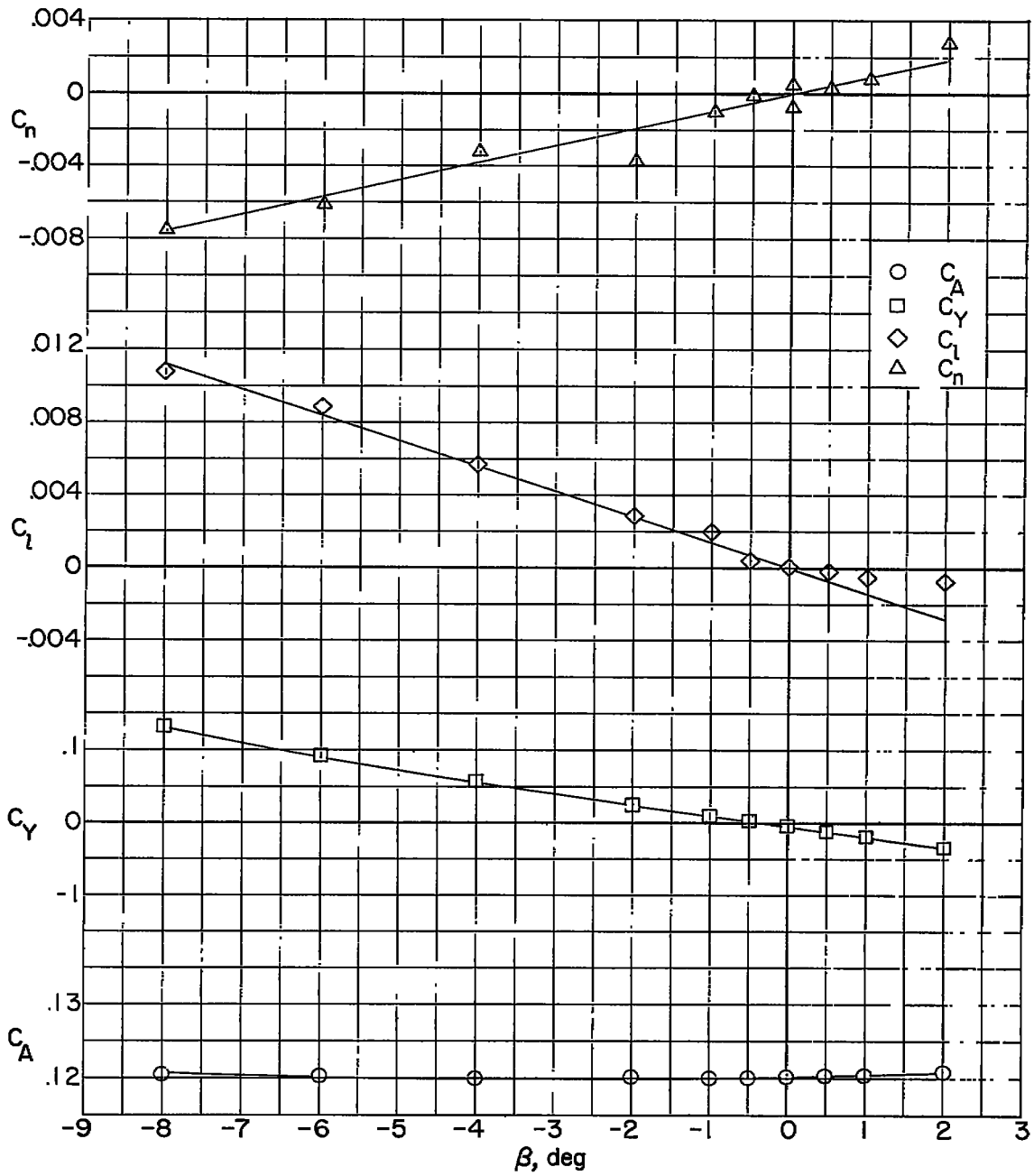

(c) Lateral characteristics in body-axis system at $\alpha = 0^\circ$.

Figure 23.- Complete configuration with $i_t = -10^\circ$ at $M = 1.94$. Concluded.

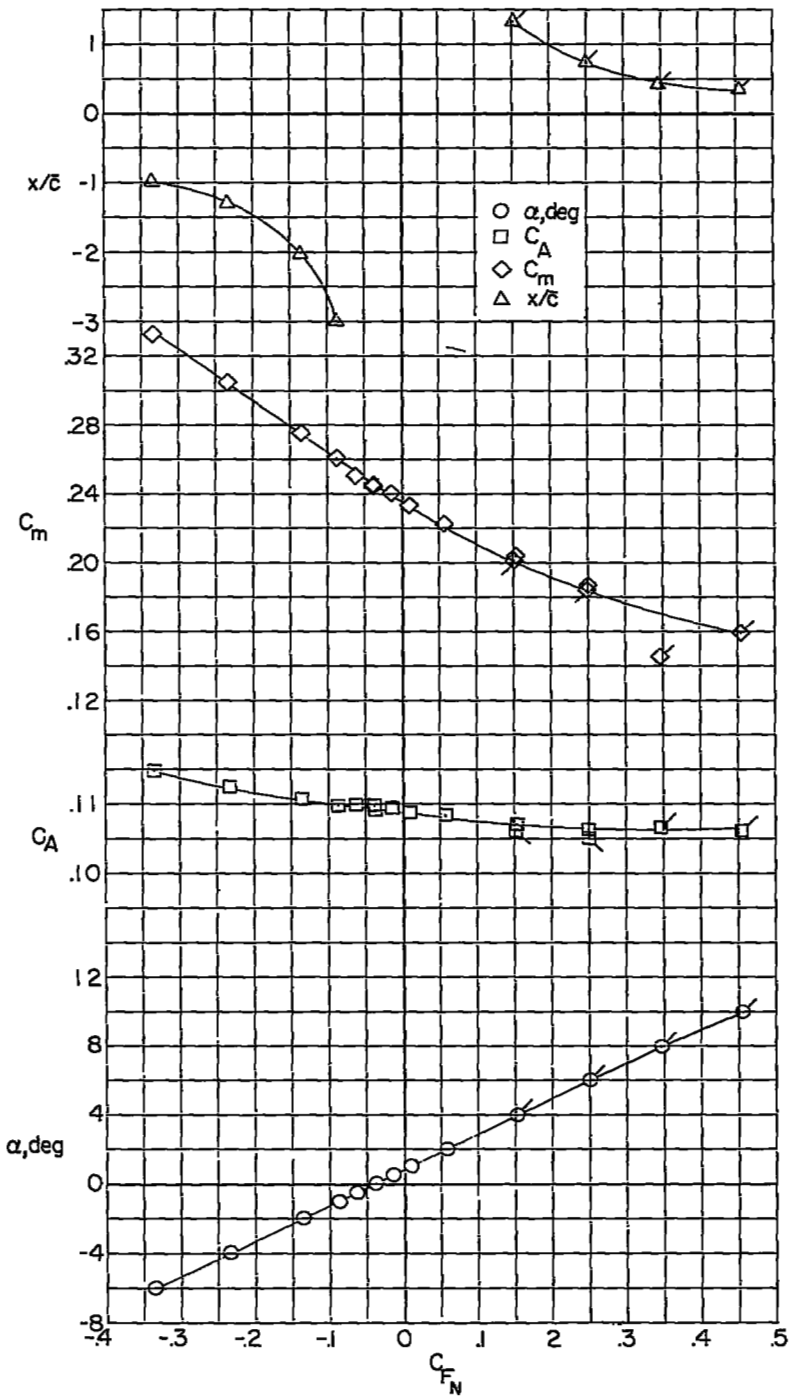

(a) Longitudinal characteristics in body-axis system at $\beta = 0^\circ$.

Figure 24.- Complete configuration with $i_t = -10^\circ$ at $M = 2.22$.

[redacted]

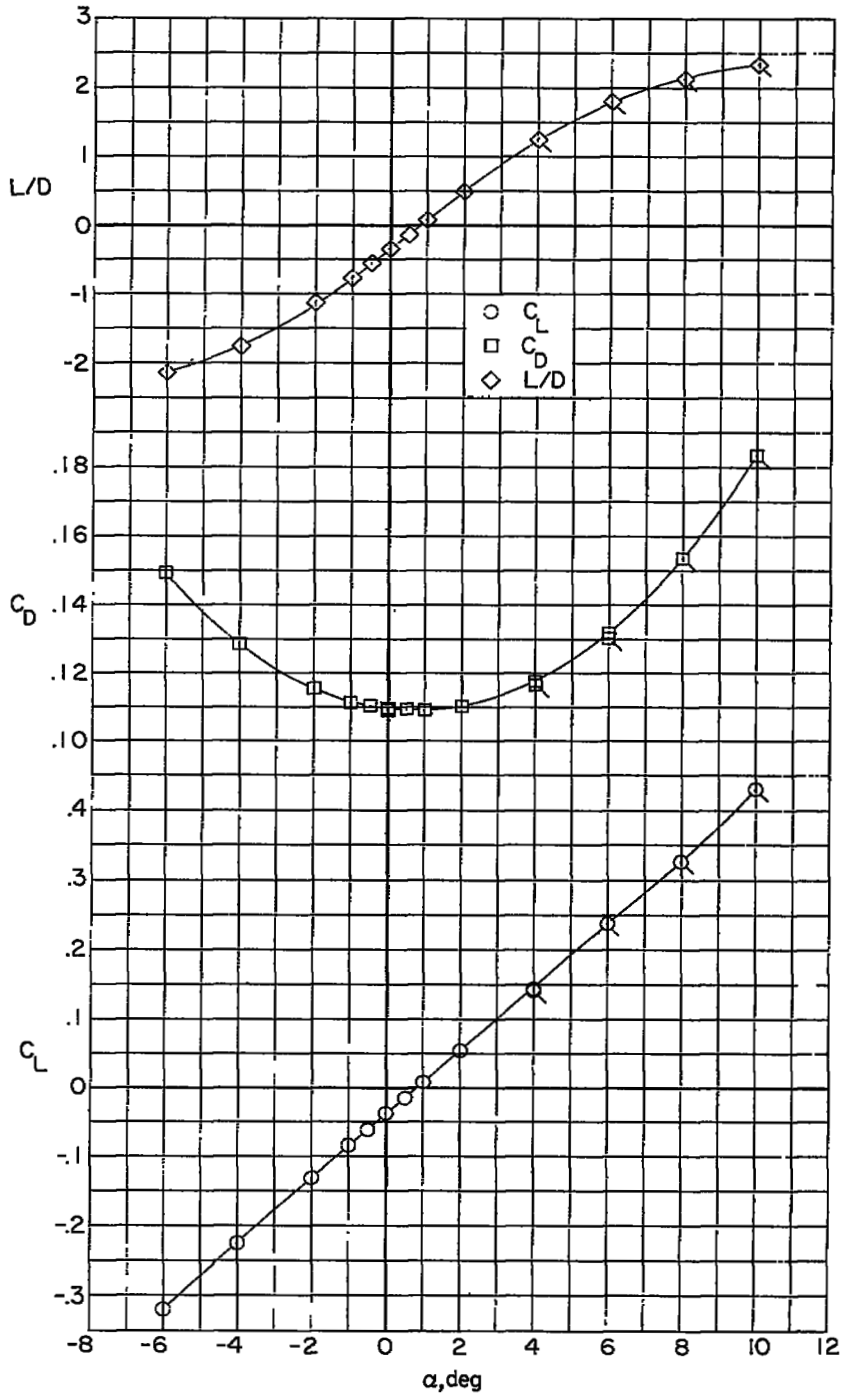

(b) Longitudinal force characteristics in stability-axis system at $\beta = 0^{\circ}$.

Figure 24.- Complete configuration with $i_t = -10^{\circ}$ at $M = 2.22$. Continued.

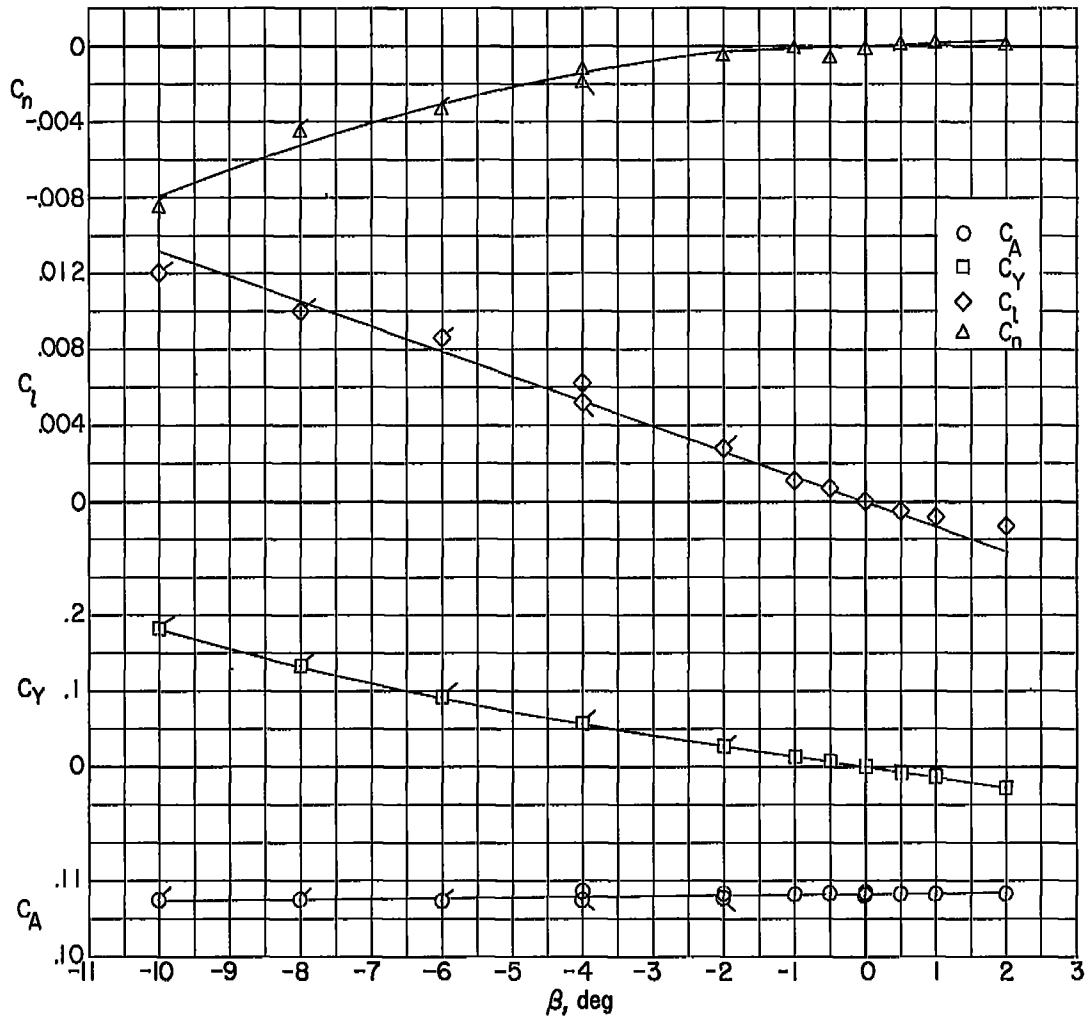

(c) Lateral characteristics in body-axis system at $\alpha = 0^\circ$.

Figure 24.- Complete configuration with $i_t = -10^\circ$ at M = 2.22. Concluded.

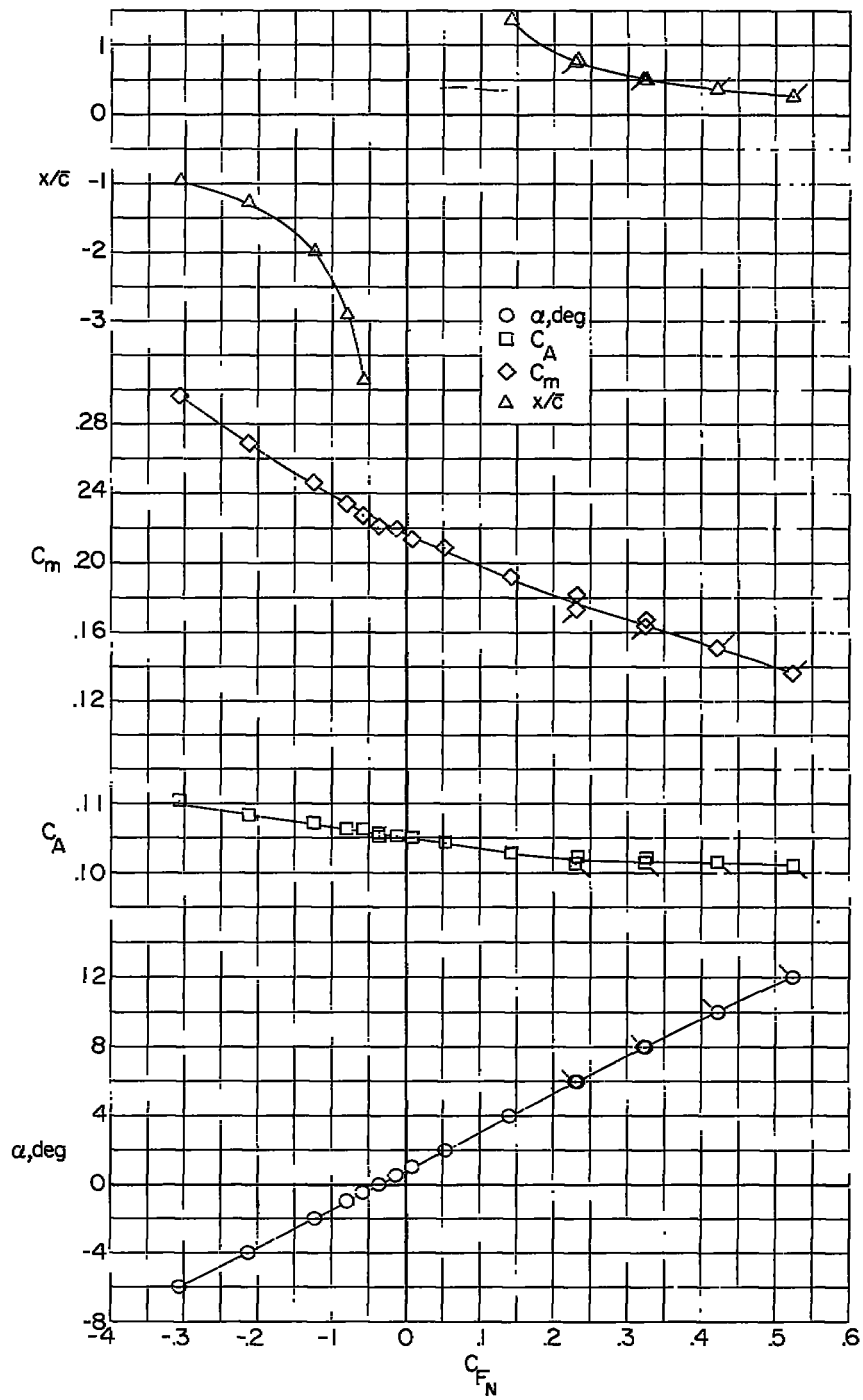

(a) Longitudinal characteristics in body-axis system at $\beta = 0^{\circ}$.

Figure 25.- Complete configuration with $i_t = -10^{\circ}$ at $M = 2.40$.

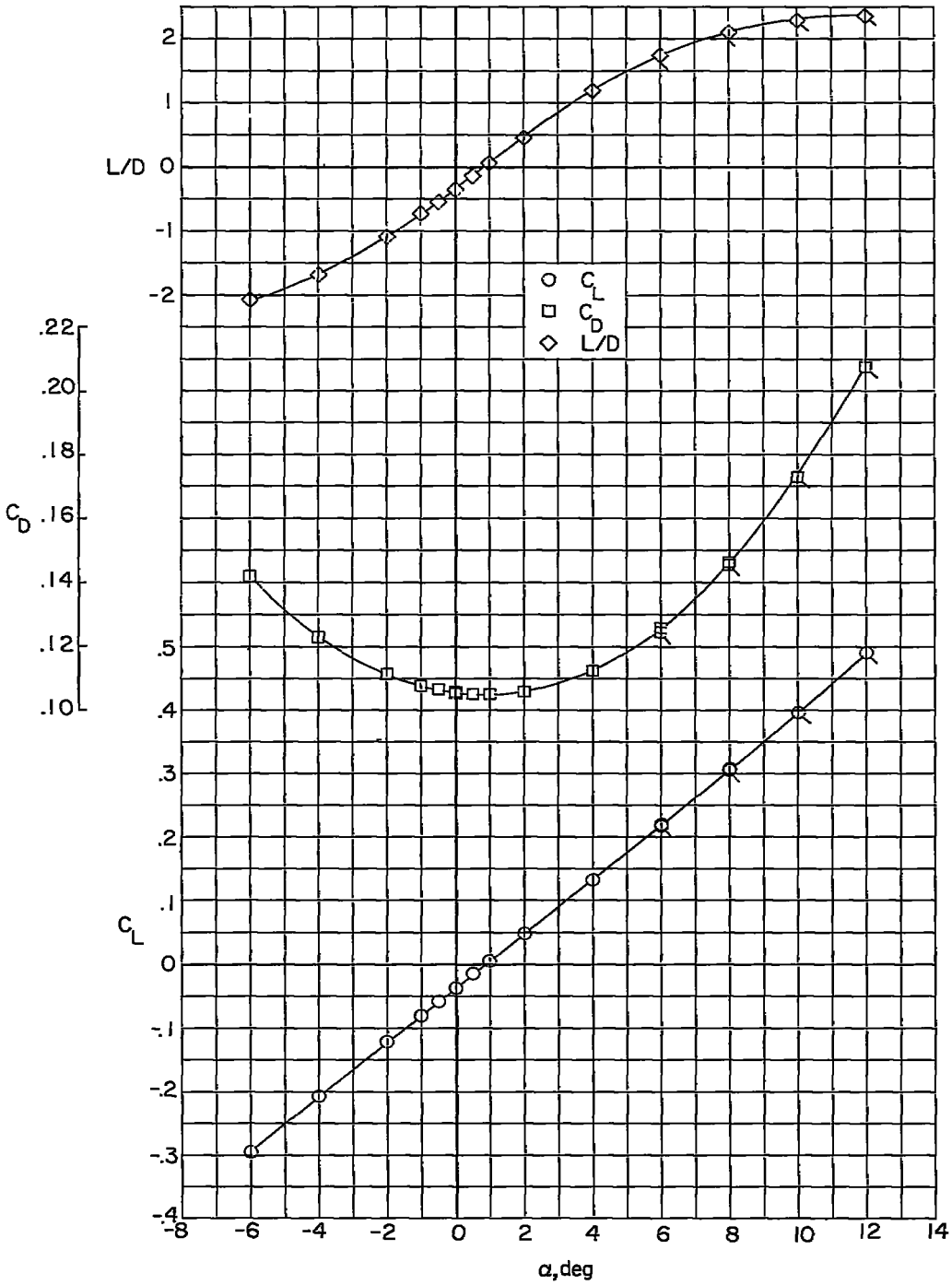

(b) Longitudinal force characteristics in stability-axis system at $\beta = 0^\circ$.

Figure 25.- Complete configuration with $i_t = -10^\circ$ at $M = 2.40$. Continued.

[redacted]

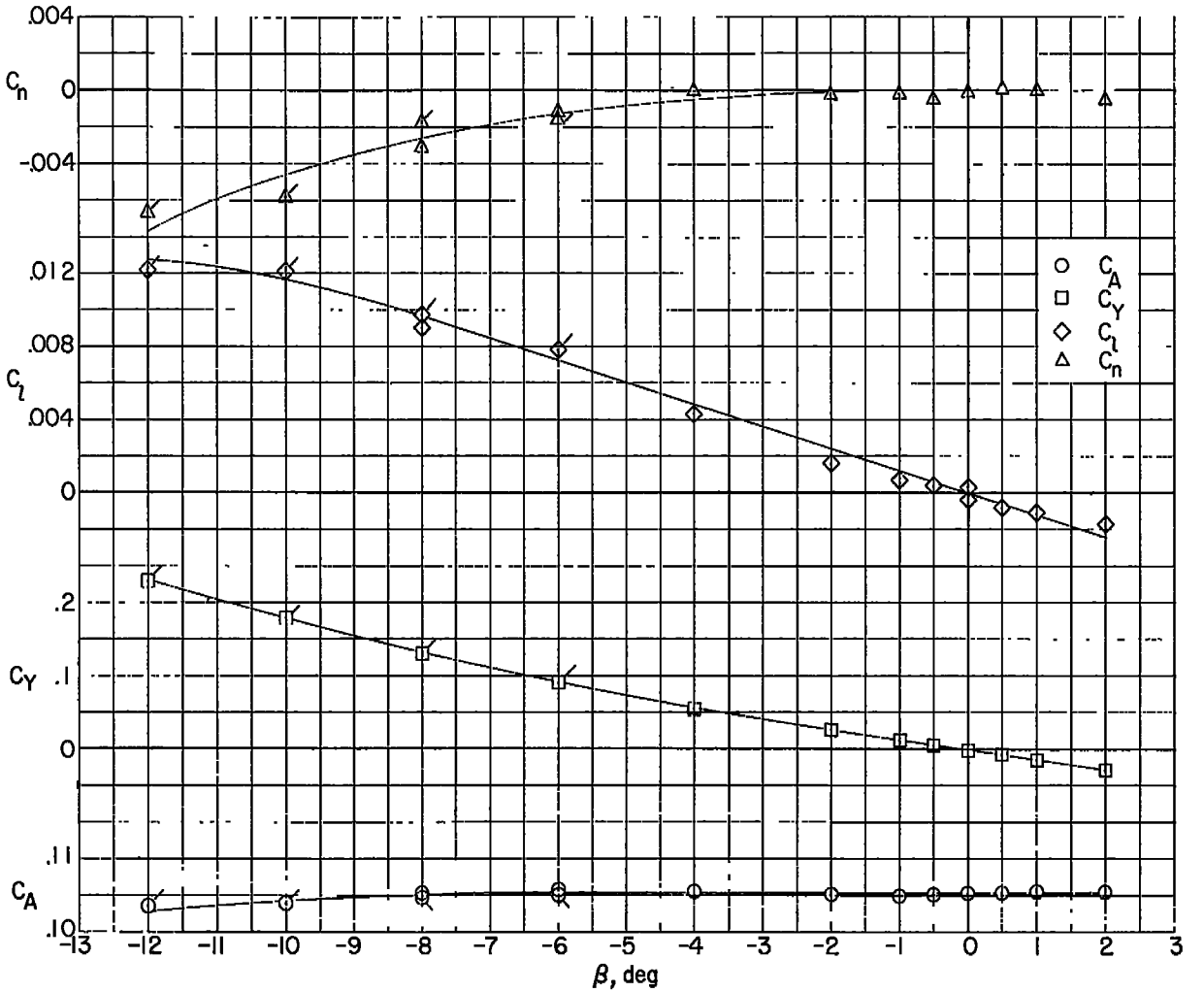

(c) Lateral characteristics in body-axis system at $\alpha = 0^\circ$.

Figure 25.- Complete configuration with $i_t = -10^\circ$ at $M = 2.40$. Concluded.

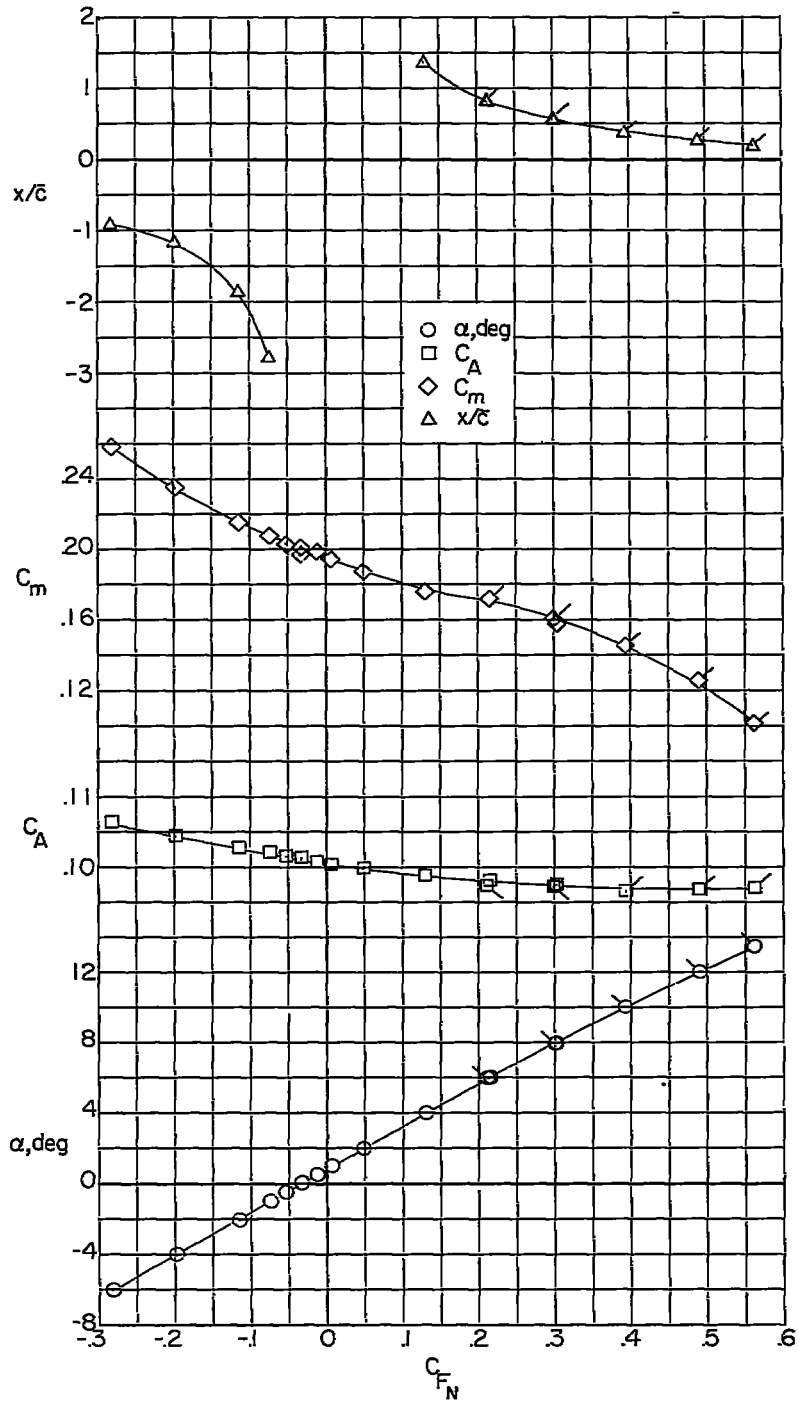

(a) Longitudinal characteristics in body-axis system at $\beta = 0^{\circ}$.

Figure 26.- Complete configuration with $i_t = -10^{\circ}$ at $M = 2.62$.

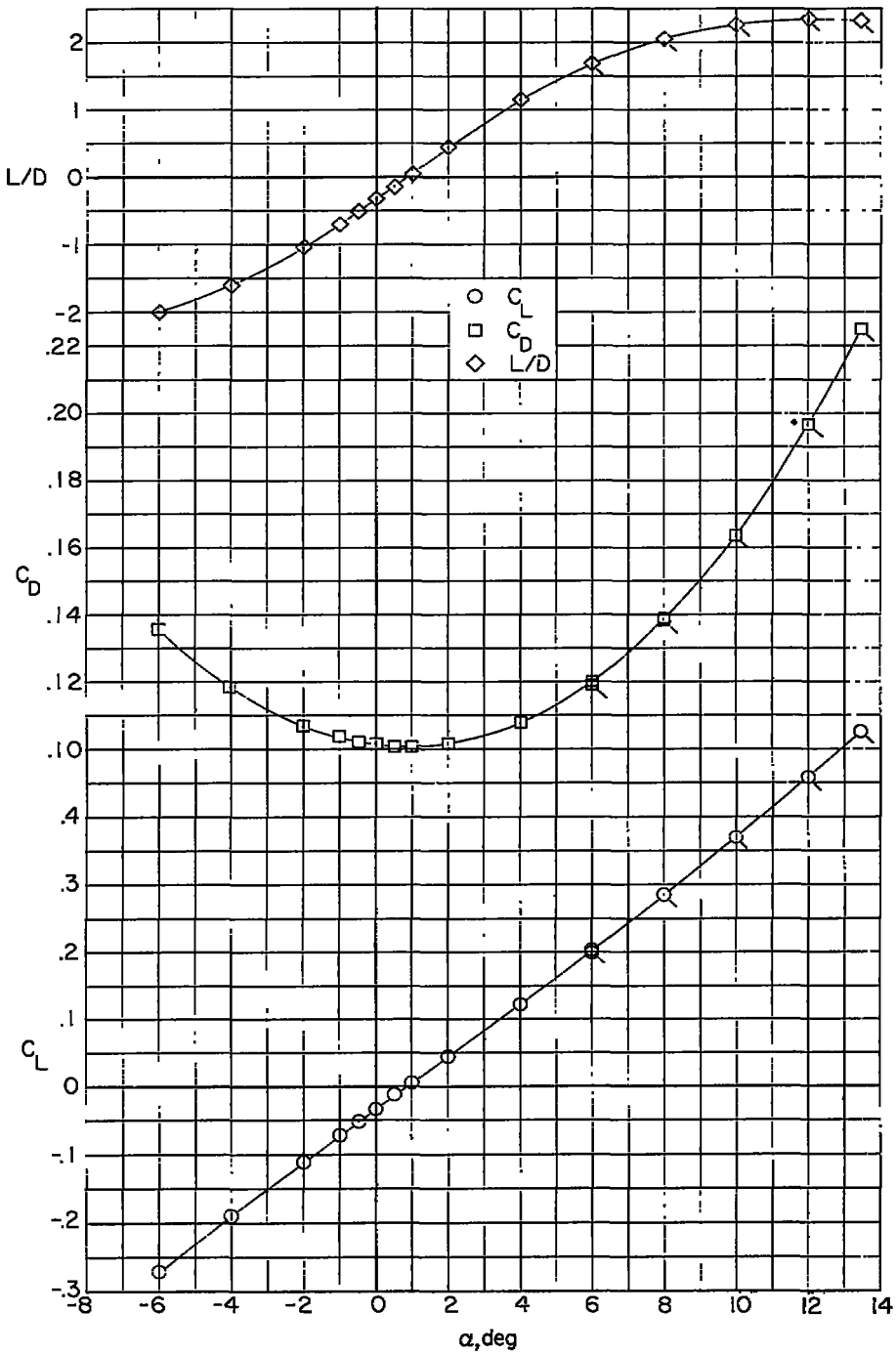

(b) Longitudinal force characteristics in stability-axis system at $\beta = 0^\circ$.

Figure 26.- Complete configuration with $i_t = -10^\circ$ at $M = 2.62$. Continued.

[redacted]

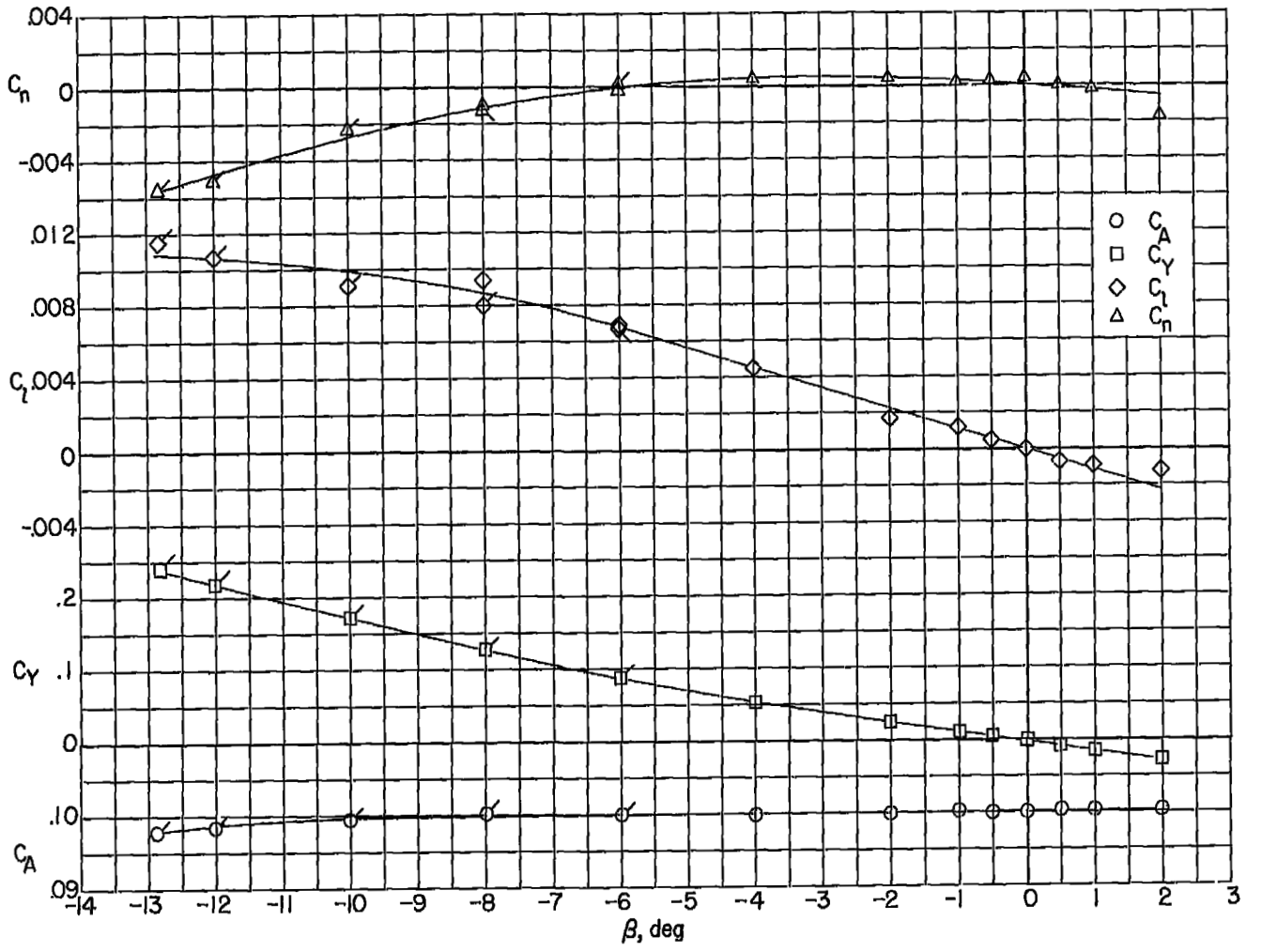

(c) Lateral characteristics in body-axis system at $\alpha = 0^\circ$.

Figure 26.- Complete configuration with $i_t = -10^\circ$ at $M = 2.62$. Concluded.

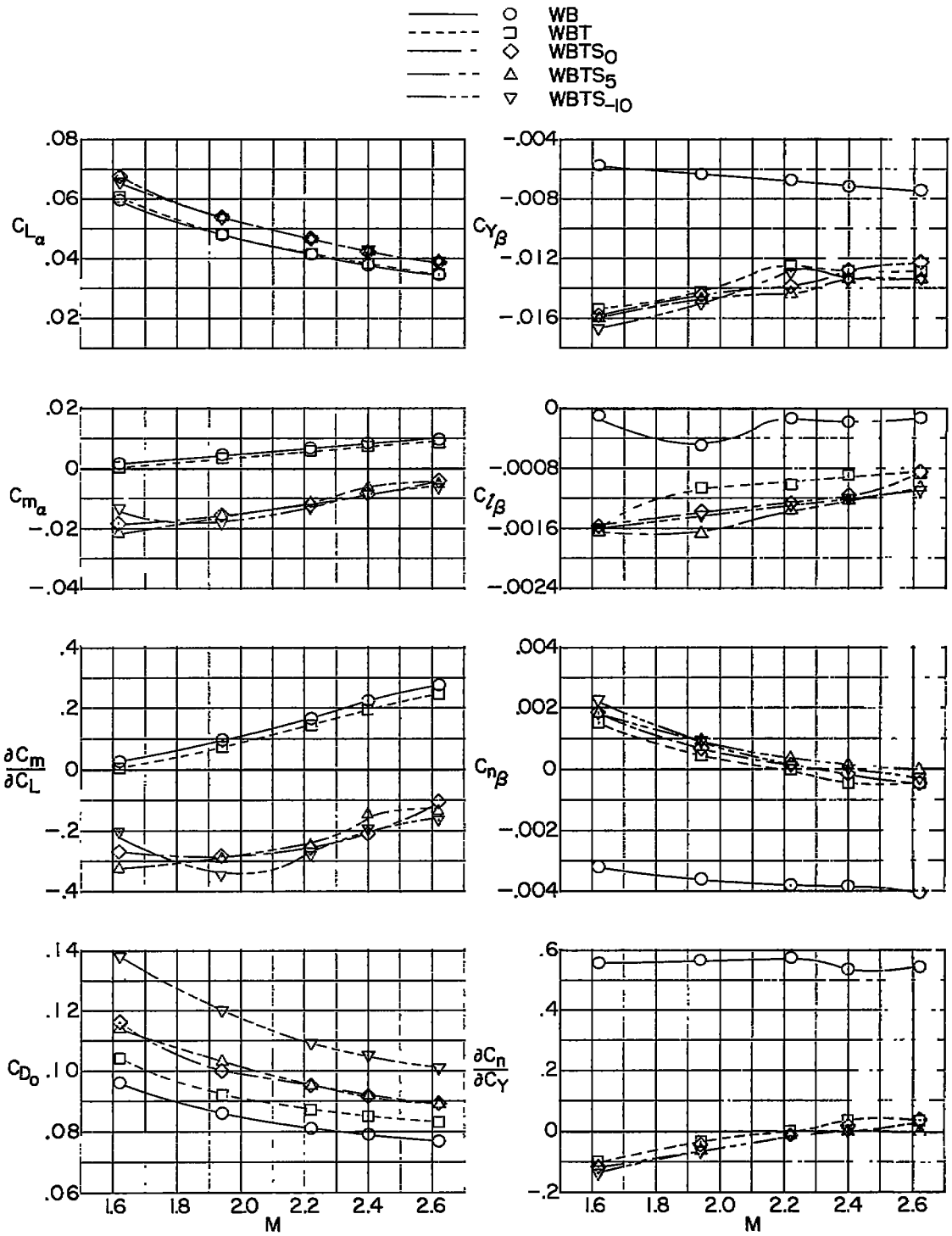

Figure 27.- Plot of static longitudinal and lateral stability derivatives and minimum drag of configurations tested against Mach number.